ELECTRON INDUCED MODIFICATIONS IN SOME POLYMERS

BY

ROSALINE MISHRA

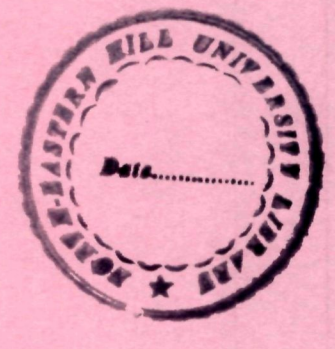

THESIS SUBMITTED

IN FULFILLMENT OF THE DEGREE OF

DOCTOR OF PHILOSOPHY IN PHYSICS

OF

NORTH-EASTERN HILL UNIVERSITY

SHILLONG – 793022, INDIA

October, 2000

Thesis

Dedicated to my

PARENTS

NORTH-EASTERN HILL UNIVERSITY
SHILLONG
October 2000

CERTIFICATE

I, Rosaline Mishra, hereby, declare that the subject matter of this thesis entitled "ELECTRON INDUCED MODIFICATIONS IN SOME POLYMERS" is the record of work done by me, that the contents of this thesis did not form basis of the award of any previous degree to me or to the best of my knowledge to anybody else, and that the thesis has not been submitted by me for any research degree in any other University / Institute.

This is being submitted to the North-Eastern Hill University for the degree of DOCTOR IN PHILOSOPHY in Physics.

Dr. D. T. Khathing
(Supervisor)

Dr. K. K. Dwivedi
(Joint Supervisor)

Rosaline Mishra.
Rosaline Mishra

Head
Department of Physics
North-Eastern Hill University
Shillong

Acknowledgements

In the innocent exuberance to delve deeper into the unfathomable sea and the glittering horizons of science, I pay glorious tributes to the galaxy of luminaries who have already illumined the track by their untiring explorations and invaluable inventions & have thus made going easier for me.

I humbly express my over-brimming gratitude to the divine reality whose unforeseen presence is exhibited in all our endeavours.

While acknowledging my deep sense of gratitude and reverence to all those who enabled me to make my thesis rendered attainable, the first and foremost are my teachers, Dr. K. K. Dwivedi, Vice Chancellor, Arunachal University, Itanagar and Dr. D. T. Khathing, Head, Regional Sophisticated Instrumentation Centre, North Eastern Hill University, Shillong. I am indebted to them for their indefatigable supervision, exacting guidance and incessant encouragement that they provided with constancy that inspired me through out the entire period of my research with them. I consider myself immensely fortunate to have them as my intellectual mentors.

My acknowledgement of gratitude is also due to Dr. D. Fink and Dr. M. Müller of Hahn Meitner Institute, Berlin for their keen interest in my work. I am indebted to them for effective and benevolent suggestions during the course of my research work. A very special feeling of acknowledgement goes to Prof. R. Brandt, Kernchemie, Philipps-University, Marburg, Germany for his encouragement during his short visit to India in 1998.

I extend my sincerest thanks to the scientific and technical staff of Hahn Meitner Institute, Berlin and Nuclear Science Centre, New Delhi for electron and heavy ion irradiation respectively. I am thankful to the scientific staff of Inter University Consortium, Indore for their generous cooperation in carrying out X-ray diffraction, A. C. Conductivity and Atomic

Force microscopy. I am grateful to the scientific staff of R.S.I.C & all the teachers of the Department of Chemistry and Physics, N.E.H.U. for making available to me all the facilities and amenities necessary for a befitting execution of my research work. I am thankful to the scientific staff of Institute of Physics, Bhubaneswar for allowing me to utilise the library facility available there.

I acknowledge the financial grant accorded in the form of Junior research fellowship by Department of Atomic Energy, Mumbai, India and in the form of Senior research fellowship by Council of Scientific and Industrial Research, New Delhi, India.

I wish to express my heartfelt gratitude to all my teachers for their encouragement throughout my career. I am very much indebted to all my seniors in the lab Dr. S. Ghosh, Dr. A. Kulshreshtha, Dr. D. Sinha and Mr. S.C. Katiyar for their ingenious help. I take this opportunity to thank all my friends who always stood by me with a note of appreciation. I humbly thank Mrs. R. Dwivedi and Mrs. N. Khathing for their motherly affection all along.

My abounding thanks are especially due to Shyam, for his consistent encouragement and unstinted support. A special feeling of gratitude is for him for being with me in my crests and troughs.

I am beholden to all my family members my Dad, Mom, Munu and Tina, who have been a perpetual and abiding fountain of inspiration for me throughout my academic pursuits. The perennial blessings of my parents constitute my intellectual and spiritual strength.

07.10.2000 *Rosaline Mishra*

Shillong.

CONTENTS

LIST OF TABLES

Table. No.	Contents	Page No.

LIST OF FIGURES

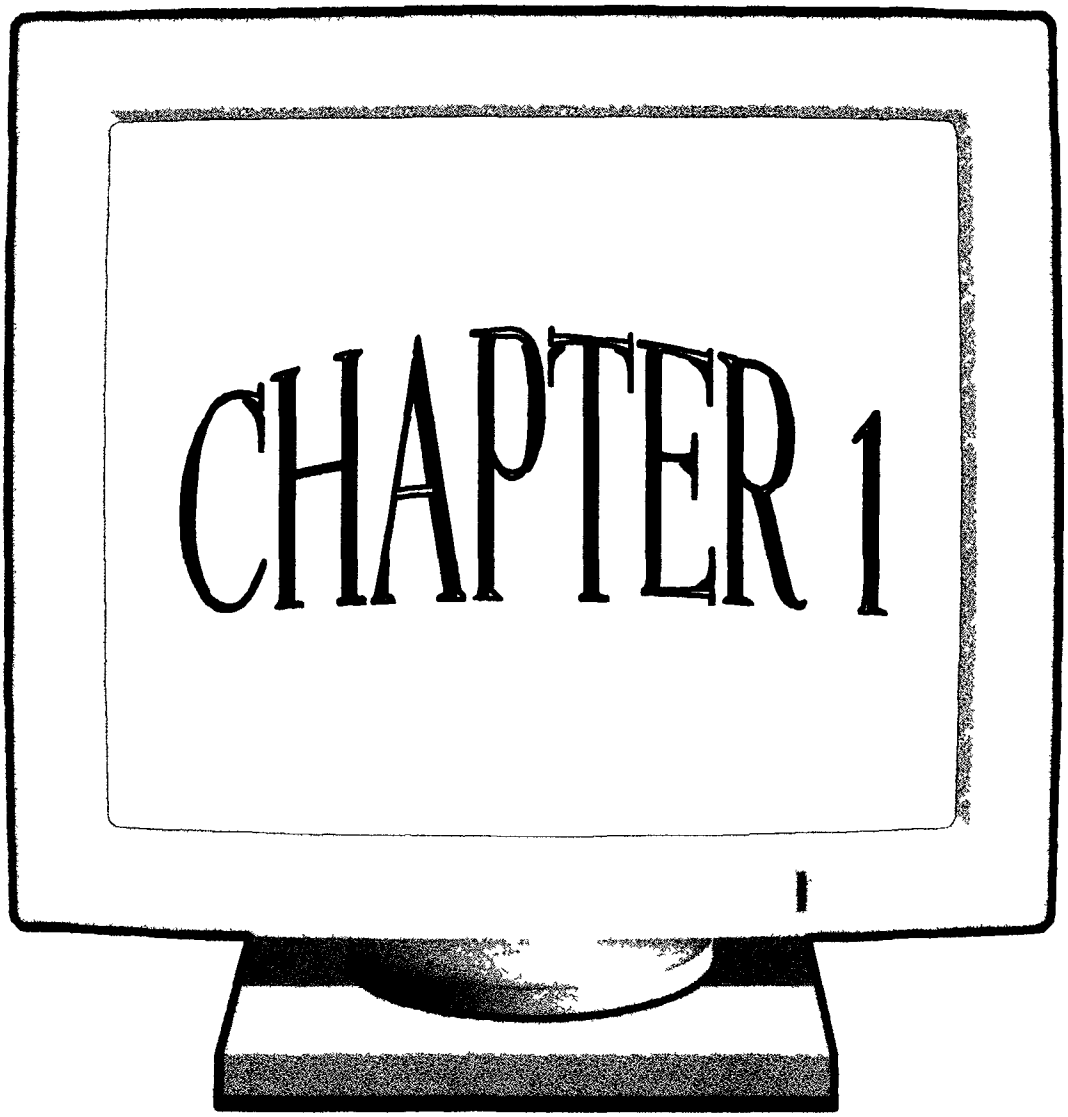
CHAPTER 1

CHAPTER 1

INTRODUCTION

1.1. POLYMERS

Polymers, also known as macromolecules, are built up of a large number of molecular units, which are linked together by covalent bonds, while separate segments of the same molecule are attracted to each other by intermolecular van der Waals forces. The covalent bonds involved are characterised by high energies (146 to 628 $kJ.mole^{-1}$), short inter-atomic distances (0.11 to 0.16 nm) and relatively constant angles between successive bonds. Covalent bonds govern the thermal and photochemical stability of the polymers. Due to a high strength to weight ratio, their lower cost, ease of moulding and lightness, polymers have diverse and extensive applications.

The structural organisation of polymers comprises of three distinct levels:

- The first level is the monomer chemical structure (primary structure) characterised by the presence of given functional groups and related electronic structure.
- The second level chain configuration (secondary structure) is characterised by spatial arrangement of the repetitive units in the polymer chains.
- The third level is the global form of macromolecule (tertiary structure) as determined by van der Waals forces, hydrogen bonds and the sum up of the conformational constraints.

A polymer single crystal looks as though it consists of many platelets (lamella) kept one over the other in decreasing order of size. The chain folding of the macromolecular chain takes place during polymerisation and then the long chain is accommodated into a narrow lamella. For a standard polymer, lamellar thickness is around 100 Å and the molecular chain length is around 100 to 1000 nm (Gowariker et al., 1996).

Polymers can exist only in solid and liquid states. Polymers in solid state can be completely amorphous, partially crystalline or

almost completely crystalline. Extension of X-ray crystallographic techniques to polymeric solids reveals that polymers do not have perfectly ordered crystal lattice and are not perfectly crystalline. Amorphous polymers are noncrystallisable and exist as glassy solids. The temperature at which the amorphous polymer changes from the glassy state to a rubbery state (glass transition temperature), a segmental mobility is observed. At flow temperature the molecular mobility sets in, the amorphous polymer changes from rubbery state to liquid state and the polymer starts flowing (Gowariker et al., 1996). Due to absence of any crystal lattice in amorphous polymer, no true melting takes place and there is no melting point associated with it. In a crystalline polymer, the segments are firmly held in crystallites by intermolecular forces. On heating the crystalline polymer at higher temperatures, the molecular mobility associated with segmental mobility abruptly sets in and the polymer starts melting. The degree of crystallinity in polymers is based on the premise that crystalline and amorphous components co-exist. Polymers in practical use are partially crystalline and consist of both crystalline and amorphous regions.

The thermal stability of a polymer is evaluated by its softening and degradation temperatures. Aromatic or heterocyclic polymers are generally known to show excellent thermal characteristics. They do not soften and retain their rigidity up to high temperatures. Stereoregular i.e. isotactic and syndiotactic polymers are found to crystallise, whereas atactic ones are unable to do so.

On one hand, polymers offer flexibility, easy processing and good insulating properties. On the other hand, the same properties limit the further applications of polymers. Ion irradiation provides a unique way to modify the polymer properties. Ion beam techniques are more and more popular as a very flexible technique to induce special properties in a large number of materials, including metals, semiconductors, ceramics, inorganic compounds and polymers.

1.2. ION INTERACTION WITH POLYMERS

Energy deposition by an impinging ion beam occurs discretely, not continuously. Electronic excitation is controlled by quantised energy levels and ionisation is restricted by a potential energy barrier, which has to be overcome for electrons to be released from the orbit. In addition to this, an atomic displacement also requires certain

threshold energy to break the bonds and move the atom over a certain potential barrier due to surrounding atoms.

The interaction steps of an ion with the polymer chains are as follows:

STEP 1: Energy is deposited by a series of adiabatic ionisation and/or excitation events and characteristic reaction sites (excited precursors) are formed according to two basic energy-loss mechanisms.

- ***Collisional energy-loss*** mechanism mainly produces a random fragmentation of polymer chains (Non-thermodynamic mechanism).

- ***Electronic energy-loss*** mechanism produces conventional ionised species by adiabatic ionisation of electronically excited species (Thermodynamic mechanism).

The characteristic interaction time, time for ionisation events and collisionaly induced bond breaking is of the order of 10^{-17} to 10^{-16} seconds.

STEP 2: Unstable species ions, radicals, recoiling atoms, excited species, created in the first step, relax through available reaction channels (Thermodynamic mechanisms). Relaxation

time for ionised species is of the order of 10^{-15} to 10^{-14} seconds and that for excited species is 10^{-16} to 10^{-12} seconds.

STEP 3: After a relatively long time, all long term rearrangements and thermalisation occur. This step affects the chain motion, de-excitation of long time radicals and decomposition of unstable bonds.

In polymers, with relatively long electronic relaxation times, part of the energy deposited by penetrating ions may be converted into atomic motion, producing defects and chemical modification in the bulk and material ejection at the surface. Ion tracks in polymers have been applied to engineer materials properties and surface morphology (Papaléo et al., 1999).

A full mechanism interpretation of the very complex beam-polymer interaction still needs a much larger amount of experimental data on suitable chemical systems and the realisation of new experiments pointing to elucidation of primarily induced chemical species with in situ measurements during irradiation. Polymers are characterised in general by a very high and very persistent reactivity. In particular, particle irradiation generates excited species or radicals, which, according to the chemical structure of polymer, can be

extremely resistant, having life-times of the order of days or months for some kind of radicals.

1.3. SPATIAL RESPONSE OF POLYMERS TO THE PERTURBATIONS

Polymers have fairly large free volume resulting in low atomic density. The spatial response of polymers to the energy input are both local and mesoscopical types.

Local response: Modification in polymer structure at the level of primary chemical structure of the monomer units. Optical properties are modified. In aliphatic polymers, the refractive index is modified due to formation of relatively high concentration of unsaturated bonds all along the irradiated polymer layer. In aromatic polymers, intrinsic modification of electronic structure takes place.

Mesoscopical response: Expansion and propagation of dynamic response over a much larger region than the primary interaction site. Modification occurs in properties related to chain configuration, as for instance, solubility and thermo-chemical properties.

Radiation damage includes changes in physical properties stable for a time scale essentially longer than the time of the slowing down of

the primary particle. It is a consequence of deposition of energy of the primary particle in the target.

1.4. ION INDUCED MODIFICATION IN POLYMERS

Ion beam treatment provides a unique way to modify the chemical, structural, optical, geometrical and electrical properties of polymer by causing irreversible modifications of structure and chemical composition (Steckenreiter et al., 1999). Ion beam induced scissions of polymeric chains typically produces charge redistribution along the skeletal backbone of a polymer molecule. This gives rise in turn to chemically unsaturated bonds and a variety of topological cross-linking rearrangements of polymer molecular fragments. There is also a simultaneous generation of free radicals. The nuclear stopping causes atomic displacements, while the electronic processes induce collective excitation of atoms and produce delta rays.

Energy deposition by an impinging ion beam occurs discretely because electronic excitation is restricted by quantised energy levels and ionisation is restricted by a certain potential barrier which has to be overcome for the electrons to be released from the orbit. This

discrete energy-loss entity is called a 'spur' (Lee, 1999). The energy-loss occurs as spurs along the ion track. Thus, changing the linear energy transfer (LET) of the impinging ion beams means changing the spur separation or spur density. For low LET ion beams, spurs are widely separated and occur independently often leading to scission. With increasing LET, more radical pairs are created within the track radius, spurs are connected or overlapped, high radical concentration gradient is established and so the effective radius increases facilitating cross-linking. It has been well established that mechanical, physical and chemical property changes in polymers are determined by the magnitude of cross-linking and scission, and that cross-linking enhances the mechanical stability while scission degrades mechanical strength.

Some modifications in polymer properties as a result of ion implantation are briefly described below:

- Formation of graphitic islands / clusters takes place as a consequence of very high locally deposited energy density. These are actually the conducting micro-composites that increase the conductivity in polymers (Davenas et al., 1997).

- Phase transition during irradiation has been observed in ferroelectric polymers (Calcagno et al., 1992).
- Ion implantation in polymers can result in drastic increase in electric conductivity (in some cases, by a factor of 10^{15}) of the pristine material (Popok et al., 1997) that opens its way to developing radically new micro-electronic devices.
- The bulk properties of polymers may not change after implantation, but rather the surface can become electrically conductive (Wang et al., 1997).
- Refractive index is modified due to formation of a relatively high concentration of unsaturated bonds all along the irradiated polymer layer (Darraud-Taupiac et al., 1997).
- Ion implantation causes a remarkable increase in hardness of polymer, increase in wear resistance and decrease in friction coefficient (Lee et al., 1991). Wear is a manifestation of bond breakage and cross-linking is responsible for improving the wear resistance in ion beam treated polymers. Ion beam irradiated polymers were reported to be three times harder than stainless steel.

- Radiation decreases the thermal conductivity of the polymers and can thus lead to higher operating temperatures and larger thermal stresses (Matzke, 1982).
- Molecular weight changes are a critical consequence of polymer irradiation, since a reduction in average molecular weight caused by main chain-scission will result in loss of mechanical strength. On the other hand cross-linking increases the molecular size thus improving the mechanical properties (Spinks and Woods 1990).
- Ion bombardment of polymers by energetic ions produces dramatic changes due to disruption of original chemical bonding as chain-scissions and cross-linking, thus changing the track registration efficiency in most of the polymers (Dwivedi et al., 1999). In general, polymers with only secondary and tertiary carbon atoms in the main chain tend to cross-link, while degradation occurs if chain includes a quaternary carbon atom.
- Disruption of original chemical bonding in polymers by ion bombardment occurs as chain-scission, cross-linking, carbonisation, gas evolution and ejection of polymer fragments with a wide distribution of molecular weights (Beardmore and Smith, 1995).

1.5. APPLICATIONS OF MODIFIED POLYMERS

Modified polymers have a wide range of applications also.

- The recent interest of using polymers as electrically conducting materials, for optical applications, light emitting diodes etc. is increasing (Das et al., 1998).
- Radiation treatment of polymers is employed to cross-link wire and cable insulation in order to improve the abrasion resistance and softening point. It is also used in the production of shrink film, tubing and packaging materials.
- Radiation induced degradation is used to form powdered Teflon which is used as a lubricant. Degradation of Teflon produces Perfluoro intermediates required in production of fluoro surfactants, fluorinated dielectrics and fluorinated finishing agents for textile industry.
- Avoidance of polymer degradation by choice of suitable polymer is utilised for satellite designs, since satellites are exposed to electrons and protons of several MeV energies, with additional stress of UV radiation, temperature fluctuations and high vacuum. The surface dose of satellite is equal to 25 MGy. y^{-1}.

- Automobile products are also irradiated to bring about partial cross-linking to increase their strength prior to conventional vulcanisation.

1.6. ELECTRON INTERACTION PHENOMENA

Heavy particles produce "tracks" densely populated with ions and excited molecules, whereas electrons deposit much of their energy in isolated spurs (micro-zones) containing a relatively small number of ions and excited states. Types of ionic and excited states will be same for both electrons and heavy particles, so that chemical process and radiolysis will be generally same, but different concentrations of reactive species in tracks and spurs will result in the products being formed in different proportions.

Electron interaction differs from heavy ion interaction in the following ways (Tayal, 1992):

1) Because of its small mass, electron, when collides with atomic electrons of the absorber, sustains deflections through much larger angles. The path of the electron is very irregular and not at all straight as the paths of heavy charged particles.

2) A heavy particle loses only a tiny fraction of its energy in each interaction with an atomic electron in its path. Random fluctuations in the amount of energy lost per interaction average out in thousands of interactions that occur during slowing down processes. Therefore, all the members of a mono-energetic beam of such particles have nearly same range. In electrons, large fraction of its energy can be lost in a single interaction. Path-lengths of electrons with same incident energy may differ.

3) Due to identity in character of the two colliding particles, exchange phenomenon must be taken into account in the theoretical investigations of electron-electron collision.

4) High speeds of the β-particles make it necessary to employ a relativistic treatment of the collision mechanism.

The relative importance of these processes vary strongly with energy of the incident electrons and depend to a small extent on the nature of absorbing material.

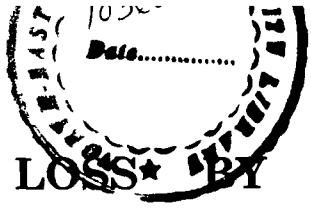

1.7. PROCESSES OF ENERGY – LOSS BY ELECTRONS

- ***Energy-loss of electrons by Bremsstrahlung emission***

Energetic electrons passing close to the nucleus of an atom, may be decelerated and according to Classical Physics will radiate electromagnetic energy (bremsstrahlung) with a rate, dE/dx (Energy-loss per unit path-length), proportional to z^2Z^2/m^2, where z and Z are the charges of the incident particle and the target nucleus respectively and m is the mass of the incident particle.

Energy-loss by bremsstrahlung will be greatest for light particles and for target materials of high atomic number. Bremsstrahlung emission produces significant changes in the stopping material, when it subsequently interacts with the material.

For electrons, the Bremsstrahlung emission is negligible below 100 keV, but increases rapidly with increasing energy. The energy of Bremsstrahlung radiation ranges from near zero to the maximum energy of the incident electrons, the energy of an individual bremsstrahlung photon depending upon the extent to which the electron, giving rise to it is slowed down. So, the

bremsstrahlung energy spectrum, which extends from zero to the energy of incident electron, is a continuous X-ray spectrum.

- ***Energy-loss of electrons by inelastic collisions:***

  Inelastic scatterings, rather than producing large angle deflections, make electrons lose energy in ionisation and excitation events with atoms. Coulomb interaction of incident electrons with atomic electrons of the stopping material produces ionisation and excitation in the target, thus, slowing down the incident electrons below the energies at which bremsstrahlung emission occurs. Inelastic scattering is relevant in the study of electron penetration through matter.

- ***Energy-loss of electrons by elastic scattering:***

  In elastic scattering with atoms, electrons suffer large angle deflections and negligible energy losses that make electrons traverse matter in tortuous paths, rather than in a rectilinear way (Idoeta, 2000). Owing to its relatively small mass, the electrons can be deflected by Coulomb electrostatic field of the atomic nucleus, which results in the elastic scattering of electrons, i.e.,

only the direction of motion is changed without any conversion of kinetic energy to any other form of energy. This scattering is more pronounced for low energy electrons and for high atomic number materials.

The technological challenges to develop new capabilities in the nanometer scale, tailoring of surfaces and the understanding of the evolution of the energy deposited around the ion path and of the modified region, are fundamental research areas in which interest has recently been aroused. The wide spread application and technological importance of the polymers evoked us to induce some desirable modifications in their properties so as to enhance their applicability. The main challenge was to modify the polymers with the electrons, which do not create tracks of their own and yet change the bulk properties.

So, for the present work five different polymeric materials have been selected on the basis of their applicability and the effect of electron irradiation on them have been studied through different experiments which are described chapter wise, as follows:

- The modification produced in four different types of polymers viz. Polypropylene, Polyethylene terephthalate, Polytetrafluoro ethylene and Polyimide, by a particular dose of 2 MeV electron has been studied by spectroscopic, thermal, track and diffraction techniques and described in **Chapter 2.**
- **Chapter 3** deals with the study of dose dependent variation in optical absorbance, transmittance, structural arrangement, roughness and thermal properties by different characterisation techniques, of a widely used polymer, Polyallyldiglycol carbonate which has been irradiated to 2 MeV electron beam.
- Modifications produced in track registration sensitivity of Polyallyldiglycol carbonate by electron irradiation has been described in **Chapter 4**. The polymer Polyallyldiglycol carbonate pre-irradiated by electrons was further irradiated by heavy ions and the overall etching response of the polymer as a function of electron dose has been investigated.
- **Chapter 5** describes the energy-loss by an electron beam when it traverses the layered metallic targets. The effect of energy-loss on the etching characteristics and thermal stability of Polyallyldiglycol carbonate has been studied. A comparative study has been carried

out to study the effect of metallic targets of different atomic numbers on the energy-loss phenomena.

- Finally in **Chapter 6**, the significant results of the present investigation are highlighted. A brief description on the potentialities and scopes of the work is presented for some future applications.

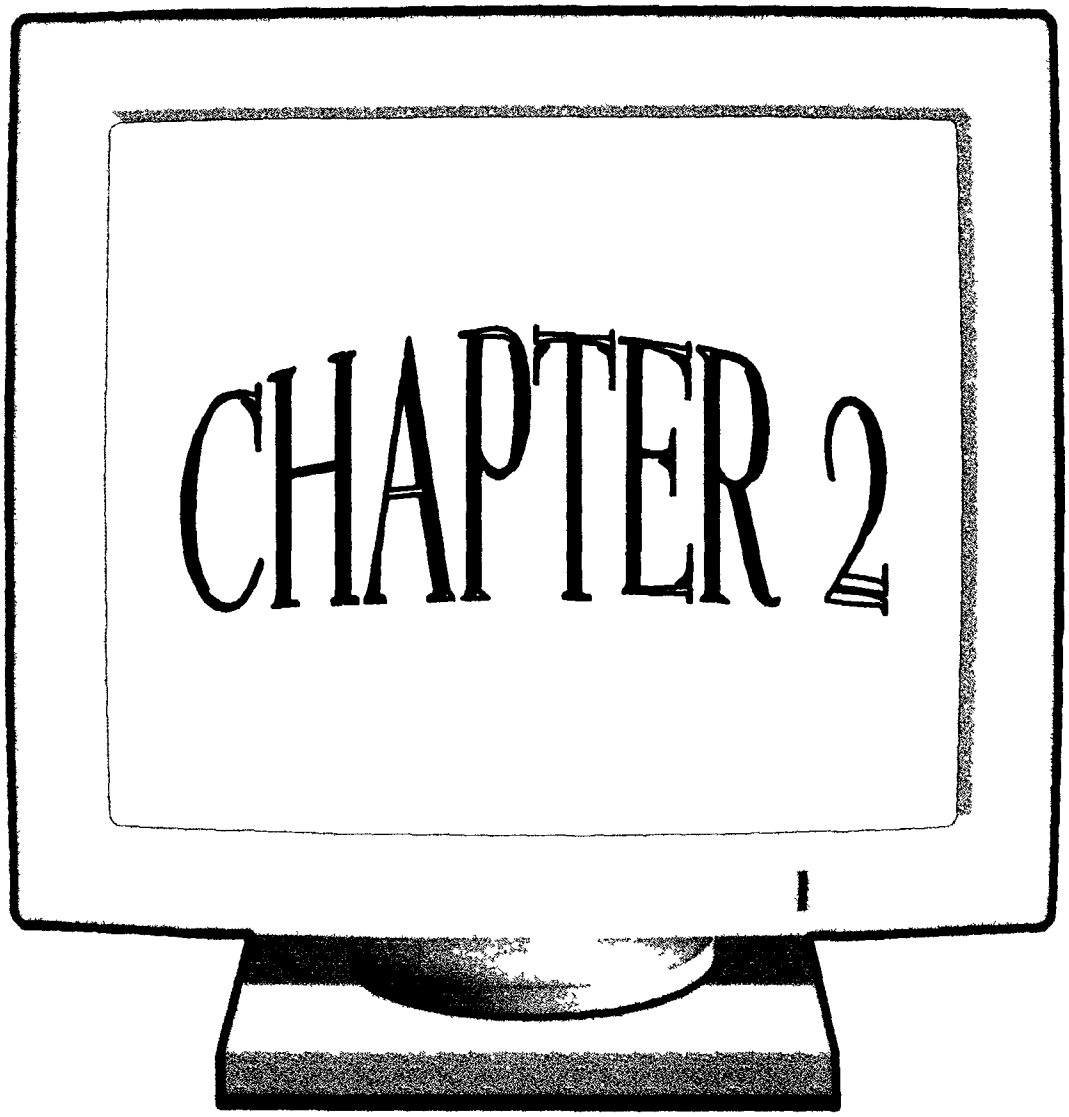
CHAPTER 2

CHAPTER 2

EFFECT OF ELECTRON IRRADIATION ON SURFACE AND BULK PROPERTIES OF SOME SELECTED POLYMERS

2.1. INTRODUCTION

Since the time their versatile properties were recognised in 1930s, polymeric materials have been the subject of immense commercial and scientific interest. Polymers exhibit ion transport, redox behaviour, electrochemical effects, in addition to light weight, flexibility, low cost and other beneficial physical properties. The application of radiation in polymer technology has been of great importance when trying to achieve some desired improvements in polymer properties.

During ion implantation in polymers, ion-electron and ion-atom

collision takes place. Ion-electron collisions lead to a momentary ionised state for atoms in their normal geometrical order. This increases the chemical activity of the atoms but does not necessarily lead to atomic re-arrangement unless such re-arrangement can reduce chemical energy of the system before electronic recombination or equilibrium takes place. Since atoms have so much more inertia than electrons, so electron recombination is favored. When ion-atom collision takes place at lower energy (< 10 keV) near the end of the ion track, a violent rearrangement of all the atoms takes place (Lee et al. 1991). Ion bombardment induces formation and transport of reactive species, which are able to permanently change the electronic and chemical properties of polymers. Ion implantation in polymers destroys the initial structure by cross-linking, scission and emission of atoms, molecules and molecular fragments. Conductivity theories on irradiated polymers assume an electronic hopping motion between the carbonaceous clusters which are supposed to be the carriers of electric conductivity in ion irradiated polymers (Fink et al., 1996(b)). In individual tracks of energetic ions, where high energy densities are deposited in small localised volumes, all polymer atoms become highly excited, hence bond free, for a short time which subsequently condense

to small carbonaceous clusters. It was found that cluster formation takes place only above a certain deposited energy density threshold of about 10^{-2} to 10^{-1} eV/Å^3 (Fink et al., 1995). A dramatic increase in polymeric conductivity sets in at mean deposited energy densities between 10^{-1} and 10^{0} eV/Å^3 (Fink et al., 1996(b)). UV-Vis spectroscopy is sensitive to optically absorbing cluster region.

When irradiation is done in presence of oxygen, the free radical R- becomes ROO-, which reacts with R'H to give ROOH and R' and the degradation can continue. In many cases, degradation is limited by molecular oxygen diffusion. The applications of radiation effects are diverse from bulk processes to interface behaviour and from thermal evolution to athermal reactions.

Track formation in polymers is complex since not only primary but also secondary processes such as formation of radicals and chemical processes are involved (Trautmann et al., 1996). Particle track technology offers the opportunity of manufacturing membranes with cylindrical pores of defined pore-size and adjustable porosity. The absolute value of track core size in polymer are of same magnitude as those in the radiation resistant inorganic crystals. In contrast to inorganic materials, the tracks in polymers possess a vast halo which

is formed by secondary reactions changing chemical properties of the radiolysis sensitive matrix at large distances from the ion path (Apel et al., 1999).

In the present work, we have studied the effect of 2 MeV electron in Polypropylene (PP), Polyethylene terephthalate (PET), Polyimide (PI) and Polytetrafluoro ethylene (PTFE). The polymers are selected on the basis of their availability and applicability. The chemical characteristics and specifications of the target polymers are discussed in the following section.

2.2. SPECIFICATIONS OF THE SELECTED POLYMERS

2.2.1. Polypropylene (PP)

The empirical formula of PP is given by C_3H_6 having a specific gravity of 0.9 $g.cm^{-3}$. It belongs to the family of polyolefins having the structure:

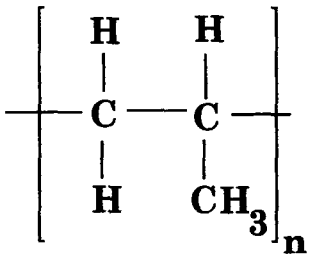

It exhibits both cross-linking and degradation under ion irradiation,

but cross-linking is dominant (Bohidar, 1994). It gives a combination of C–C bond rupture and C–C bond formation. It has a glass transition of -8°C and a melting point of 208°C. It is the lightest known industrial polymer because of its high strength to weight ratio and is produced by polymerisation of propylene. Being highly crystalline PP exhibits high stiffness, hardness and tensile strength and has excellent mechanical and dielectric properties. It finds its applications in electrical appliances such as radio, television, refrigerator, etc. It is extensively used for producing package films, storage tanks and monofilaments.

2.2.2. Polyethylene terephthalate (PET)

PET is a polyester popularly known as Terylene having the structure:

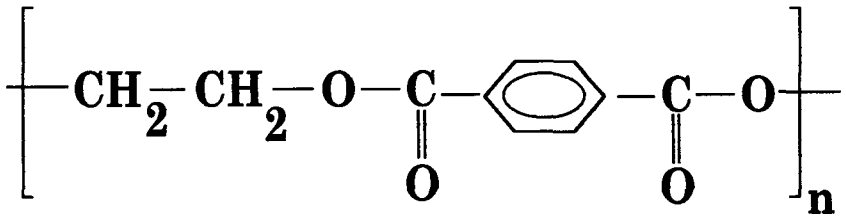

It's empirical formula is $C_{10}H_8O_4$ and specific gravity is 1.41 $g.cm^{-3}$. It is semicrystalline in nature. The crystalline lamella surrounded by the amorphous region makes the whole structure mechanically intact. It has a very good mechanical strength up to 175°C. It has a glass

transition temperature of 73°C to 80°C and a high melting point of 245-265°C due to the presence of aromatic ring. It is resistant to heat and moisture. It is virtually unattacked by chemicals. It is extensively used to make textile fibres. Literature survey indicates that irradiation of PET by Krypton and Molybdenum ions result in the formation of alkyne groups in the polymer (Steckenreiter et al., 1997). Even at the highest dose, the aromatic rings are not destroyed but di-substituted benzene groups are modified to mono-substituted ones. Formation of olefins, carboxylic acids, alcohols and carbondioxide in PET has been reported due to electron and UV irradiation. Chain-scissioning, cross-linking, molecular emission and formation of double bonds are the effects of electron irradiation. An additional effect on PET by swift heavy ions is the formation of alkyne group. The main effects of heavy ion irradiation in keV - MeV range on PET are loss of hydrogen, decrease of optical band-gap and breaking of C-H bonding. In PET the C-H bond is stronger than C-O and Oxygen is depleted more than Hydrogen by ion bombardment (Lee et al., 1991). The analysis of polarisation spectra in heavy ion irradiated PET shows the production of hydroxyterephthalates and dihydroxyterephthalates in the polymer backbone as radiolysis products and molecular orientation

in the ion tracks (Eßer et al., 1999). Heavy ion irradiated PET undergoes main chain-scission by bond breaking in the aliphatic part of the main chain rather than destruction of benzene ring and thus leading to amorphisation of the polymer (Steckenreiter et al., 1999).

2.2.3. Polyimide (PI)

Polyimides form a class of thermally stable polymers that can withstand higher operational temperatures than most of the polymeric materials in use today. Its empirical formula is $C_{22}H_{10}N_2O_5$ and the specific gravity is 1.4 $g.cm^{-3}$. Aromatic Polyimides are one of the most stable and environmentally resistant heterochain polymers having the structure:

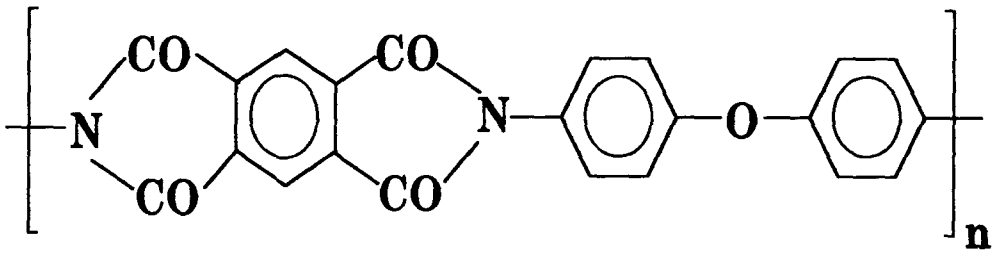

The presence of imide and aromatic rings in the structure of the polymer is at the origin of improved heat resistance and stability to ionising radiations, which led to a wide spread use of this category of polymers in many modern technologies. Ion beam irradiation on Polymides produces dramatic modifications in their electronic

properties by production of a composite system involving graphitic nanoparticles dispersed in a polymeric medium, which accounts for percolation transition to a conducting state when critical concentration of carbon clusters is reached (Davenas et al., 1997). Ion beam irradiation in Polyimide also leads to dramatic modifications of the diffusion, which result from creation of static free volume. It is widely used not only for electrical insulation but also for passivation and multilayer interconnection in microelectronics, because of its good electrical insulation and dielectric properties, excellent thermostability and mechanical strength. Photo-sensitive PI is used in high-energy implantation for IC fabrication as a marking material (Xu et al., 1991). Pyrolysis produces dramatic loss of imide structures with a progressive depletion of oxygen and nitrogen containing groups along with a drastic change in electrical properties of Polyimide, from initial insulating ($\rho = 10^{16}$ Ωcm) to a semiconducting ($\rho < 10^{2}$ Ωcm) at pyrolysis temperature, of the order of 700°C to a metallic ($\rho = 10^{-2}$ Ωcm) at 900°C. A drastic increase in conductivity has been reported when Polyimide is heated between 800°C to 850°C, due to formation of dense heterocyclic carbon ring networks in the polymer (Marletta and Iacona, 1995). The threshold for homogeneous track etching in PI has

been reported to be higher (Trautmann et al., 1996). With an increase in the dose of Argon ions on Polyimide, the surface of the implanted region of the polymer changed colour from dark brown to lustrous black and revealed electrical conductivity. Further, it has been found that atoms implanted in Polyimide films migrate and aggregate in form of tiny islands in the surface region and the polymer is carbonized as a result of scission of chemical bonds and subsequent out diffusion of nitrogen and oxygen atoms (Yoshida and Iwaki, 1987). Ion beam induced electrical conduction of PI films can find potential applications for encapsulation of micro-electronics. It can withstand a temperature of 425°C without undergoing any degradation. Therefore, it finds application in surface coating of supersonic aircrafts. Main chain-scission leading to degradation of the polymer has been evidenced in Polyimide by Krypton and Molybdenum ion irradiation, along with the formation of triple bond species such as alkynes and cyanates (Steckenreiter et al., 1999). Further it has been found that the hardness of the B, N, C - implanted Polyimide is over three times harder than stainless steel and about two times harder than implanted stainless steel. Implanted Polyimide showed remarkable wear resistance and decrease in friction coefficient (Lee et al., 1991). A

remarkable dye uptake of Polyimide is an indirect consequence of the electronic destruction processes of the irradiated polymer (Fink et al., 1996(a)).

2.2.4. Polytetrafluoro ethylene (PTFE)

PTFE belongs to the family of fluoroplastics having the empirical formula C_2H_4 and specific gravity 2.2 $g.cm^{-3}$. Its structure is given by,

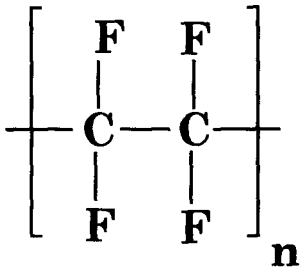

This is a linear polymer having no branching at all. It is a highly crystalline polymer having a melting point of 330°C. It has a very low dielectric constant. Its high thermal stability is attributed to very high dissociation energy (452 $kJ.mole^{-1}$) of C-F bond. Besides the highly electronegative nature, Fluorine protects C-C bond from external attack. Ionising radiations are known to induce scissions of bonds giving rise to radicals and evolved gases. In addition, stable radicals are formed and crosslinking frequently occurs (Betz et al., 1996). It is resistant to radiation in the presence of oxygen, but rapidly

deteriorates when oxygen is present, becoming extremely brittle. The entire polymer is rapidly degraded once a free radical centre has been formed in some part of the molecule. According to the literature survey, the energy provided by fast electrons is sufficient to cause dissociation of C-C and C-F bonds during irradiation (Schierholz et al., 1999). As a consequence, short-chain oligomers are formed. Further short-chain oligomers also arise from radical reactions that are induced by absorption of thermal energy. However, the temperature resistance of PTFE is reduced drastically by electron irradiation.

It is used for making pump valves and pipes where chemical resistance is required. It finds its application in surface coating of household appliances. PTFE micropowder that is produced by exposing the polymer to electron beam radiation is commonly used as an additive in a wide variety of applications (Gangal, 1989), including as a component of lubricants.

2.3. EXPERIMENTAL ASPECTS

2.3.1. Preparation of the targets

Ten pieces of each of size (2x2) cm^2 were cut from commercially available sheets of PTFE, PI, PP and PET. Thickness of the polymers

were measured by a sensitive Heidenhain depth- measuring device. The measuring length of the gauze (CT-60) of the device has a glass scale with DIADUR line grating (grating with pitch 1.0 μm). The glass scale has a rigid connection to the plunger. The scale grating is photo-electrically scanned. The measuring gauze is connected to the digital VRZ-210 display unit. The least count of this device is ± 0.1 μm. Thickness of the samples was measured at 10-15 different places chosen at random. They were found to be 200 μm, 8 μm, 10 μm and 13 μm for PTFE, PP, PI and PET respectively.

The samples were then washed thoroughly with soap solution and then several times with deionised water. The cleaned samples were dried inside a vacuum desiccator. A polymer stack was prepared having 10 foils each of the above mentioned polymers and covered at both ends by radiation sensitive Polyvinyl acetate (PVA). This target assembly was then taken for electron irradiation. PVA was used to check the uniformity of the impinging beam from decolourisation of the blue dye in the irradiated region.

2.3.2. Irradiation and cooling

Irradiation of the first target stack was done by a 2 MeV electron beam from an electron generator at the Hahn-Meitner Institute,

Berlin. The electron beam was allowed to pass through a collimator and was allowed to fall on the target stack placed perpendicularly at a distance of 2 metres from the collimator. The dose of 2 MeV electron was 23 kGy. The beam size was bigger than (2 x 2) cm^2, which covered the whole target area.

Irradiated target stacks were allowed to cool for about 24 hours. The samples were then separated, marked and preserved in plastic boxes.

2.3.3. Polymer characterisation

After irradiation, the characterisation of the samples were performed by different spectroscopic techniques (UV-Vis spectroscopy, Fourier Transform IR spectroscopy, Electron Spin Resonance spectroscopy), thermal techniques (Thermogravimetric Analysis, Differential Scanning Calorimetry), Structural analysis technique (X-ray diffraction), Track technique, Conductivity measurement technique and Atomic Force microscopy.

a) *UV-Vis Spectroscopy*

UV-Vis spectroscopy is used for structure elucidation and is based on the law governing the absorption of electromagnetic radiation in matter, i.e., "The intensity of a beam of monochromatic

light decreases exponentially with increase in concentration of the absorbing substance". When an electromagnetic radiation in UV-Vis region (200nm - 800nm) falls on the target material, a part of the incident radiation is absorbed which in turn excites the lower energy orbitals to higher energy orbitals. The amount of energy absorbed at each wavelength of UV-Vis region, is measured by the spectrophotometer.

UV-Vis spectroscopy for the first foil of irradiated samples were done by a Beckman DU-650 spectrophotometer. All the spectra were taken with pristine samples as reference. The scanning speed of the apparatus was 1200 nm/min and the scanning wavelength region was 200 nm to 800 nm. The wave-length range of absorption edges were found to be within 200-345 nm for PTFE, 400-550 nm for PI, 300-330 nm for PET and 200-255 nm for PP. Information about optical band-gap is accessible from the absorption edge of UV-Vis spectra of irradiated polymers. The UV-Vis spectra of irradiated samples show an increase in absorption with increase in radiation dose towards the longer wavelength region. The red-shift in the spectra with increasing dose can be correlated with optical band-gap (E_g) by Tauc's expression (Fink et al., 1995):

$$\omega^2 \varepsilon(\lambda) = (\hbar\omega - E_g)^2 \qquad \text{-------- (2.1)}$$

where, $\varepsilon(\lambda)$ is the optical absorbance at wavelength λ.

The values of $\sqrt{\varepsilon} / \lambda$ are plotted against $1 / \lambda$ to determine the gap-wavelength (λ_g) from the intersection of the extrapolated curve with the abscissa.

The band-gap is derived from the relation,

$$E_g = hc/ \lambda_g. \qquad \text{-------- (2.2)}$$

In determining the wavelength gap, the best linear fit of the points on the curve $\sqrt{\varepsilon} / \lambda$ vs. $1 / \lambda$ was always taken. The maximum probable error in determining the energy band-gap was ± 0.1 eV.

b) *Fourier Transform Infra-red Spectroscopy*

IR spectroscopy is based on the simple fact that a chemical substance shows marked selective absorption in the infra-red region, after which the molecules vibrate at different rates giving rise to close packed absorption bands. Fourier transform is the mathematical operation used to convert an interferrogram to a single beam spectrum.

All FT-IR spectra of the first foil of irradiated samples along with their pristine were recorded in transmission mode using model NICOLET, IMPACT 410, Fourier transforming instrument keeping air as

reference. All the measurements were done in the range of 4000 cm^{-1} to 500 cm^{-1} wave number. The spectra were obtained for the polymer's transmittance as a function of wave number. The variation of transmittance in the pristine and electron irradiated samples were compared and the peak analysis was done to study the variation in position and intensity of the bands, disappearance of some existing bands and the emergence of new bands.

While recording the spectra, the errors might be due to stray radiation, zero setting of the instrument, non-continuous sample, atmospheric absorption, slit width, scan speed etc. For a relatively ideal sample, the accuracy is expected to be from better than ± 1% to ± 3% of the amount present.

c) *Electron Spin Resonance Spectroscopy*

ESR is the branch of absorption spectroscopy in which radiations of microwave frequency are absorbed by a paramagnetic substance to induce transitions between magnetic energy levels of electrons with unpaired spins. It is a powerful tool in the investigation of radiation-induced para-magnetic defects (free radicals).

The ESR measurements have been done using a Varian (E-109, X-band) spectrometer with 100 kHz field modulation. Samples were

cut into (0.5 x 0.5) cm^2 sizes, placed in quartz tube and their spectra were recorded at room temperature. A 9.6 GHz frequency was used for this instrument. The instrumental settings were:

Field set: 3382 Gauss, Scan range: 1000 Gauss; Time constant: 0.25 sec; Scan time: 4 minutes; Modulation amplitude: 0.5x1; Receiver gain: $6.3x10^4$; Microwave power: 2 mW.

The spectra obtained were analysed for emergence of free radicals.

d) *Thermogravimetric Analysis*

Thermogravimetric analysis involves the weighing of the substance under investigation while it is being heated at a predetermined rate. Thus this technique offers a possibility of studying the complete thermal decomposition behaviour of a substance. Thermogravimetric analysis has been done for the irradiated polymer using a simple automatic Perkin Elmer Delta series Thermal Analysis system. The samples were cut into very small pieces, crimped in small aluminium pans and weighed in a micro-balance, with a weighing precision up to 10 ppm. The samples were then heated up to 600°C, which resulted in weight-loss of the sample. The heating rate for this instrument was 20°C/min. The temperature range scanned was from 30°C to 600°C. The resulting weight loss is

recorded as a function of temperature in TGA thermogram. The thermogram is a plot of mass percentage as a function of temperature obtained after complete decomposition of the samples. This weight loss results from chemical reactions, decomposition, solvent and water evolution, oxidation etc. The temperature error in recording the TGA thermogram was ± 2°C.

e) *Differential Scanning Calorimetry*

DSC is a thermal technique in which differences in heat flow in a substance and a reference are measured as a function of sample temperature while both are subjected to a controlled temperature program. It measures the gains and losses of heat accompanying the phase transitions. The measurements were done using a Perkin Elmer Delta-series Thermal analysis system. Nitrogen was used as flushing gas. The samples were cut into small pieces and crimped in aluminium pans. The samples were weighed in a thermobalance. Aluminium was taken as the reference material. Heat power was adjusted to maintain a constant temperature in the sample and the reference. The thermograms were obtained for heat flow in the sample as a function of temperature. The type of thermal reactions (endothermic / exothermic) shown by the polymer on application of heat was studied.

f) *X - Ray Diffraction*

XRD involves the diffraction of X-rays by crystals having geometrically periodic arrangements of atoms separated by distances comparable to X-ray wavelengths. XRD patterns were recorded using Cu - Kα radiation ($\lambda = 1.54$ Å) 8.04 keV energy from the Rigaku θ - 2θ X-ray spectrometer at Inter University Consortium, Indore, India. A rotating anode source and a Sodium Iodine scintillation detector have been used. The dimension of the entrance slit was 0.2 mm and the step size was 0.04 mm. The samples were cut to sizes of (1 x 1) cm^2, fixed in the sample holder and placed in the XRD chamber. The value of the diffraction angle (2θ) ranged from 3° to 90°. The spectra were obtained for structural analysis of the samples.

g) *Atomic Force Microscopy*

AFM is used to investigate the surface morphology, to probe the surface forces and to study the nano-mechanical properties of the samples. It is capable of imaging the electromagnetic forces between the surfaces, on the length scale of 10^{-11} to 10^{-7} m. The resolution of this instrument is in the range of 10^{-8} to 10^{-13} N. The atomic force microscopy was done at Inter University Consortium, Indore, India, using Digital instrument, Nanoscope E, in contact mode. The samples

were cleaned and glued down to the sample puck using cyanoacrylate glue (superglue). The sample puck was placed on the top of the scanner tube. The instrument consists of a microscopic force censor (cantilever) made of silicon nitride that is used to sense the force between the sample and the tip while scanning the sample surface. The laser spot is positioned on to the cantilever. The photodiode is then positioned to maximise the signal and the spot is fine adjusted on to the very tip of the cantilever. The deflection of the cantilever as well as the local height of the sample was recorded during the course of scanning. Three-dimensional images of the surface scanned were then obtained. Further surface roughness of the irradiated samples were measured at 20 different fields on the sample surface at random and the mean was taken as the surface roughness of the sample.

h) *Track Etch Method*

The irradiated polymers PET and PI along with their pristine were further exposed to fission fragments from ^{252}Cf having half-life of 2.65 years and activities $5.7x10^3$ fission/minute, at an angle of 90° for 30 minutes. The irradiation was done inside a desiccator in air. Before etching, the samples were washed in soap solution to remove all the greasy substances and contamination from the sample surface. The

samples were then dried between layers of soft filter paper and later in a vacuum desiccator.

PET samples were etched in 6.25N NaOH solution at different etching temperatures viz. 55°C, 60°C, 65°C and 70°C. The PI samples were etched in NaOCl solution at different etching temperatures viz. 50°C, 55°C, 60°C, 65°C.

The fission fragment diameters were then measured by Leitz optical microscope at 625x magnification. The bulk etch-rate was determined by track diameter method. The rate of increase of the fission track diameters was determined by plotting etching time versus track diameter. The bulk etch-rate (V_G) was then derived from the slope of the obtained curve. Mathematically,

$$V_G \approx D / 2t \qquad \text{-------(2.3)}$$

where, D = diameter of fission fragment tracks, in μm

t = etching time in hours.

The activation energy for bulk etching was determined by plotting log V_G against the reciprocal of the etching temperature. Mathematically, the bulk etch-rate can be co-related to activation energy of etching by the following equation:

$$V_G = A\, e^{-Ea / kT} \qquad \text{------(2.4)}$$

where, A is a constant,

E_a is the activation energy for bulk etching in kJ mol^{-1},

k is the Boltzman's constant,

T is the temperature in absolute units.

Thus, $\log V_G = -E_a / 2.303\ kT + \log A$ ------(2.5)

If m is the numerical value of the slope of the plot of log V_G versus reciprocal of etching temperature then E_a can be given as (Saxena and Dwivedi, 1986):

$E_a = 19.165\ m$ ------(2.6)

The track diameters were measured to an accuracy of ± 1.12 μm leading to an error of ± 0.4 μm/h in bulk etch rate determination.

i) ***Conductivity Measurement***

A. C. Conductivity measurement of electron irradiated PP along with the pristine PP were done by a Low Frequency (L. F.) Impedance analyser at Inter University Consortium, Indore, India.

Sample preparation:

A 2 MeV electron irradiated PP sample was cut to a size of (1 x 1) cm^2 and cleaned. Silver paste was applied as a coating on the polymer and it was allowed to dry.

A. C. Conductivity Set-up:

The A. C. Conductivity set-up comprised of a stainless steel chamber, Hewlett Packard L. F. Impedance analyser and a Lake Shore 340 Temperature controller. The steel chamber consisted of a sample holder, heater coil and two platinum resistance thermometers. The sample holder was connected to the heater coil. Two platinum resistance thermometers were connected, one near the heater coil and the other near the sample to see the temperature difference. The L. F. Impedance analyser had a frequency range of 5 Hz to 13 MHz with an accuracy of about ± 50 ppm at room temperature. Its operating temperature was between 0°C to 55°C and relative humidity was less than or equal to 95% at 40°C. The Lake Shore 340 temperature controller controls the heat supplied to the heater and maintained the same temperature both near the heater and the sample. Both the Impedance analyser and the temperature controller are connected to the stainless steel chamber.

Measurement of A. C. Conductivity:

After the silver paste dried completely, the sample was mounted on the sample holder. The frequency was varied from 50 kHz to 5 MHz and the corresponding conductance was measured in micro-Siemen

(μS). All these measurements were done at room temperature.

The same procedure was repeated for measuring A. C. Conductivity of the pristine PP.

2.4. RESULTS AND DISCUSSION

All the four irradiated polymers (PET, PP, PTFE and PI) along with their pristine were characterised by the above mentioned techniques. The results obtained are compiled polymer-wise and analysed as mentioned below.

2.4.1. Polyethylene terepthalate (PET)

a) Spectroscopic analysis

Spectral analysis of the pristine and the irradiated PET samples were done using FT-IR, UV-Vis and ESR techniques.

FT-IR spectral analysis

The vibration mode of the chemical bonds in the polymer are characterised by the absorption bands in the FT-IR spectra. The spectra obtained by the spectrophotometer for the irradiated as well as the pristine are shown in Fig. 2.1 ((a) wave number regions from 4000 cm^{-1} to 1800 cm^{-1} and (b) wave number regions from 1800 cm^{-1} to 700

cm^{-1}). The variation in intensity of the absorbance bands after irradiation was analysed and the individual peak studies were done. The absorbance corresponding to certain wave numbers for both pristine and the irradiated PET and interpretation of the absorbance peaks are shown in Table 2.1. PET is a condensed polymer of terephthalic acid and ethylene glycol. The IR peaks belong to C=C double bonds of Phenyl ring, C–H bonding of Phenyl ring and CH_2 group. Irradiation induced stretching of all functional units of the polymer and a deformation of phenyl ring as a whole. The fact that the position of all IR lines changed slightly without any emergence of new peaks, indicates that the irradiation affected regions are distributed randomly all over the polymer molecules and that there do not exist especially radiation sensitive functional groups in the polymer. The following inferences are derived from the spectral analysis:

a) Amorphisation of PET under electron irradiation was monitored by specific bands of trans configuration of the ethylene glycol residue at 1471 cm^{-1} due to CH_2 bending, at 850 cm^{-1} due to CH_2 rocking and at 972 cm^{-1} due to the C–O stretching vibration of the trans configuration of the ethylene glycol residue (Steckenreiter et al., 1997). Amorphisation of the crystalline fraction of the polymer is

evident from the band at 1471 cm^{-1}. Increase in absorbance of this band indicates a dramatic loss of crystallinity of the polymer. Increase in absorbance of the band at 873 cm^{-1} implies amorphisation of the polymer due to irradiation.

b) The increase in absorbance lines characteristic for vibration bands of para-substituted benzene rings illustrates the stability of the benzene ring. So, even under electron irradiation the aromatic systems are stable owing to delocalisation of excitation energy (Chapiro, 1988). Earlier it has also been found that bond breaking at the aliphatic parts of the main chain occurs more likely than the destruction of the benzene ring (Steckenreiter et al., 1997).

c) Nothing has been found at 3294 cm^{-1}, which is usually assigned to the characteristic C–H stretching mode of alkyne end group (Steckenreiter et al., 1997).

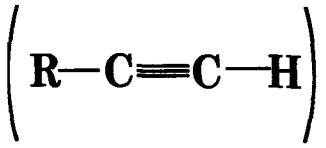

An overall degradation by oxidation processes is evidenced by an increase of the entire wavelength area. Increase in absorbance due to electron irradiation is ascribed to oxidative degradation of the entire polymer, in particular to the formation of alcohols and

carboxylic acids. Polymer degradation is more pronounced because of its irradiation in oxygen atmosphere. Amorphisation of the polymer indicates that PET has undergone some chain-scission by electron bombardment.

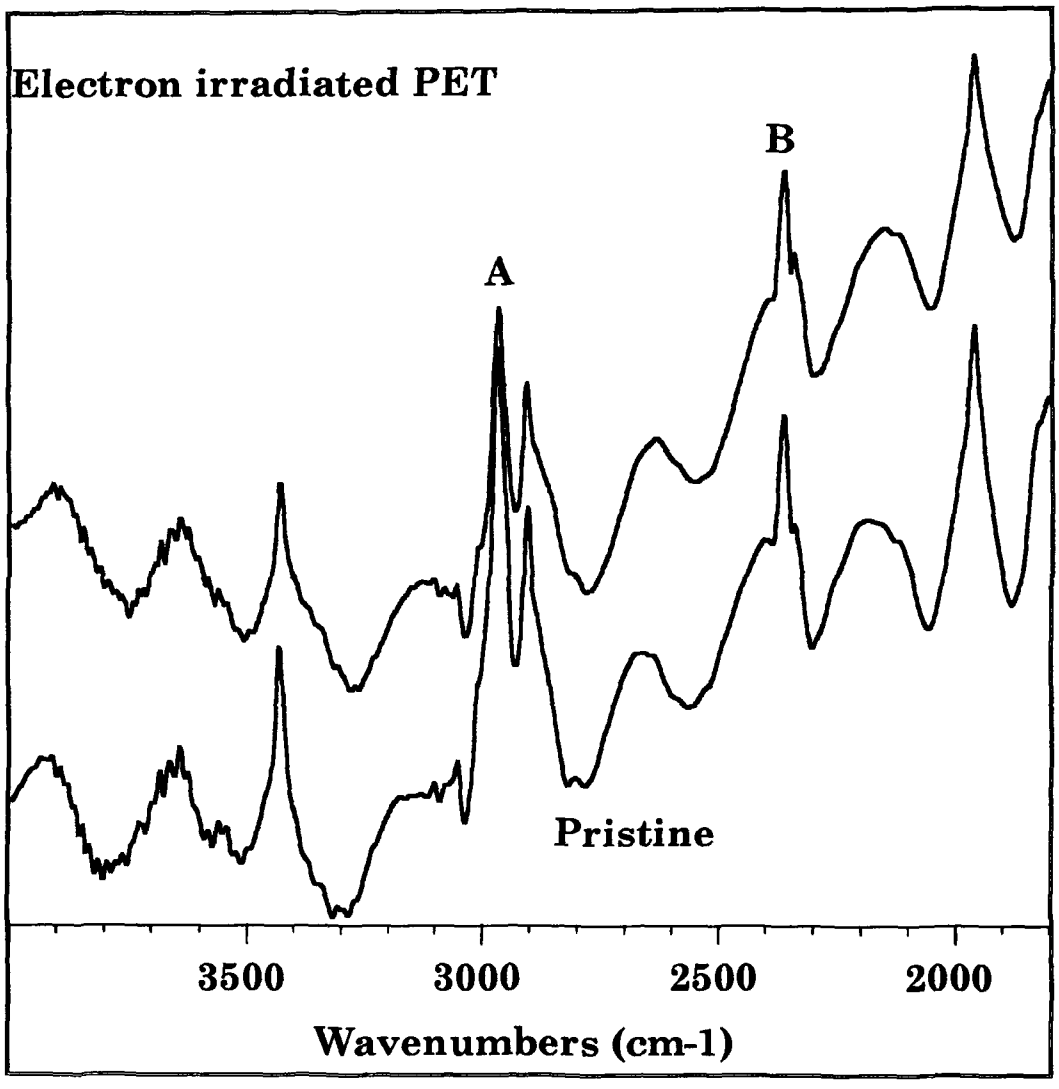

Fig. 2.1(a). FT-IR spectra of pristine and electron irradiated PET (23 kGy) in the wave number region 4000 cm^{-1} to 1800 cm^{-1}.

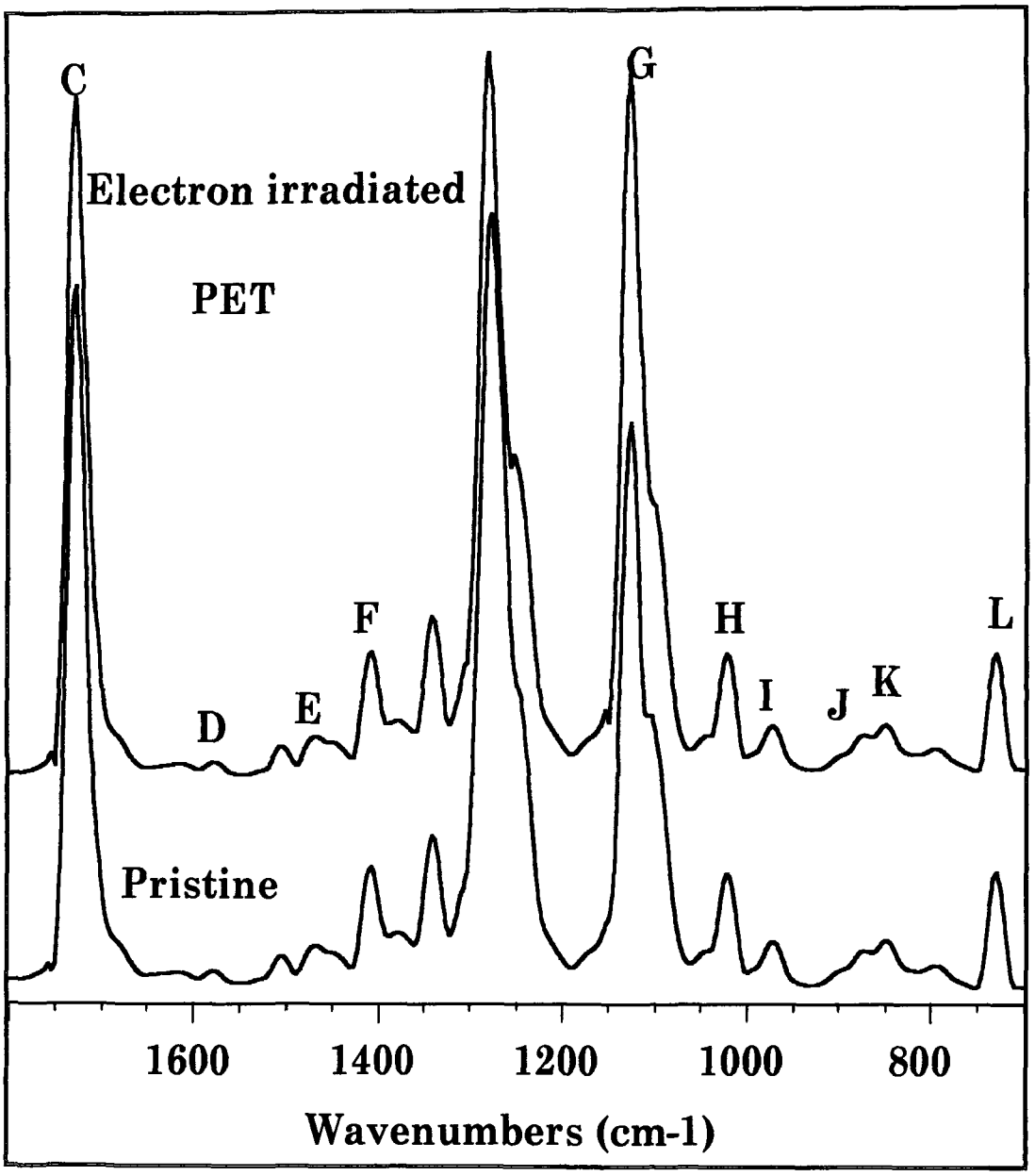

Fig. 2.1 (b). FT-IR spectra of pristine and electron irradiated PET (23 kGy) in the wave number region 1800 cm^{-1} to 700 cm^{-1}.

Table 2.1. Interpretation of IR absorption peaks for pristine and electron irradiated PET (23 kGy) along with their absorbances (Abs) at their corresponding wave numbers (1/λ).

Pristine		Irradiated		Interpretation
1/λ (cm^{-1})	Abs	1/λ (cm^{-1})	Abs	
A. 2970	0.2	2969	0.2	CH stretching of CH_2 groups.*
B. 2363	0.2	2362	0.3	CO_2 from air.*
C. 1729	2.3	1726	6.0	C=O stretching vibration.
D. 1615	0.4	1615	0.4	C-C stretching of phenyl ring.** Vibration band of para-sustituted benzene rings.**
E. 1466	0.6	1471	0.8	CH_2 bending.**
F. 1409	1.0	1410	1.7	Vibration band of para-sustituted benzene rings.**
G. 1133	5.7	1124	6.0	Vibration band of para-sustituted benzene rings.**
H. 1021	0.6	1021	1.8	C-O-C stretching of ester.**
I. 972	0.7	972	0.9	C-O stretching vibration of trans configuration of ethylene glycol residue.**
J. 871	0.6	874	0.8	Vibration band of para-sustituted benzene rings.**
K. 850	0.7	849	0.9	CH_2 rocking.** CH deformation of phenyl ring.*
L. 731	1.0	729	1.8	Ring deformation of phenyl ring.* Bending vibration of CH_2 group of crystal phase.**

* (Fink et al., 1994)

**(Steckenreiter et al., 1997)

ESR spectral analysis

ESR spectral analysis did not show the presence of any free radical in the irradiated PET. The irradiated samples were kept at room temperature for a few months which indicates that the free radicals formed have been annihilated during that time.

UV-Vis Spectral studies

The UV-Vis spectra of the irradiated along with the pristine PET showed no significant changes in the absorbance of the irradiated polymer. Correlating the absorption edge to the optical band-gap by Tauc's expression, the band gap was calculated to be 3.9 eV in case of both the pristine and the irradiated PET. This stability can be attributed to the presence of aromatic groups in the repeating units of the polymer, which helps in delocalisation of excitation energy.

b) Thermal analysis

Thermal analysis of the pristine and the irradiated PET were done by Thermogravimetric analysis and Differential Scanning Calorimetry.

Thermogravimetric Analysis

The TGA thermograms of irradiated and the pristine PET are shown in Fig. 2.2.

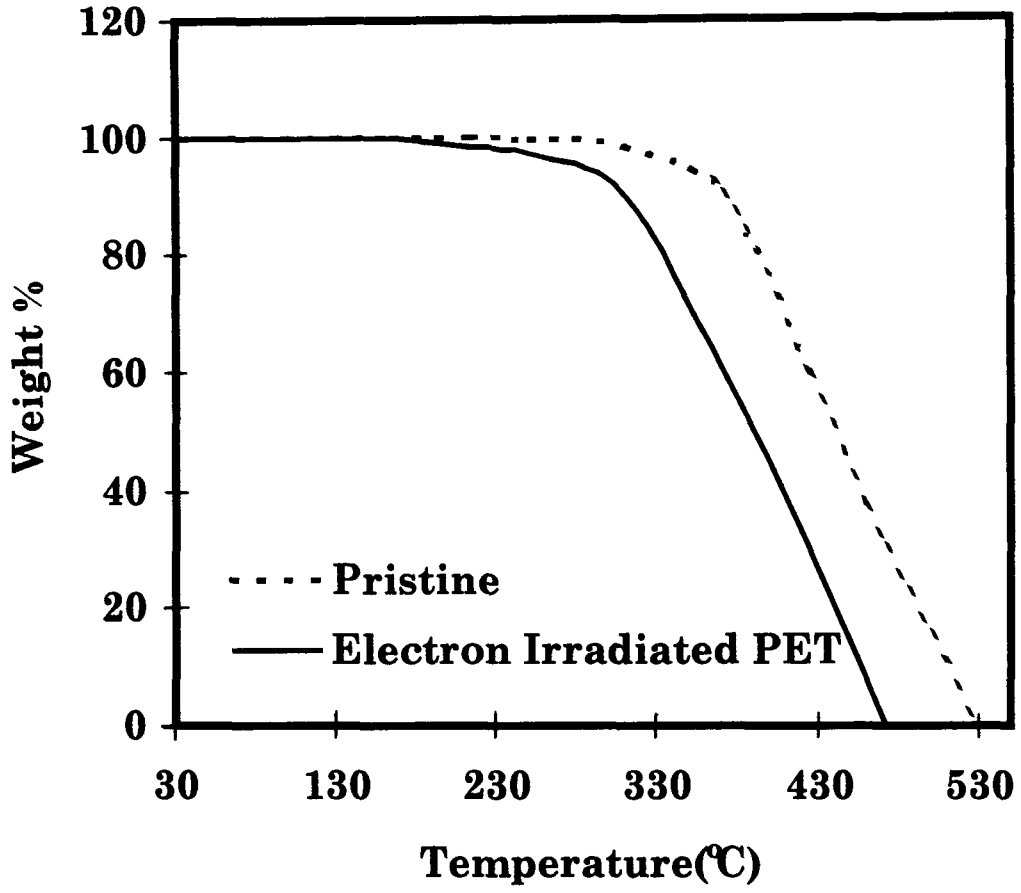

Fig. 2.2. TGA thermograms of the pristine and the electron irradiated PET (23 kGy).

The analysis of the thermograms indicates that the polymer remains stable up to certain temperature and then undergoes a 2-step decomposition, first at a slow rate and then at a very fast rate till complete decomposition. This weight-loss of the sample results from chemical reactions, decomposition, solvent and water evolution,

oxidation, etc. The results are compiled in Table 2.2. The pristine sample remains completely stable from 30°C to 165°C, with no weight loss at all. This stable zone is followed by a very slow rate of decomposition from 165°C to 371°C, with about 10% weight loss, after which the fast rate of sample decomposition occurs till 530°C, where the pristine PET is completely decomposed.

Table 2.2. Thermal analysis data derived from the TGA thermograms for pristine and electron irradiated PET (23 kGy).

Weight (mg)	Temperature range (°C)	Total weight loss %	Interpretation
Pristine PET			
0.8	30 – 165	0	Stable
	165 – 371	10	Slow decomposition
	371 – 530	100	Fast decomposition
Electron Irradiated PET (23 kGy)			
0.4	30 – 97	0.0	Stable
	97 – 359	12.0	Slow decomposition
	359 – 472	100.0	Fast decomposition

The irradiated sample remains stable up to a relatively lower temperature (about 97°C), after which slow decomposition starts and continues up to 359°C, with 12% weight loss. There is a subsequent fast rate of decomposition up to a 100% weight loss of the sample when the sample is further heated above 359°C. The sample is completely decomposed at 472°C. Hence, the TGA thermograms show a decrease in thermal stability of the irradiated polymer.

Differential Scanning Calorimetry

At the scanning rate of 20°C/min, the pristine sample was scanned at a temperature range of 60°C to 510°C. The thermogram shown in Fig. 2.3 indicates an exothermal peak of crystallisation at 208°C involving heat of 3083 J/g, as recorded from the instrument. DSC curves of the pristine shows melting endotherm at 229°C.

The irradiated sample was also scanned in the same temperature range at the same rate and the thermogram is shown in Fig. 2.3. The sample shows an exothermic peak of crystallisation at 208°C involving 575 J/gram of heat. The irradiated PET shows melting transformation at 222°C.

The data derived from the thermograms of the pristine and the

irradiated PET are compiled in Table 2.3.

Table 2.3. Thermal analysis data derived from the DSC thermograms for pristine and electron irradiated PET (23 kGy).

Peak	Temperature(°C)	Specification	Explanation
Pristine PET			
A	208	Exothermal	Crystallisation
B	229	Endothermal	Melting
Irradiated PET (23 kGy)			
A	208	Exothermal	Crystallisation
B	222	Endothermal	Melting

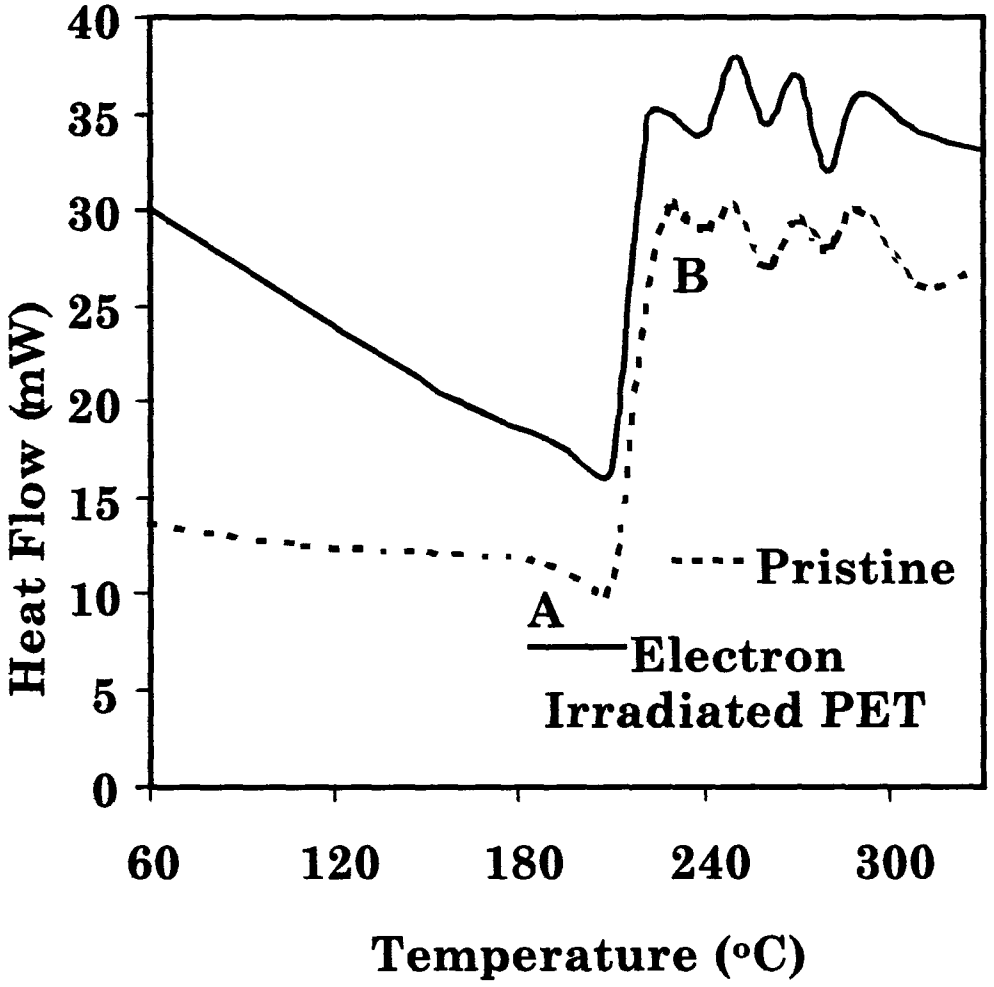

Fig. 2.3. DSC thermograms of the pristine and the electron irradiated PET (23 kGy).

c) Structural Analysis

Structural analysis of the pristine and irradiated PET was done by X-ray diffraction technique.

X-ray diffraction analysis

The XRD spectra for the pristine and irradiated PET are shown in Fig. 2.4. The spectra show the main sharp peak of pristine sample at 2θ of 26.26°. The sharp peak indicates the crystalline nature of the polymer. The main peak of the irradiated sample is slightly shifted to 2θ = 26.38°. Moreover, a slight decrease in intensity of the main peak is also observed from the spectra. The shifting of the main peak and the decrease in peak intensity indicate the destruction of the crystal structure, which might be due to chain-scissioning after electron irradiation. The values of intensity of the main peak are tabulated in the Table 2.4.

Table 2.4. Position (2θ), Intensity (I) and full width half maximum (FWHM) of the main peak in the pristine and electron irradiated PET (23 kGy) obtained from XRD spectra.

Sample	2θ (degrees)	I(Rel)	I(CPS)	FWHM
Pristine	26.26	100.0	7825.0	0.7
Irradiated	26.38	100.0	7204.0	0.9

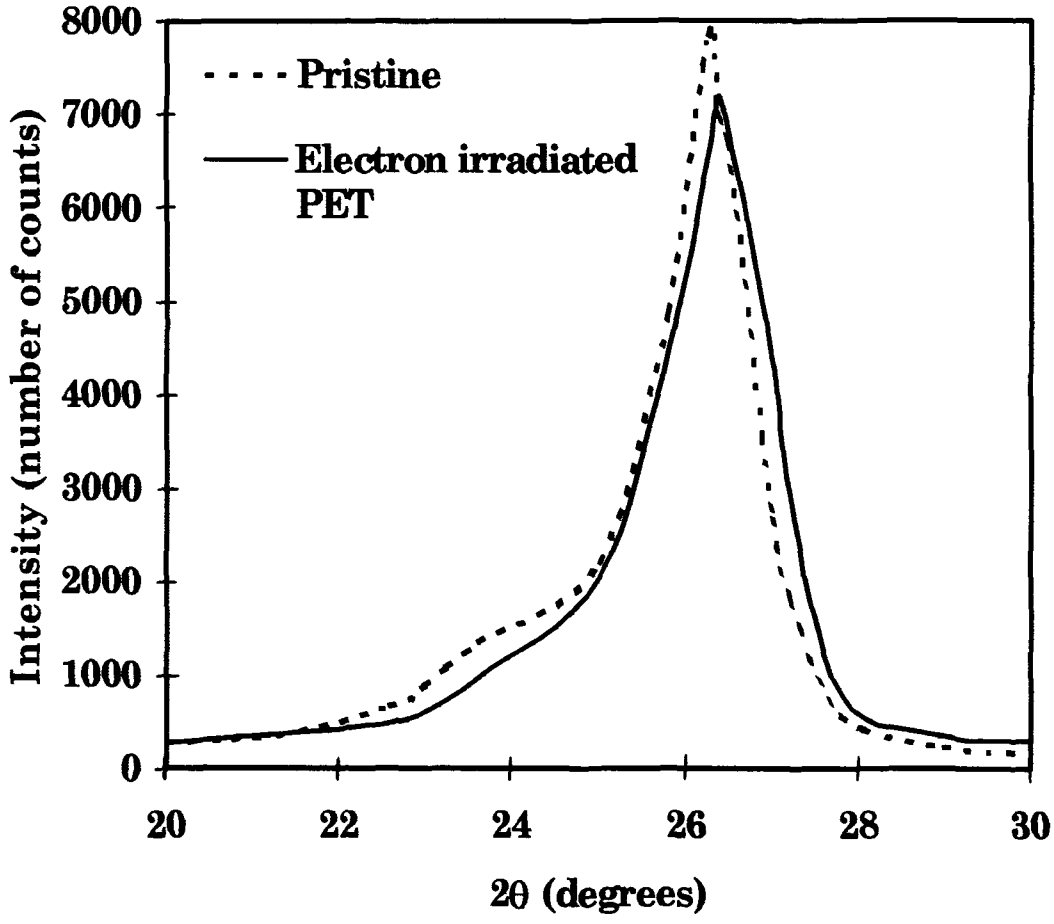

Fig. 2.4. X-ray diffraction spectra of the pristine and the electron irradiated (23 kGy) PET.

d) Track Studies

The bulk etch-rate for PET was calculated from the slope of the plot of fission track diameters versus etching time and it was found to increase after electron irradiation as shown in Table 2.5. The electron irradiation converted the polymer into easily etchable material. It was

also observed that the irradiated sample, after etching became somewhat opaque or in other words its opacity increased.

The activation energy was calculated from the slope of the plot of inverse of etching temperature in absolute units and log of bulk etch-rate as shown in Fig. 2.5. The activation energy was found to decrease after irradiation as shown in Table 2.5, implying that a comparatively less energy is needed to activate the molecules after irradiation.

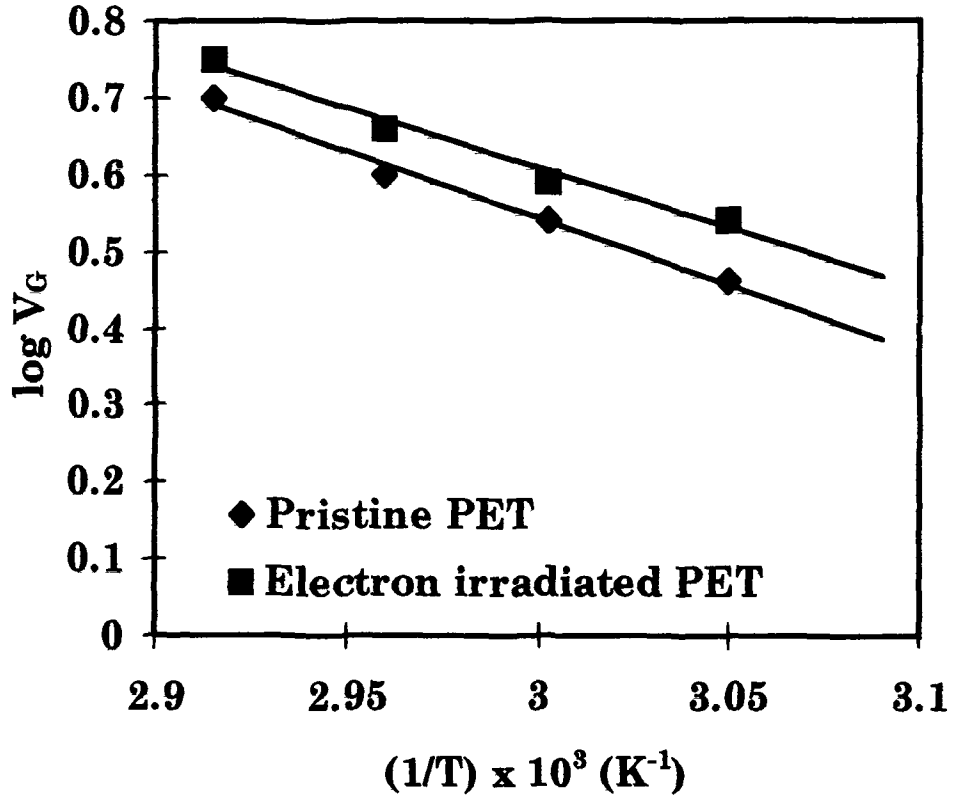

Fig. 2.5. The plot of log V_G versus inverse of etching temperature for the pristine and the electron irradiated PET (23 kGy).

Table 2.5. Bulk etch-rate of pristine and electron irradiated PET (23 kGy) at different etching temperatures and the corresponding activation energies of etching.

Temperature of etching (°C)	Bulk etch rate (μm/h)		Activation energy of etching (kJ.mole^{-1})	
	Pristine	Irradiated	Pristine	Irradiated
55	2.9 ± 0.4	3.5 ± 0.4		
60	3.5 ± 0.4	3.9 ± 0.4	33.0 ± 0.4	30.0 ± 0.4
65	4.0 ± 0.4	4.6 ± 0.4		
70	5.0 ± 0.4	5.6 ± 0.4		

e) Atomic Force Microscopy

The 3-dimensional images of the surface topography have been obtained from AFM for both pristine and irradiated samples in nanoscopic level and are shown in Fig. 2.6 (a) and (b) respectively. The surface roughness of the pristine and the electron irradiated PET has been measured at about 20 different fields on the polymer surface at random. The mean surface roughness was calculated to be 5.7 ± 0.4 nm for the pristine PET and 3.7 ± 0.5 nm for the electron irradiated PET. Thus, the electron irradiation made the polymer surface more smooth.

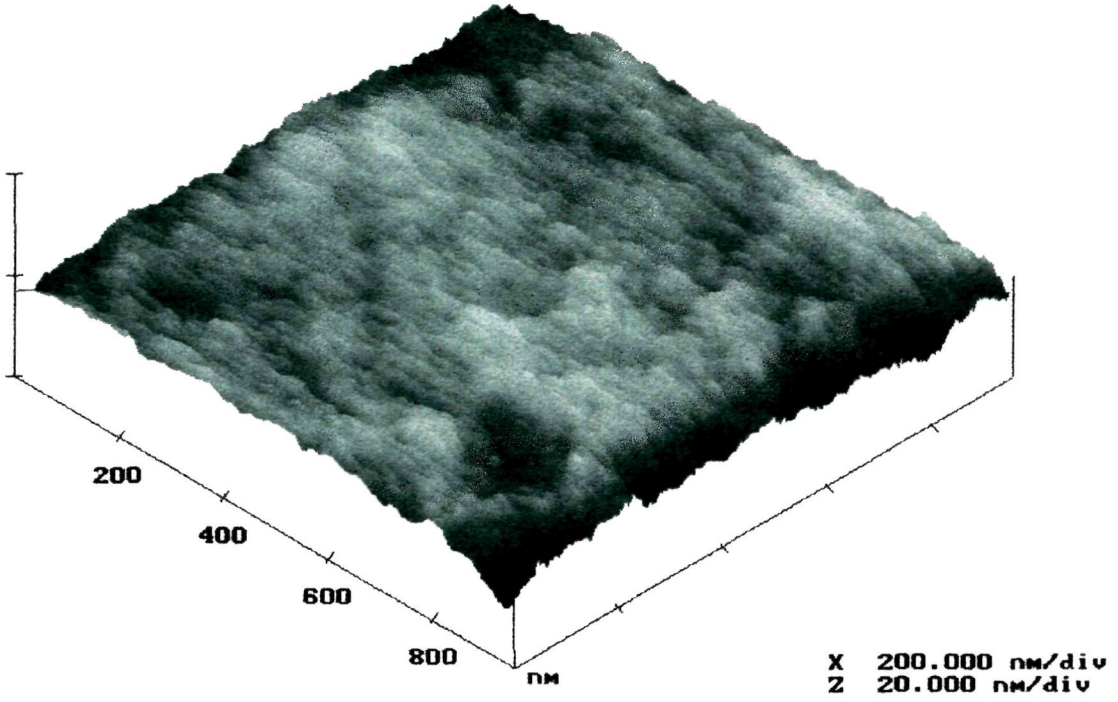

Fig. 2.6.(a) The AFM image of the pristine PET.

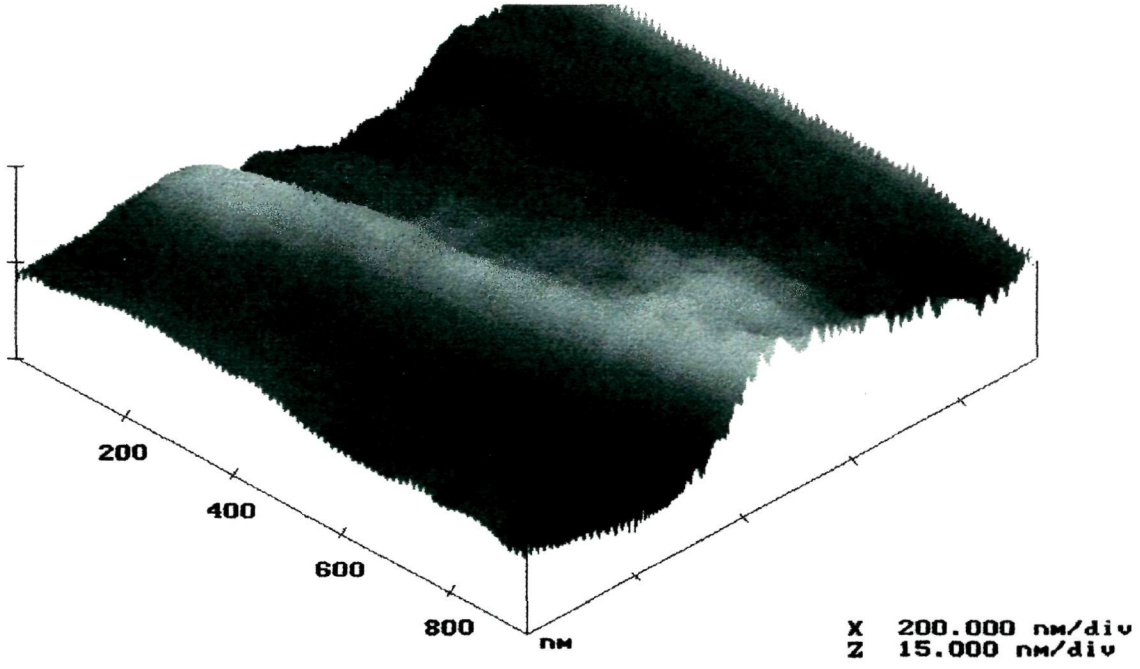

Fig. 2.6.(b) The AFM image of the electron irradiated PET (23 kGy).

2.4.2. Polypropylene

a) Spectroscopic analysis

Spectral analysis of the pristine and the irradiated PP samples were done using FT-IR, UV-Vis and ESR techniques.

FT-IR spectral analysis

The FT-IR spectra of the pristine and the irradiated PP are shown in Fig. 2.7. All the bands studied from the spectra were the characteristic bands of the pristine PP indicating the isotactic nature of the polymer. The presence of the same bands in the irradiated PP indicates that the isotactic nature of PP was not destroyed due to electron irradiation. The symmetric and assymetric stretching, scissors or bending and wagging of CH_3 and CH_2 group frequencies were observed both in the pristine as well as in the irradiated PP. The assymetric stretching vibration of CH_3 and CH_2 groups were observed at 2957 cm^{-1} and 2920 cm^{-1} respectively. CH_2 wagging vibration observed at 1303 cm^{-1} was of low intensity. Due to irradiation, the chain length of hydrocarbon increases thus introducing more CH_2 groups, there by increasing the absorbance of CH_2 wagging vibrations from 0.1 in the pristine to 0.4 in the irradiated PP.

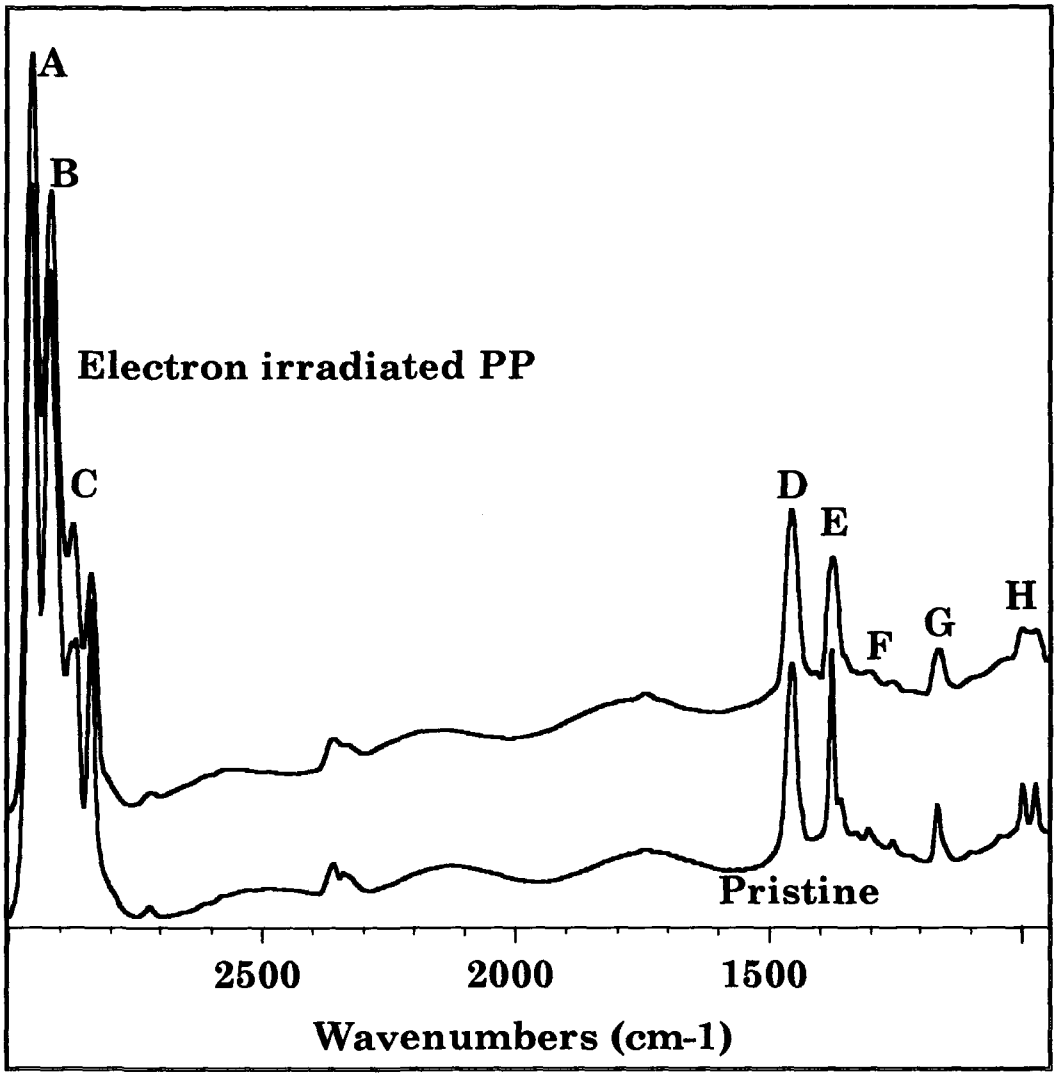

Fig. 2.7. The FT-IR spectra of the pristine and the electron irradiated PP (23 kGy).

This implies that the chain length of the hydrocarbon increased owing to cross-linking induced by electron irradiation in the polymer. The CH_3 symmetric stretching was observed at 2870 cm^{-1}, in both the

pristine and the irradiated sample. The symmetric and asymmetric scissoring vibration of the methyl group was observed at 1376 cm^{-1} and 1455 cm^{-1} respectively. The absorbance bands representing the 3/1 helix structure of PP were found in the pristine as well as in the irradiated PP at 1166 cm^{-1} and 974 cm^{-1}, showing that the helix structure was not affected by electron irradiation.

Table 2.6. Interpretation of IR absorption peaks for pristine and electron irradiated PP (23 kGy) along with their absorbances.

Wave no. (cm^{-1})	Absorbance		Interpretation
	Pristine	Irradiated	
2957 (A)	1.6	2.0	CH_3 assymetric stretch.*
2920 (B)	1.3	1.5	CH_2 assymetric stretch.*
2870 (C)	0.6	0.7	CH_3 symmetric stretch.*
1455 (D)	0.5	0.7	CH_3 assymetric scissors.*
1376 (E)	0.4	0.8	CH_3 symmetric scissors.*
1303 (F)	0.1	0.4	CH_2 wag.*
1166 (G)	1.3	1.4	3/1 helix structure.*
974 (H)	0.3	0.3	3/1 helix structure.*

*(Alpert et al., 1970)

UV-Vis Spectroscopic Studies

The UV-Vis spectra for irradiated and the pristine Polypropylene is shown in Fig. 2.8. The variation in absorbance due to electron irradiation are given at some selected wavelengths in Table 2.7.

Table 2.7. Variation of absorbance due to electron irradiation (23 kGy) in PP at some selected wavelengths in the UV-visible range.

Wavelength (nm)	Absorbance	
	Pristine	Irradiated
200.0	0.54	0.55
205.0	0.39	0.39
210.0	0.27	0.29
215.0	0.20	0.25
220.0	0.17	0.22
225.0	0.16	0.21
230.0	0.15	0.20
235.0	0.14	0.18
240.0	0.12	0.16
245.0	0.11	0.15
250.0	0.10	0.14
255.0	0.10	0.13

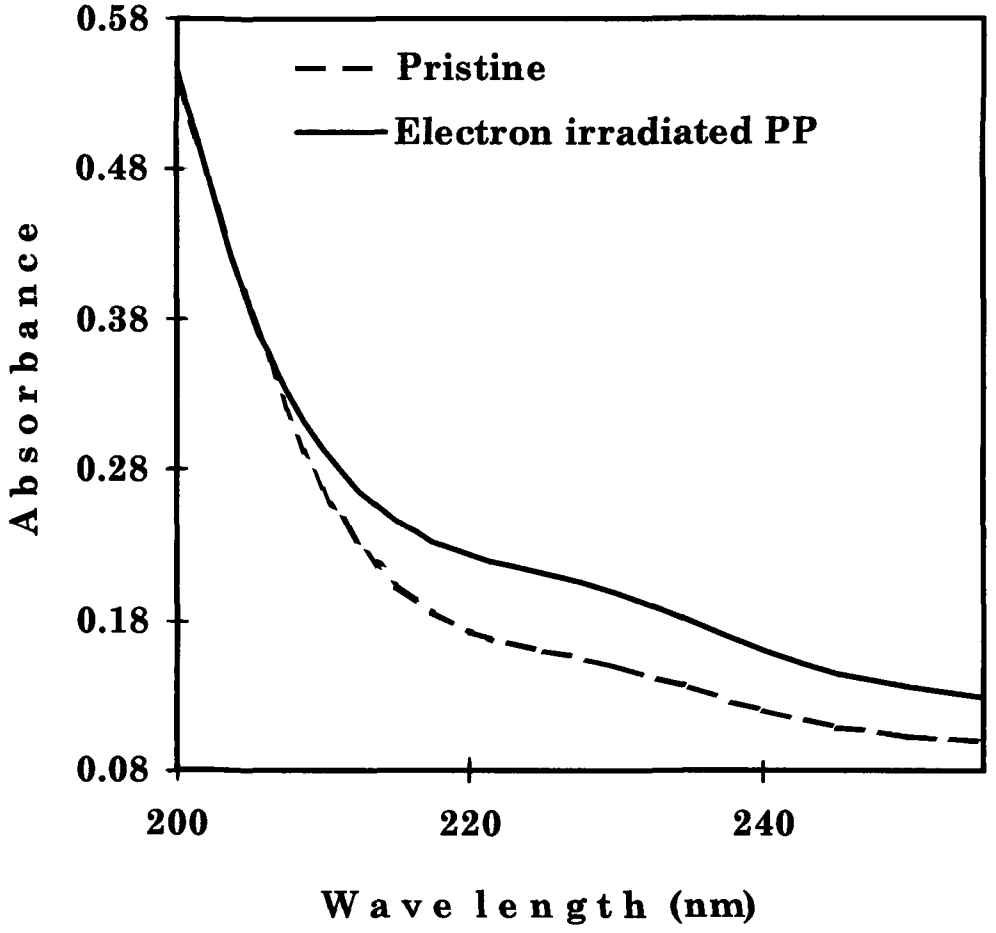

Fig. 2.8. The UV-Vis spectra of the pristine and the electron irradiated PP (23 kGy).

It is evident from the spectra that, the absorbance edge shifted from UV to visible region due to electron irradiation. The shift in

absorbance edge from UV to visible region was correlated to energy band-gap by Tauc's expression. The energy band-gap was calculated to be 5.2 eV in the pristine PP, which was found to be reduced to 4.9 eV after irradiation. This decrease in energy band-gap can be correlated to an increase in conductivity of the polymer due to electron irradiation.

ESR spectral analysis

ESR spectral analysis shows the absence of any free radical in the irradiated PP. The irradiated samples were kept at room temperature for a few months which indicates that the free radicals formed might have been annihilated in the due course of time.

b) A. C. Conductance Measurement

The increase in conductivity as revealed from UV-Vis spectral analysis was further cross-checked by A. C. Conductance measurement of the pristine as well as the irradiated PP. The conductance of the pristine and the irradiated samples as a function of frequency are shown in Table 2.8. The A. C. Conductance of the irradiated PP and the pristine was found to increase with increase in frequency, as shown in Fig. 2.9 and the conductance of the irradiated

sample was found to be more than that of pristine. This data is in agreement with the results obtained from UV-Vis spectral analysis.

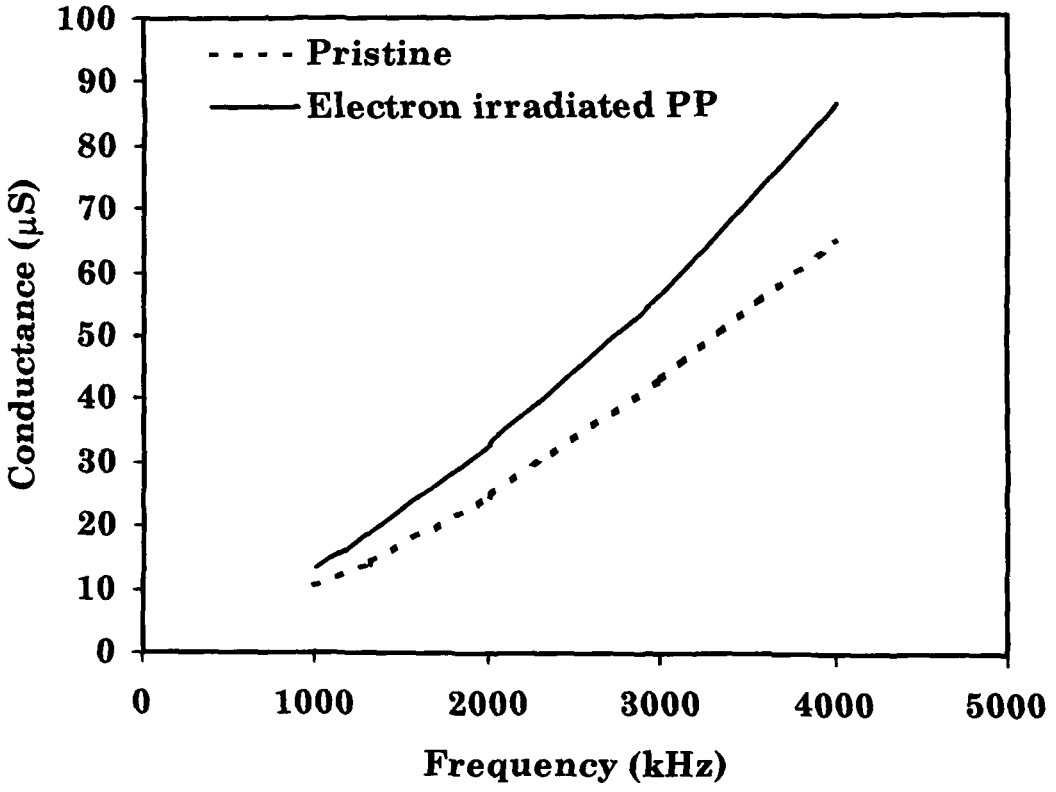

Fig. 2.9. The plot showing the increase in conductance (micro-Siemen) with frequency of the pristine and the electron irradiated PP (23 kGy).

Table 2.8. A. C. Conductance of the pristine and the electron irradiated PP (23 kGy) as a function of applied frequency.

Frequency (kHz)	Conductance (μS)	
	Pristine	Irradiated
510	4.9	6.1
1000	10.5	13.5
1300	-	18.9
1310	14.4	-
2000	-	32.9
2010	25.2	-
3000	43.3	56.8
4000	65.1	86.3

c) Thermal Analysis

Thermal analysis of the pristine and the electron irradiated PP samples were done by TGA and DSC techniques.

Thermogravimetric Analysis

The TGA thermograms of the irradiated PP along with the pristine are shown in Fig. 2.10, which shows an increase in thermal stability due to electron irradiation. TGA revealed a double step decomposition pattern of the polymer in both the pristine as well as the irradiated polymer, as shown in Table 2.9.

The pristine sample remained stable from 30°C to 102°C without undergoing any weight loss. This stable zone was followed by a slow rate of decomposition from 102°C to 266°C. In this slow decomposition zone, there was a weight loss of only about 6%. A faster rate of decomposition continued after that till the sample was completely decomposed at 374°C. A weight loss of about 94% was recorded in this fast decomposition zone.

Table 2.9. Data derived from TGA thermogram of irradiated (23 kGy dose of electron) and pristine PP indicating their thermal decomposition behaviour.

Weight (mg)	Temperature range (°C)	Total weight loss %	Interpretation
		Pristine PP	
0.4	30 – 102	0	Stable zone
	102 – 266	6	Slow decomposition
	266 – 374	100	Fast decomposition
		Irradiated PP	
0.4	30 – 138	0.0	Stable zone
	138 – 335	10.0	Slow decomposition
	335 – 440	100.0	Fast decomposition

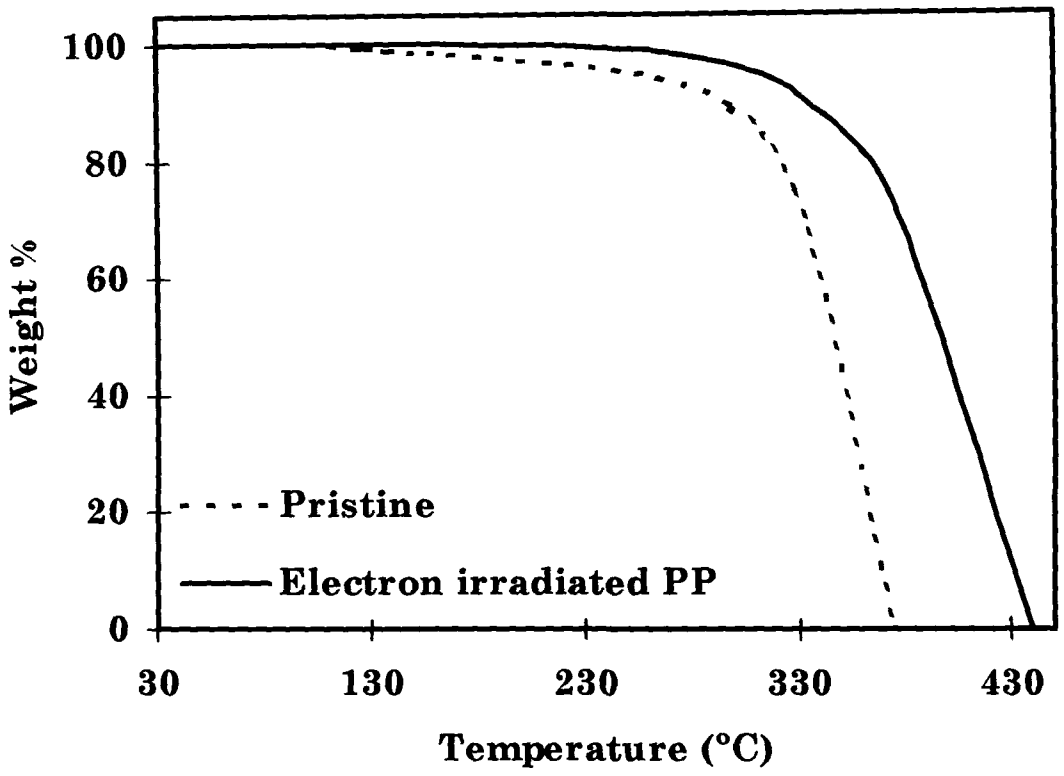

Fig. 2.10. The TGA thermogram of the pristine and the electron irradiated PP (23 kGy).

Similarly, the irradiated polymer remained stable up to a comparatively higher temperature, i.e., up to 138°C. It also followed the same trend of a double step decomposition as that of the pristine. A slower rate of decomposition took place from 138°C to 335°C where the sample lost about 10% of its initial weight. This was followed by a fast decomposition mechanism from 335°C to 440°C, with a weight loss

of 90%. The irradiated sample was completely decomposed at 440°C. It was thus observed that the thermal stability of PP increased due to electron irradiation.

Differential Scanning Calorimetry

The DSC thermograms of the pristine and the irradiated PP are shown in Fig. 2.11. The analysis of the thermogram is given in Table 2.10. In the pristine sample, a sharp exothermic peak of crystallisation was observed at 203°C (A). This sharp exothermic peak was followed by an endothermic peak of melting at 212°C (B). In the irradiated PP, continuous exotherm of crystallisation was observed from 138°C to 215°C (A). This exotherm is followed by a phase transition resulting in melting endotherm at 221°C (B).

Table 2.10. Data derived from DSC thermogram of electron irradiated (23 kGy) and pristine PP.

Peak	Temperature (°C)	Specification	Interpretation
Pristine PP			
A	203	Exothermic	Crystallisation
B	212	Endothermic	Melting
Irradiated PP			
A	138 – 215	Exothermic	Crystallisation
B	221	Endothermic	Melting

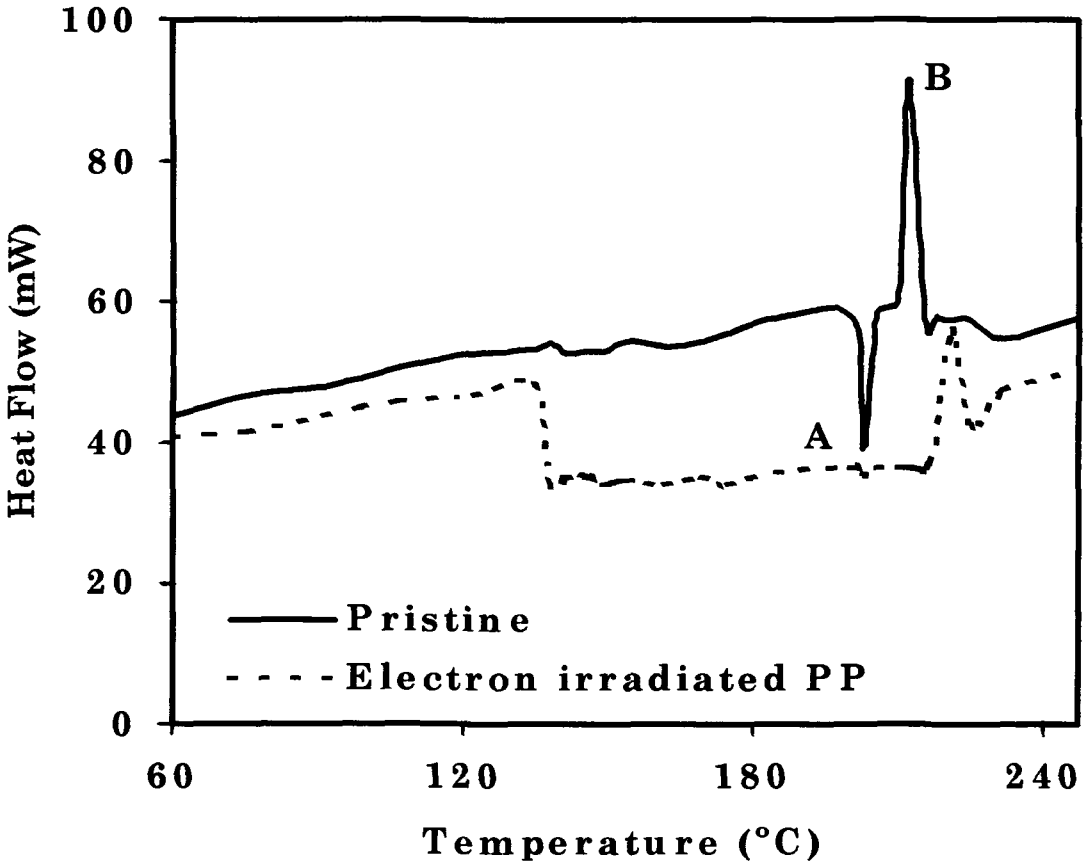

Fig. 2.11. The DSC thermograms of the pristine and the electron irradiated PP (23 kGy).

d) Structural analysis:

Structural analysis of PP samples were done by X-ray diffraction analysis.

X-ray diffraction

The X-ray diffraction spectra for the pristine and the irradiated PP are shown in Fig. 2.12. The main sharp peak in case of the pristine

sample was found at 2θ = 18.0° (C). This main peak in case of the irradiated PP shifted to 2θ = 16.9°. The sharpness of the peak indicated the crystallinity of the polymer. The intensity of this main peak increased after irradiation. An additional new peak was observed at 2θ = 9.5° (A) due to electron irradiation. This increase in the intensity of the main peak, as shown in Table 2.11, and the emergence of new peak indicated the increase in crystallinity of the polymer after electron irradiation.

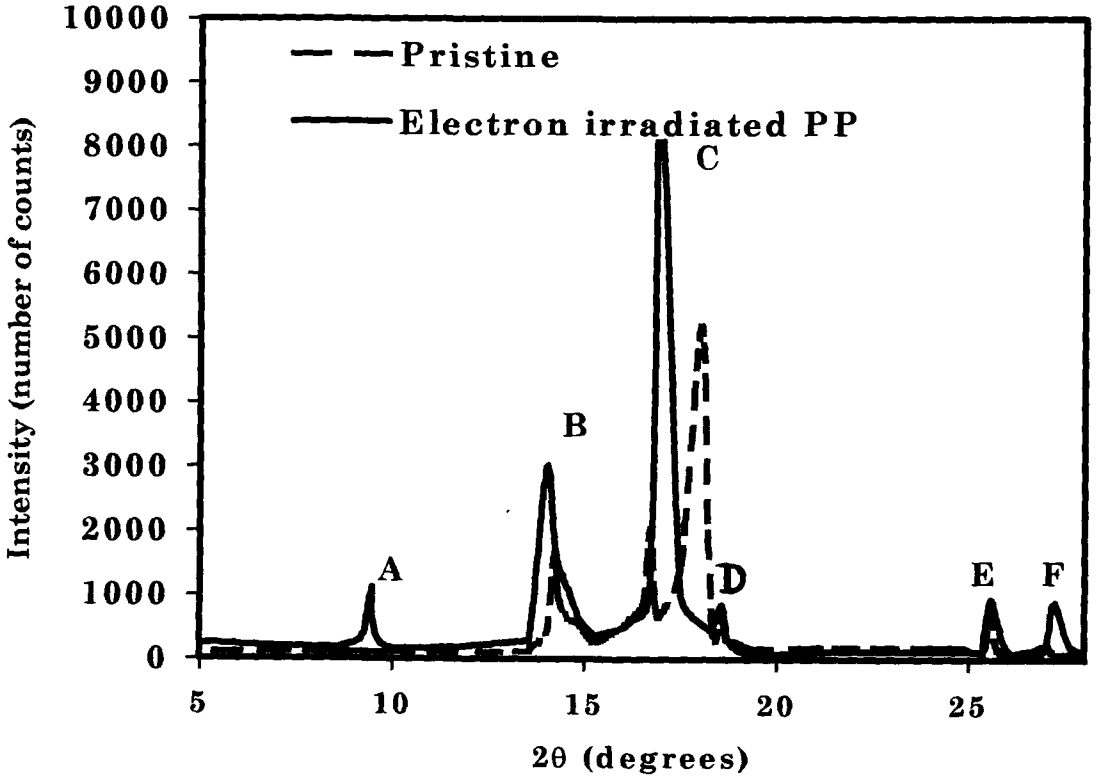

Fig. 2.12. The XRD spectra of the pristine and the electron irradiated PP (23 kGy).

Table 2.11. Position (2θ), Intensity (I) and full width half maximum (FWHM) of the XRD peaks in the pristine (P) and the electron irradiated (E) PP (23 kGy) obtained from XRD spectra.

2θ (degrees)		I(REL)		I(CPS)		FWHM	
P	E	P	E	P	E	P	E
-	9.5 (A)	-	13	-	1124	-	0.2
14.2	14.0 (B)	32	34	1658	2986	0.9	0.8
18.0	16.9 (C)	100	100	5225	8904	0.9	0.7
18.6	18.6 (D)	12	10	643	849	1.3	0.7
25.6	25.6 (E)	13	11	684	942	0.5	0.5
28.7	28.7 (F)	3	11	147	971	0.9	0.7

e) Atomic Force Microscopy

The 3-dimensional images of the surface topography were obtained from AFM for both pristine and electron irradiated (23 kGy) samples in nanoscopic level. The 3-D image of the pristine PP is shown in Fig. 2.13 (a) and that of the irradiated PP is shown in Fig. 2.13 (b). The surface roughness of the samples were measured at about 20 different fields on the polymer surface at random and were calculated to be 7.23 ± 0.4 nm for the pristine PP and 6.6 ± 0.4 nm for the irradiated one. Thus, the electron irradiation made the polymer surface more smooth.

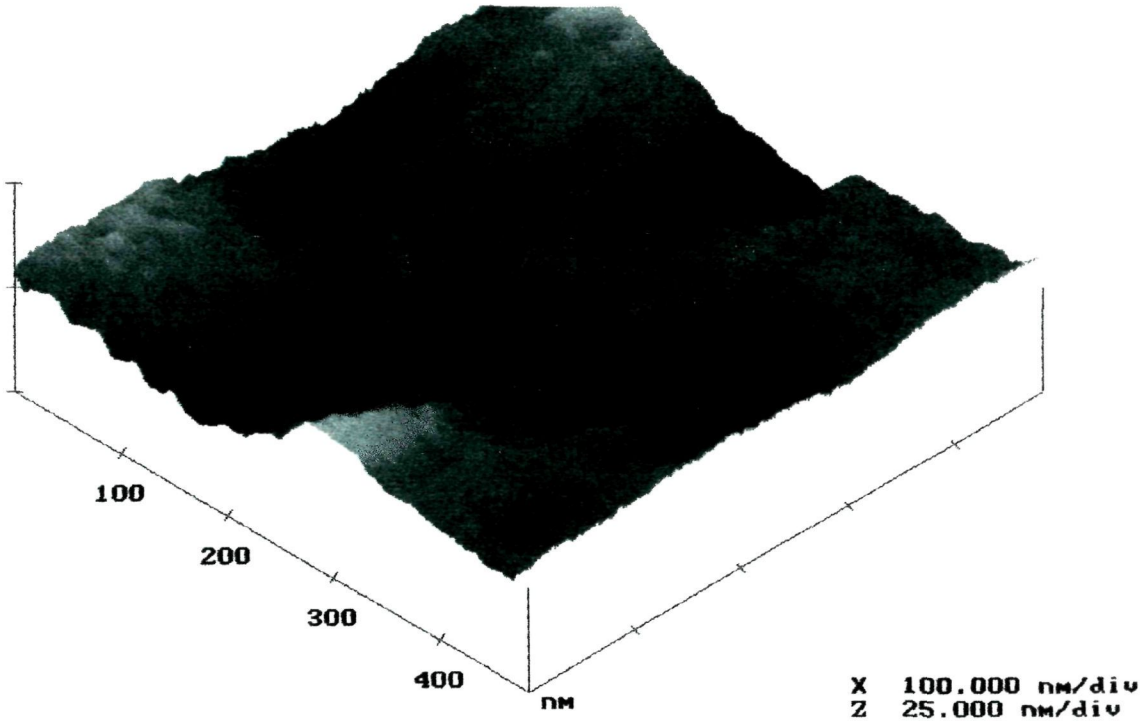

Fig. 2.13.(a) The AFM image of the pristine PP.

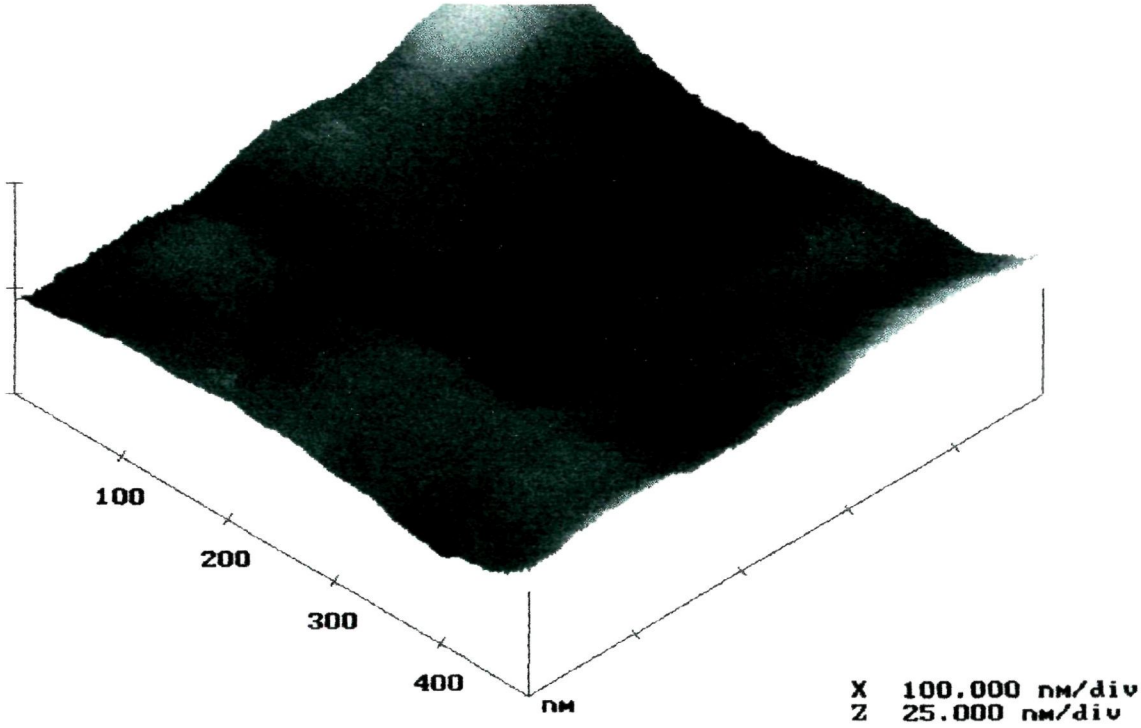

Fig. 2.13.(b) The AFM image of the electron irradiated (23 kGy) PP.

2.4.3. Polytetrafluoro ethylene (PTFE)

a) Spectroscopic analysis:

Spectral analysis of the pristine and the electron irradiated PTFE samples were done using FT-IR, UV-Vis and ESR techniques.

FT-IR spectral analysis

The FT-IR absorbance spectra for the pristine and the electron irradiated PTFE samples are shown in Fig. 2.14. The analysis of the spectra for the pristine and the electron irradiated PTFE showed the C-F stretching vibration from 1000 cm^{-1} to 1300 cm^{-1}. The shouldering effect due to increasing strain by electron irradiation on PTFE is prominent from the spectra of the irradiated PTFE in this wave number region. The C-F bond of PTFE has suffered a large amount of C-F stretching due to electron irradiation.

The electron irradiated PTFE showed an additional band assigned to carbonyl stretching vibrations (Schierholz et al., 1999). The band is located at 1882 cm^{-1} (A) and is originated from carbonyl fluoride group (-COF). The band at 1793 cm^{-1} (B) is assigned to terminal double bonds in the form of $-CF=CF_2$ in the polymer chain structure (Caro et al., 1999).

Many new peaks were found to emerge due to irradiation which

could be owing to the emission of complex molecules viz. CF_2, CF_4, C_2F_6, etc. (Calcagno et al., 1992) after irradiation.

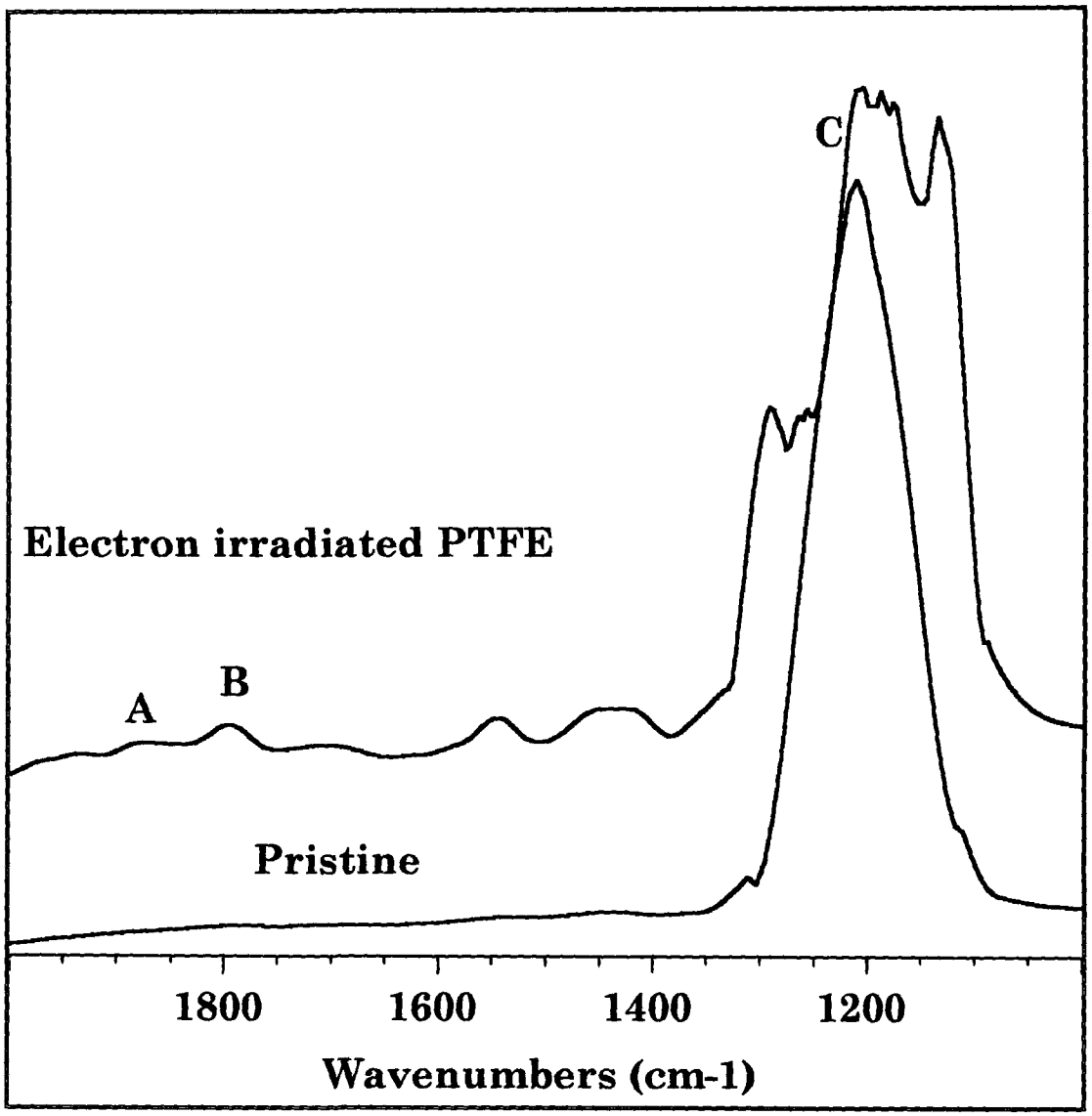

Fig. 2.14. FT-IR spectra of the pristine and the PTFE irradiated to a dose of 23 kGy of 2 MeV electron.

UV-Vis Spectral Studies

The UV-Vis spectra for electron irradiated (23 kGy) and the pristine PTFE are shown in Fig. 2.15. It is evident from the spectra that the absorbance edge shifted from UV to visible region due to electron irradiation. The variation in absorbance due to electron irradiation at some selected wavelengths are listed in Table 2.12.

Table 2.12. Variation in absorbance in the pristine and the electron irradiated PTFE (23 kGy) at some selected wavelengths (λ) as revealed from the UV-Vis spectra.

Pristine		Irradiated	
λ (nm)	Absorbance	λ (nm)	Absorbance
202.0	2.49	209.0	2.60
273.0	1.97	268.0	2.08
277.0	1.96	278.0	2.04
285.0	1.94	287.0	2.03
302.0	1.90	291.0	2.02
306.0	1.90	300.0	1.98
310.0	1.89	306.0	1.98
316.0	1.88	316.0	1.95
336.0	1.86	332.0	1.94

It is evident from the above data that, the absorbance increases after irradiation. The shift of absorption edges from lower to higher wavelength side was correlated with energy band-gap (E_g) by Tauc's expression. The energy band-gap in pristine sample was found to be 1.5 eV, which was reduced to about 50% after irradiation. The band-gap for the PTFE irradiated by 26 kGy dose of 2 MeV electron was found to be 0.7 eV.

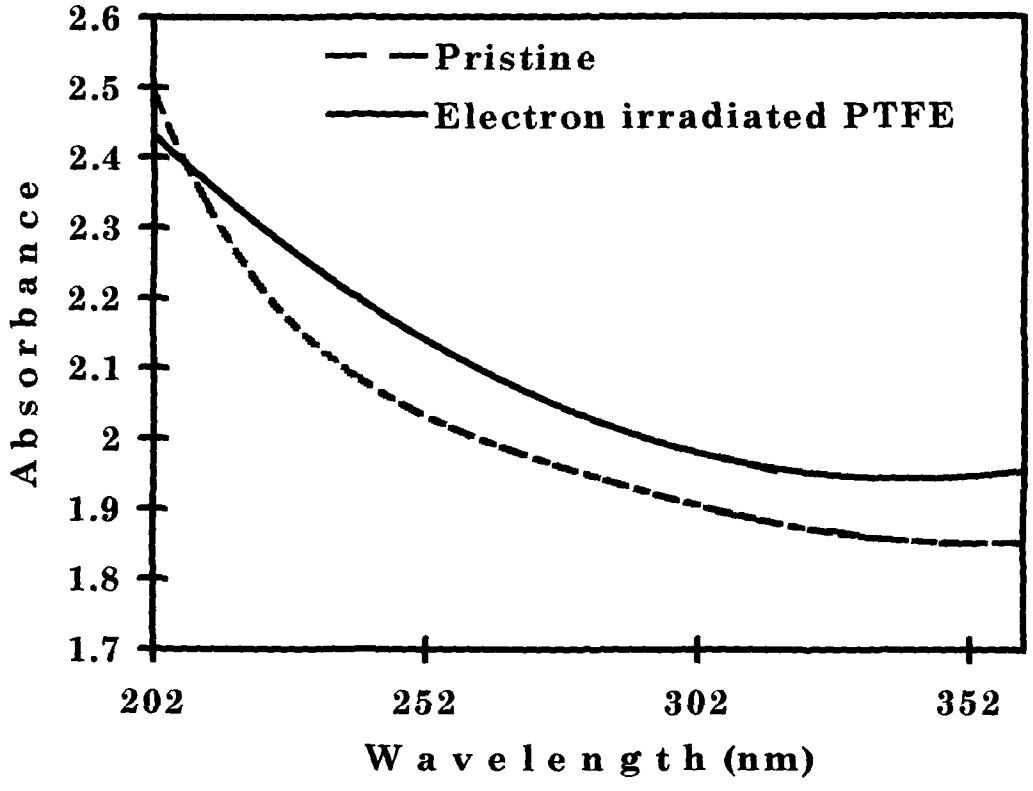

Fig. 2.15. UV-Vis spectra of the pristine and the electron irradiated PTFE (23 kGy).

PTFE is a typical example of a polymer where the only effects of irradiation are scission production and emission of large fragments produced along the particle trajectory (Calcagno et al., 1992). The cleavage of bonds and emission of free radicals decreases the energy band-gap after irradiation.

Electron Spin Resonance Spectroscopy

Fig. 2.16 represents the ESR spectra for the pristine and the electron irradiated PTFE. A signal of free radical is observed for the electron irradiated PTFE. The width of the signal formed is around 50 Gauss. The irradiation was done in the presence of oxygen. In the presence of oxygen a number of radiolysis products were formed (CF_4 and C_2F_6 in small amounts, high proportion of COF_2). These products were formed by random splitting of C-C bonds and to a small extent of C-F bonds to give radicals. Oxygen will add to organic radicals to give peroxy-radicals which can react together to form alkoxy radicals as follows:

$$-CF_2-\dot{C}F_2 + O_2 \longrightarrow -CF_2-CF_2O_2^{\bullet}$$

$$2-CF_2-CF_2O_2^{\bullet} \longrightarrow 2-CF_2CF_2\dot{O} + O_2$$

Dissociation of alkoxy radicals further produces carbonyl fluoride and a new organic radical by one $-CF_2-$ unit

$$-CF_2-CF_2O^{\bullet} \longrightarrow -CF_2^{\bullet} + COF_2$$

This free radical was detected by the ESR spectrophotometer.

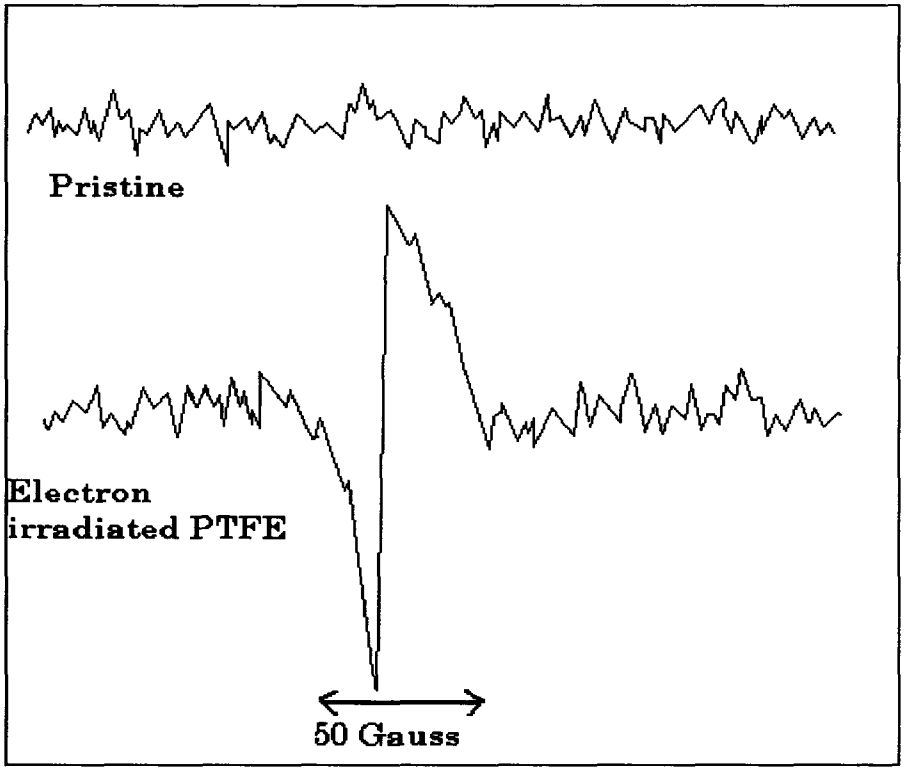

Fig. 2.16. ESR spectra of the pristine and the electron irradiated PTFE (23 kGy).

The reduction in energy band-gap (E_g) by about 50% as revealed from UV-Vis spectral analysis can be attributed to the formation of this stable free radical, which is in accordance with the conductivity theory.

c) Thermal Analysis

Thermal analysis of the samples was done by TGA and DSC techniques.

Thermogravimetric Analysis

The TGA thermograms of the electron irradiated (23 kGy) PTFE along with the pristine one are shown in Fig. 2.17. It was quite evident from the thermograms that, there was a decrease in thermal stability due to electron irradiation though PTFE is a very thermally stable polymer. The pristine polymer remained stable up to 264°C, whereas the temperature of stability in the electron irradiated PTFE was decreased to 250°C. Both the pristine and the irradiated PTFE exhibited a two step thermal decomposition behavior, as shown in Table 2.14. The pristine sample completely decomposed at 639°C, whereas the complete decomposition temperature in the irradiated PTFE decreased to 622°C. The decrease in thermal stability in PTFE

was due to chain-scissioning by electron irradiation in the polymer, which reduced the strength of the polymer.

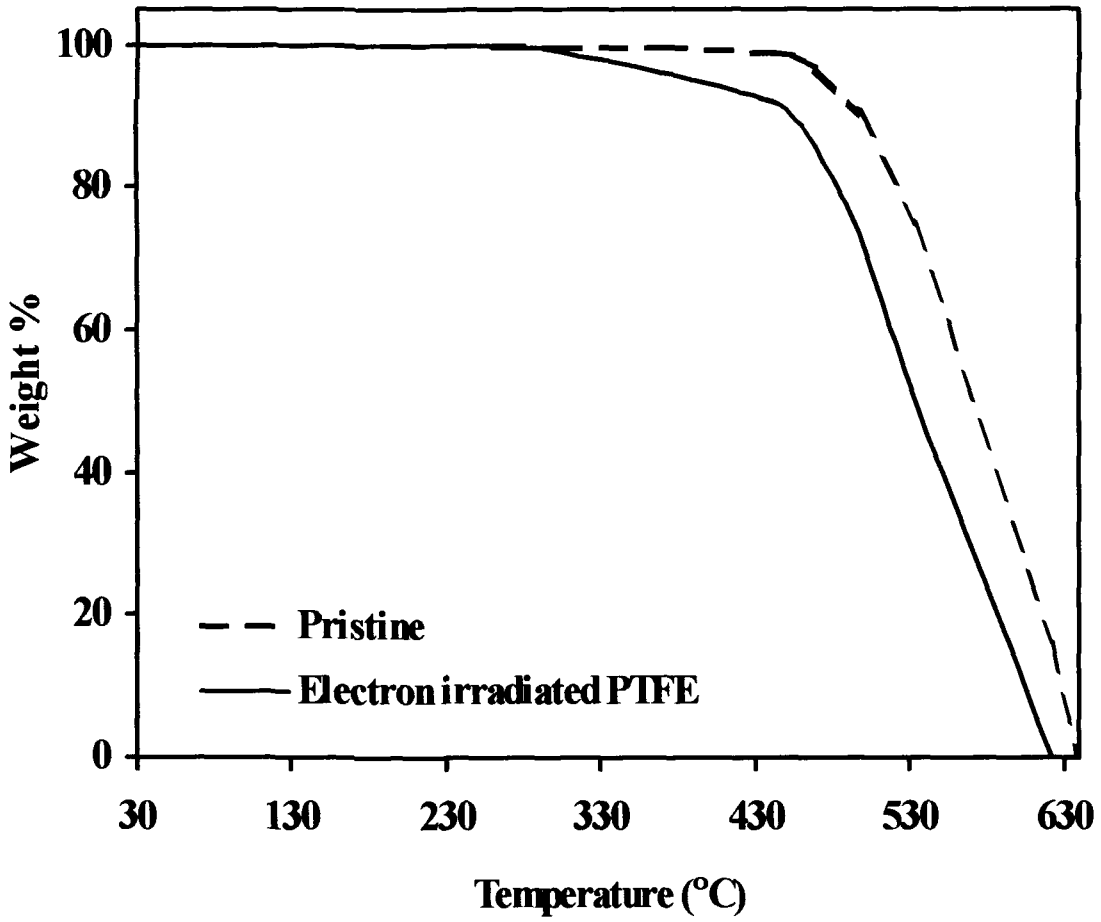

Fig. 2.17. TGA thermograms of the pristine and the electron irradiated PTFE (23 kGy).

Table 2.13. Data derived from TGA thermogram of the electron irradiated (23 kGy) and the pristine PTFE indicating their thermal decomposition behaviour.

Weight (mg)	Temperature range (°C)	Total weight loss %	Interpretation
PTFE (pristine)			
4.4	30 – 264	0	Stable zone
	264 – 470	3	Slow decomposition
	470 – 639	100	Fast decomposition
PTFE (irradiated)			
2.7	30 – 250	0	Stable zone
	250 – 443	8	Slow decomposition
	443 – 622	100	Fast decomposition

Differential Scanning Calorimetry

The DSC thermograms of the pristine and the irradiated PTFE are shown in Fig. 2.18. The analysis of the thermograms is compiled in Table 2.14.

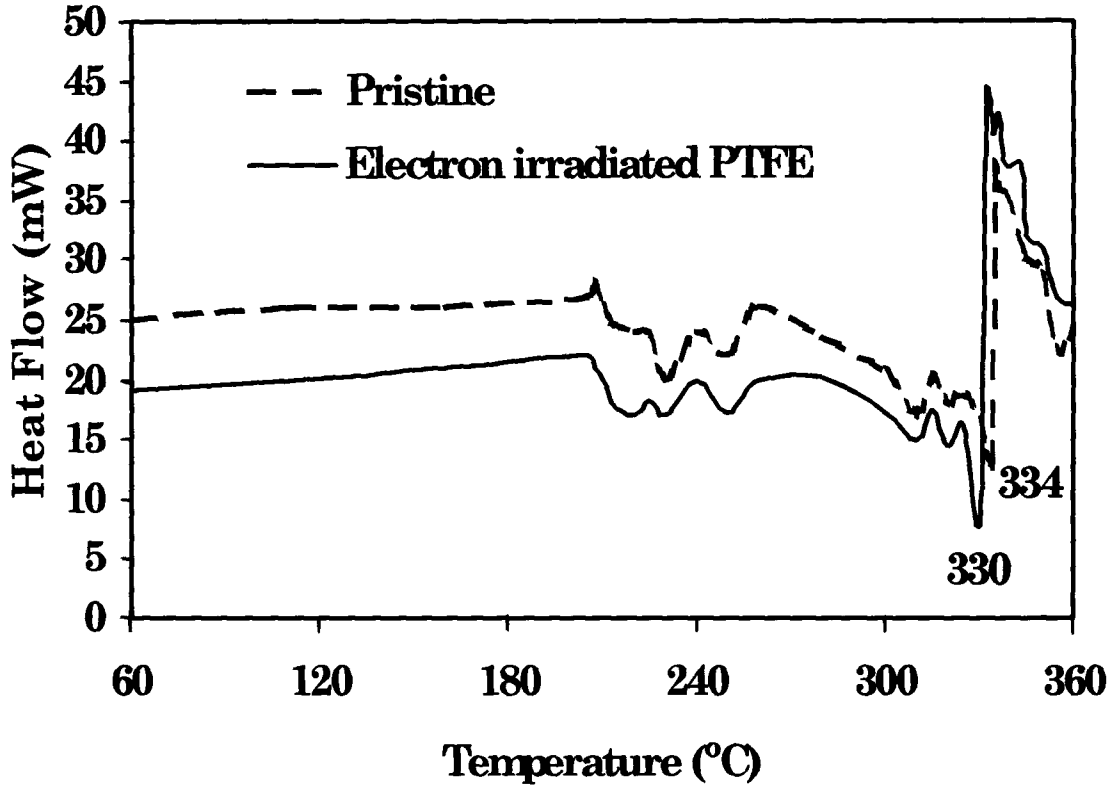

Fig. 2.18. DSC thermograms of the pristine and the electron irradiated PTFE (23 kGy).

The DSC thermograms of both the pristine and the electron irradiated PTFE showed some exothermic distortions at the initial temperature. In the pristine PTFE, these exothermic distortions started from 208°C to 334°C, after which a sharp transition from the exothermic to endothermic behaviour occurred and the melting

endotherm was observed at 334°C. A similar trend was also observed in the electron irradiated PTFE in which the exothermic to endothermic transition occurred at 330°C, thus, showing a melting endotherm at that point. Thus, a decrease in melting temperature was recorded from the DSC thermal analysis.

Table 2.14. Thermal analysis data derived from DSC spectra for the electron irradiated (23 kGy) and the pristine PTFE.

Temperature (°C)	Specification	Interpretation
Pristine PTFE		
334± 2	Endothermic	Melting
Irradiated PTFE		
330± 2	Endothermic	Melting

d) Structural analysis:

Structural analysis of PTFE after irradiation was done by X-ray diffraction analysis.

X-ray diffraction analysis

The X-ray diffraction spectra of the pristine and the irradiated PTFE are shown in Fig. 2.19. The main peak in the pristine polymer was found at $2\theta = 21.79°$. This main peak in the irradiated PTFE was

found to shift to 2θ = 18.06°. The intensity of the main peak was also reduced due to the electron irradiation (Table 2.16). There was formation of a new peak at 2θ = 75°, due to irradiation, as shown in the XRD spectra, but they were of very low intensity.

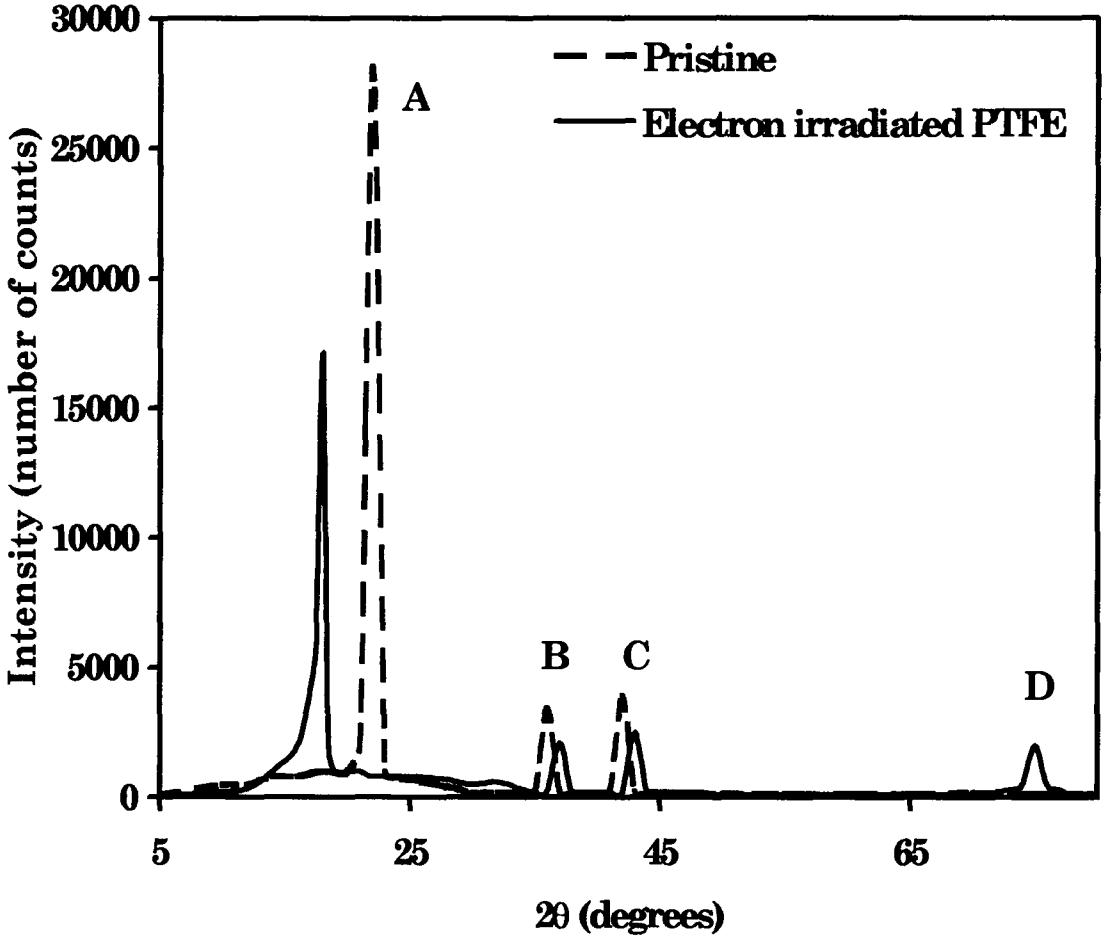

Fig. 2.19. XRD spectra of the pristine and the electron irradiated PTFE (23 kGy).

Table 2.15. Position (2θ), Intensity (I) and full width half maximum (FWHM) of the pristine (P) and the electron irradiated (E) PTFE (23 kGy) as obtained from the XRD spectra.

2θ (degrees)		I(REL)		I(CPS)		FWHM	
P	E	P	E	P	E	P	E
(A) 21.79	18.06	100.0	100.0	28166.0	17132.0	2.6	2.8
(B) 36.00	37.00	7.5	19.9	3103.0	2124.0	0.4	0.3
(C) 42.00	43.00	3.8	22.7	3896.0	1085.0	2.9	0.3
(D)	75.00		3.4		581.0		0.5

e) Atomic Force Microscopy

The 3-dimensional images of the surface topography were obtained from AFM for both pristine and irradiated PTFE samples in nanoscopic level. The 3-D image of the pristine polymer is shown in Fig. 2.20 (a) and that of the electron irradiated PTFE is shown in Fig. 2.20 (b). The surface roughness of the pristine was measured at about 20 different fields and the mean roughness was found to be 19.4 ± 0.4 nm, which increased to 22.05 ± 0.5 nm. Thus, electron irradiation made the polymer surface more rough.

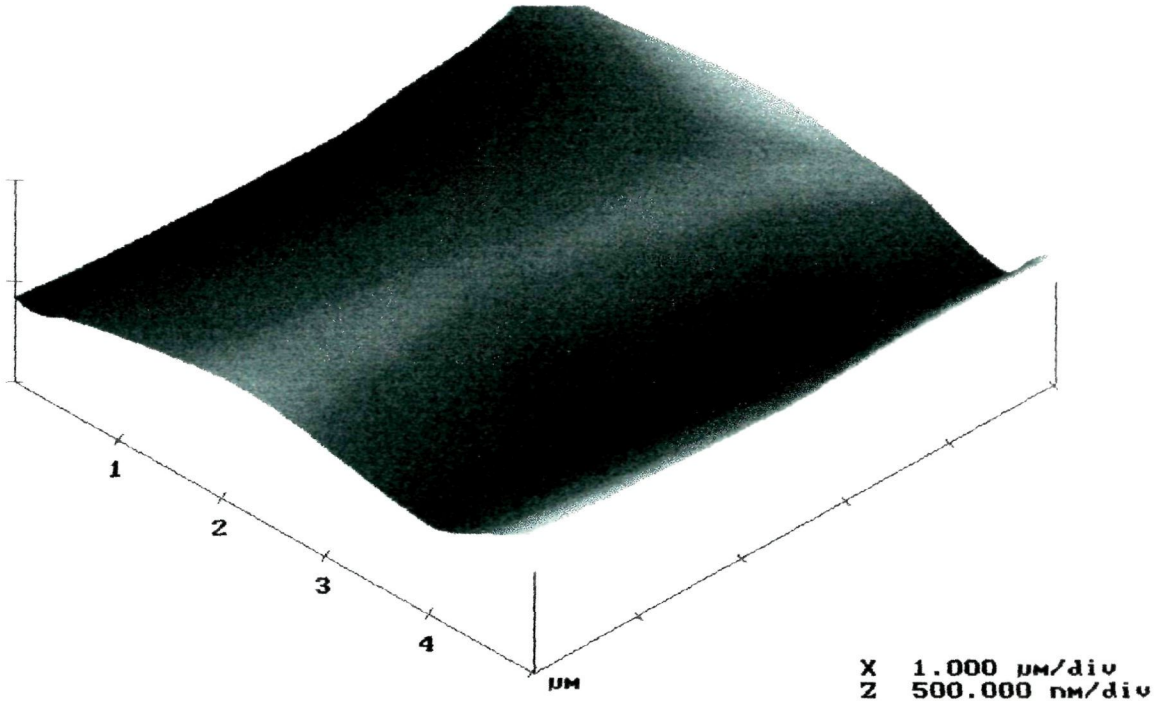

Fig. 2.20(a) AFM image of the pristine PTFE.

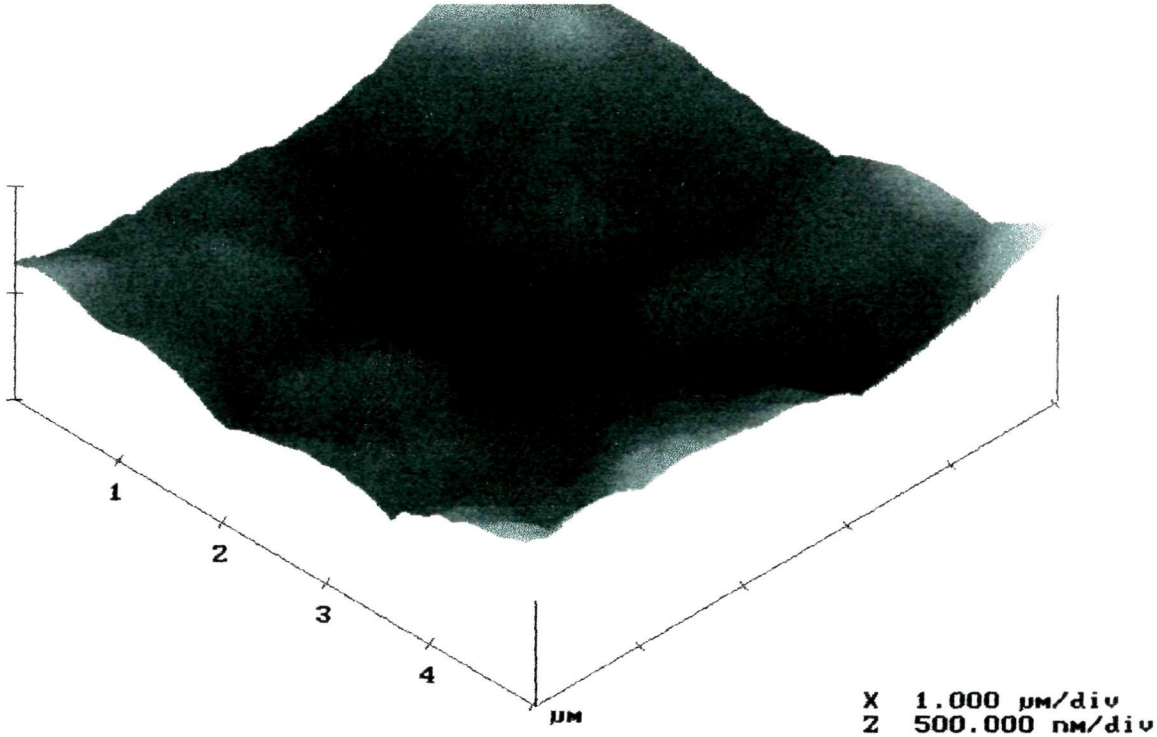

Fig. 2.20(b) AFM image of the electron irradiated PTFE (23 kGy).

2.4.4. Polyimide (PI)

a) Spectroscopic analysis:

Spectral analysis of the pristine and the electron irradiated PI samples were done using FT-IR, UV-Vis and ESR techniques.

FT-IR spectral analysis

The absorbance bands obtained from the FT-IR spectra for the pristine and the irradiated PI are shown in the Fig. 2.21. Radiation induced changes as observed in the spectra do not occur transiently during irradiation only, but reflect a stationary irreversible state of the modified polymer. The change in absorbance due to irradiation at certain frequencies and the interpretation of the absorbance bands are given in Table 2.16. The absorption bands corresponding to carbonyl, phenyl, aromatic ether and C–H vibration of phenyl rings were observed at 1777 to 1725 cm^{-1}, 1500 cm^{-1}, 1250 to 1094 cm^{-1} and 883 to 606 cm^{-1} respectively. The absorbance concerned with C–H deformation (940 - 640 cm^{-1}) and for C–C stretching (1600 cm^{-1} and 1500 cm^{-1}) of phenyl rings increased after irradiation. It has already been observed that, PI degraded by ion irradiation as a multi-step process, in which first a modification of chemical structure occurred without losing much of the O and N constituents and with little

resistivity change (Fink et al., 1994). Moreover, it is a well known fact that, aromatic additives or groups in the repeating units of polymer act as stabilising elements against electron irradiation induced degradation due to delocalisation of excitation energy in the aromatic units (Chapiro et al., 1988). The absorbance at 3295 cm^{-1}, corresponding to C-H stretching mode of alkyne end group was not observed in the present case. Similarly, evidence for unsaturated carbon-nitrogen bonds at 2260 cm^{-1} were not observed. The increase in absorbance in the wide region between 3500 cm^{-1} to 3200 cm^{-1} is possibly originated from oxidative degradation of hydrogen bonds of amides. As evident from the spectra, electron irradiation led only to modification of the existing lines but not to the formation of entirely new structures.

This degradation process was enhanced due to electron irradiation in the presence of air. The degradation was characterised by the decay of imide group at 1118 cm^{-1}. Moreover, appearance of methylene group at 2926 cm^{-1} due to breaking of benzene rings in PI due to Molybdenum ion irradiation (Steckenreiter et al., 1999) was not observed in the present case.

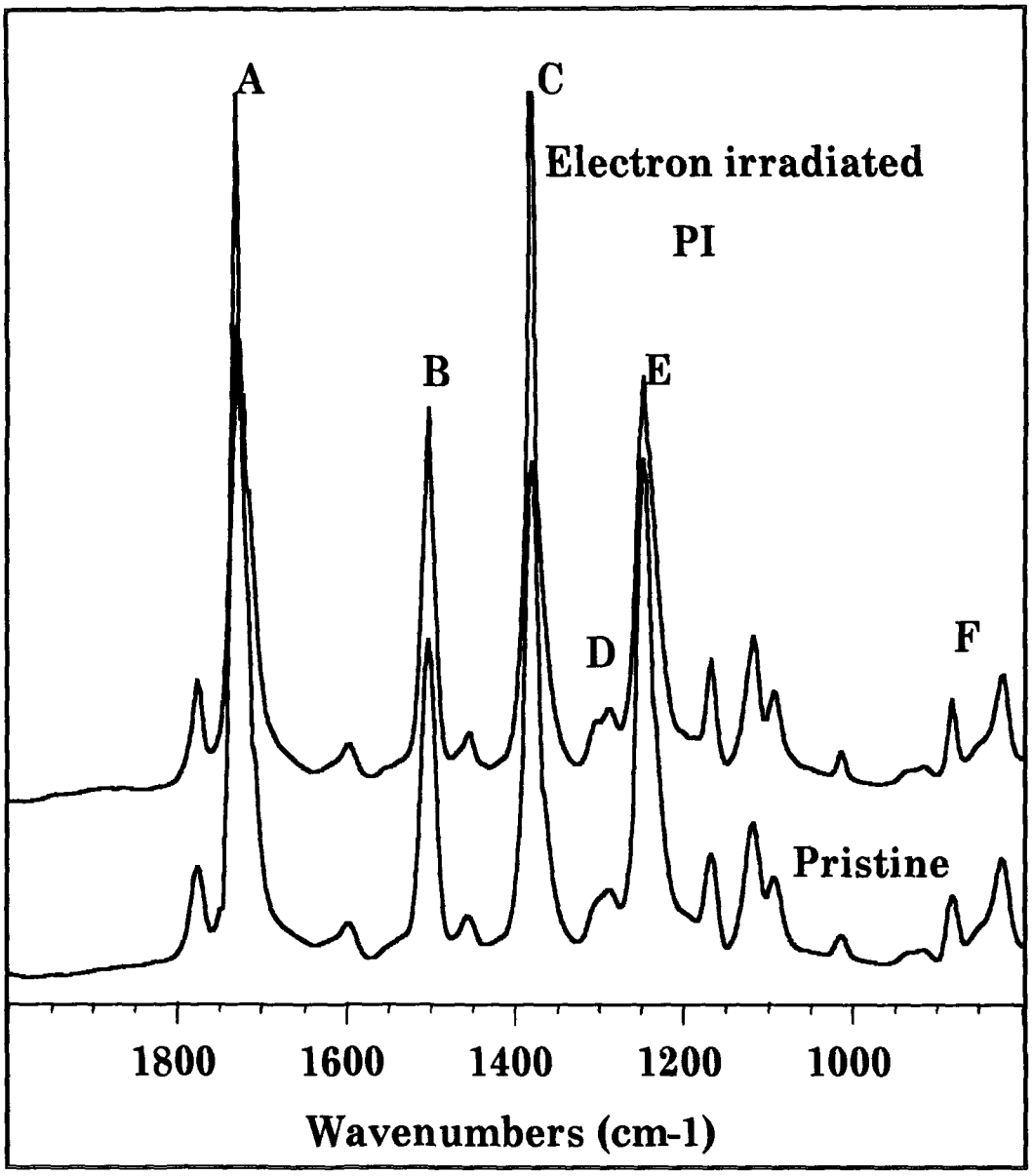

Fig. 2.21. FT-IR spectra of the pristine PI and the one irradiated by 23 kGy dose of 2 MeV electron.

Table 2.16. Interpretation of absorbance bands in Polyimide at some selected frequencies.

Peak name	Wave number(cm^{-1})	Interpretation
A	1777 1732 1725	Stretching vibration of carbonyl group (C=O).
B	1598 1504	Skeletal in-plane Phenyl ring vibration (C-C stretching of Phenyl rings).
C	1383	C-N vibrations of aromatic tertiary amines.
D	1289	C-O-C group vibration between two aromatic cycles.
E	1250 1169 1118 1094	Vibration of aromatic ether group.
F	883 823 725 606	C-H deformation of Phenyl ring.

UV-Vis Spectral analysis

It was quite evident from the UV-Vis spectra of the pristine and the irradiated PI that, there was no change in the absorbance spectra of the polymer after irradiation. In other words, electron irradiation was not able to induce any significant change in the absorbance of the polymer in the UV-Visible region. There was no shift in absorbance edge from UV to visible region. The optical band-gap (E_g) derived from the absorbance spectra was found to be 2.3 eV for the pristine and the irradiated PI.

ESR spectral analysis

ESR spectral analysis showed the absence of any free radical in the irradiated PI.

b) Thermal Analysis

Thermal analysis of the samples was done by TGA and DSC techniques.

Thermogravimetric Analysis

The thermograms obtained for the pristine and the irradiated PI are shown in Fig. 2.22. Thermograms showed the absence of stable zone (0% weight loss) in both the pristine and the irradiated PI, i.e.,

the samples started to decompose slowly as soon as they were heated.

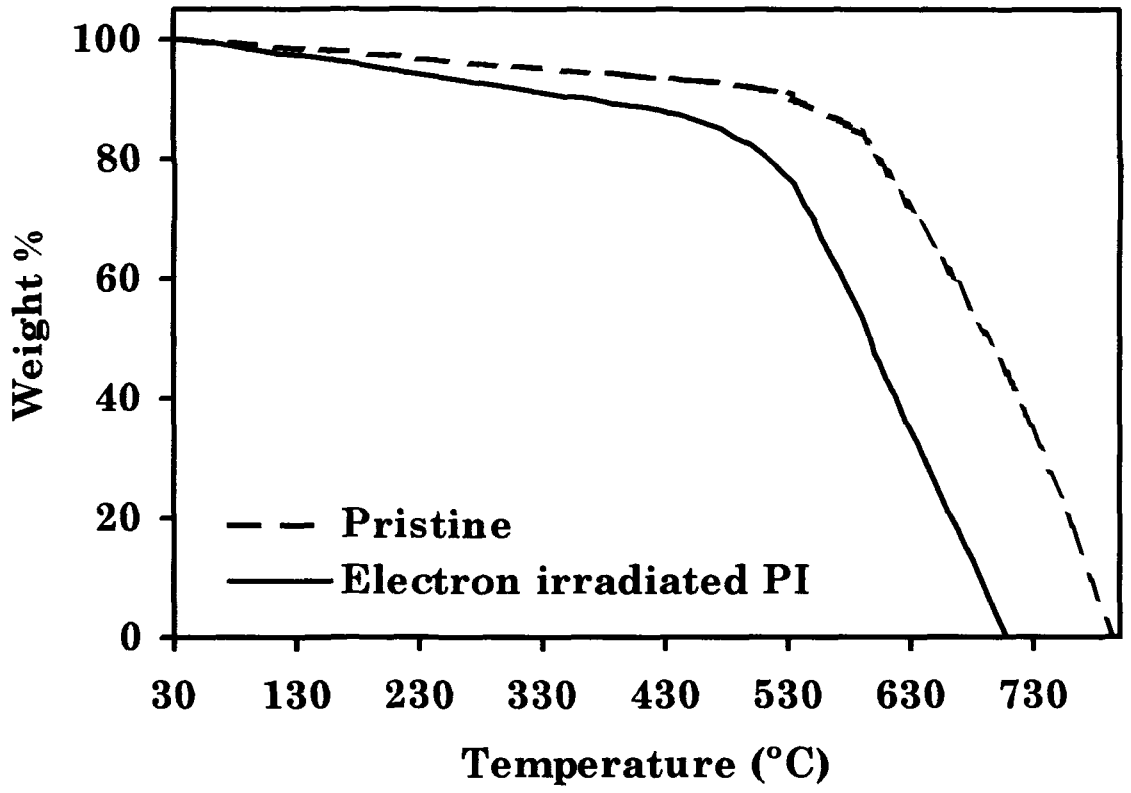

Fig. 2.22. TGA thermograms of the pristine and the electron irradiated (23 kGy) PI.

A 2-step decomposition was observed in both the pristine and the irradiated sample. In the pristine sample, the slow decomposition zone terminated at 584°C and the fast decomposition followed. The pristine sample got completely decomposed at 794°C. In the electron

irradiated PI, the slow decomposition zone terminated at 534°C and the sample got completely decomposed at 669°C as given in Table 2.17. This decrease in thermal decomposition temperature in PI was due to chain-scissioning in the polymer by electron irradiation. In PI the C-H bond was stronger than C-O and Oxygen was depleted more than Hydrogen. Since it has strong C=O (715 kJ/mol) bonds, oxygen loss in PI was due to breakage of C-C and C-N bonds.

Table 2.17. Data derived from TGA thermogram of the electron irradiated (23 kGy) and the pristine PI indicating their thermal decomposition behaviour.

Temperature range (°C)	Total weight loss %	Interpretation
	Pristine PI	
30 – 40	0	Stable zone
40 – 584	15	Slow decomposition
584 – 794	100	Fast decomposition
	Irradiated PI	
30 – 40	0	Stable zone
40 – 534	24	Slow decomposition
534 – 669	100	Fast decomposition

Differential Scanning Calorimetry

The DSC thermograms for the pristine and the electron irradiated PI are shown in Fig. 2.23.

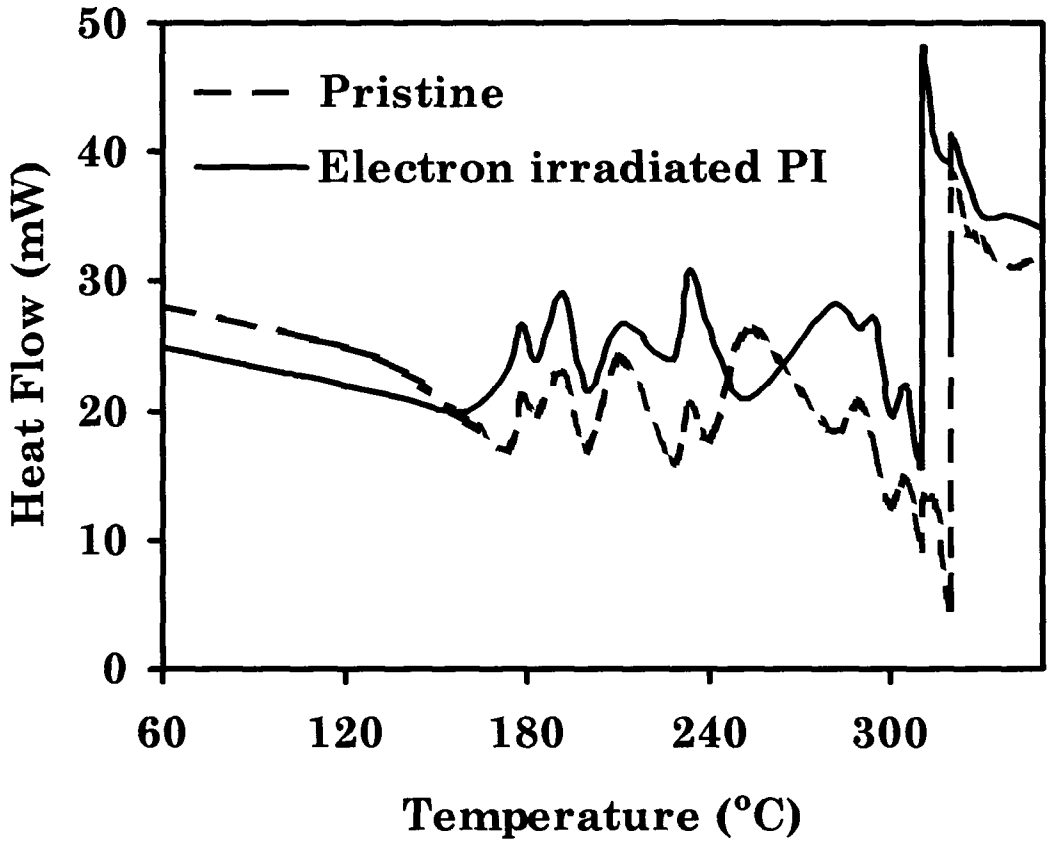

Fig. 2.23. DSC thermograms of the pristine and the electron irradiated PI (23 kGy).

The pristine PI showed thermic distortions till 320°C, at which a sharp transition occurred. This transition resulted in a sharp endotherm

signifying the melting of the pristine polymer. The similar thermic distortions were also observed in the electron irradiated PI. The irradiated PI showed an endothermic transition with a melting point at 310°C. Thus, a decrease in melting temperature of PI was observed possibly due to degradation of PI by electron irradiation.

c) Track studies

The bulk etch-rate (V_G) of the pristine and the electron irradiated PI for fission fragments was calculated from the slope of the plot of fission track diameters versus etching time and was found to increase after electron irradiation as mentioned in Table 2.18. Electron irradiation has, therefore, converted the polymer into an easily etchable material. The increase in bulk etch-rate also showed that the electron irradiation had caused the chain-scissioning in the polymer. The activation energy was calculated from the slope of the plot of inverse of etching temperature (in absolute units) and log of bulk etch-rate as shown in Fig. 2.24. The activation energy was found to decrease by about 34%, i.e., from 73 $kJ.mole^{-1}$ to 48 $kJ.mole^{-1}$ for the irradiated PI, implying that a comparatively less energy was needed to activate the molecules of PI pre-irradiated to electrons. Electron irradiation in PI in the presence of oxygen inhibited cross-linking and

increased the formation of oxygenated compounds, accompanying the degradation of the polymeric molecule (Sasuga, 1988). The oxygenated compounds, which mainly consist of carboxyl and hydroxyl group are considered to relate to the mechanism of etching dissolution. In the present case also the chain-scission caused by electron irradiation in PI accelerates the bulk etch-rates of the polymer thereby decreasing its activation energy of etching.

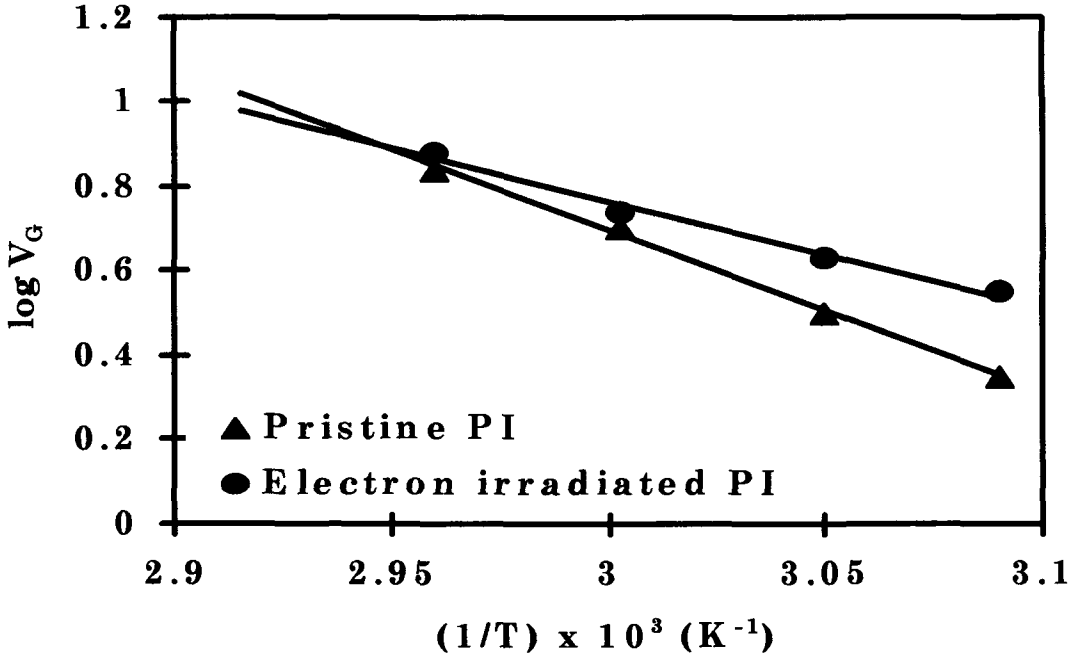

Fig. 2.24. A plot of log V_G versus inverse of etching temperature in the pristine and the electron irradiated PI (23 kGy).

Table 5.19. Bulk etch-rate (V_G) of pristine (P) and electron irradiated PI (E) (23 kGy) at different etching temperatures (ET) and their corresponding activation energies of etching (E_a).

ET (°C)	V_G (μm/h)		E_a (kJ.mole^{-1})	
	P	E	P	E
50	2.2 ± 0.4	3.6 ± 0.4	73.0 ± 0.4	48.0 ± 0.4
55	3.2 ± 0.4	4.3 ± 0.4		
60	5.0 ± 0.4	5.5 ± 0.4		
65	6.9 ± 0.4	7.6 ± 0.4		

d) Atomic Force Microscopy

The 3-dimensional images of the surface topography were obtained from AFM for both pristine and electron irradiated PI in the nanoscopic level. The 3-D image of the pristine polymer is shown in Fig. 2.25 (a) and that of the irradiated PI is shown in Fig. 2.25 (b). The surface roughness of pristine was measured at about 20 different fields on the polymer surface at random. The value mean of surface roughness was found to be 5.6 ± 0.5 nm for the pristine PI, which was reduced to 4.7 ± 0.5 nm for the irradiated one. Thus, electron irradiation enhanced the smoothness of the polymer surface.

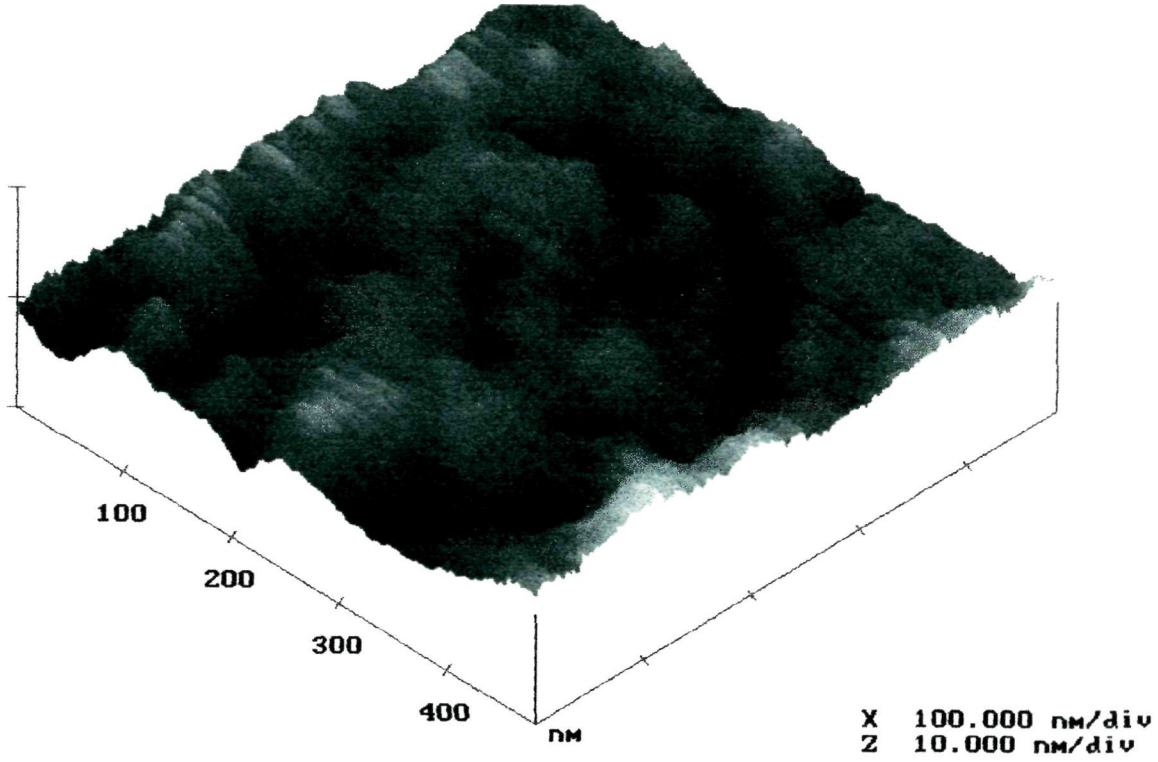

Fig. 2.25(a) AFM image of the pristine PI.

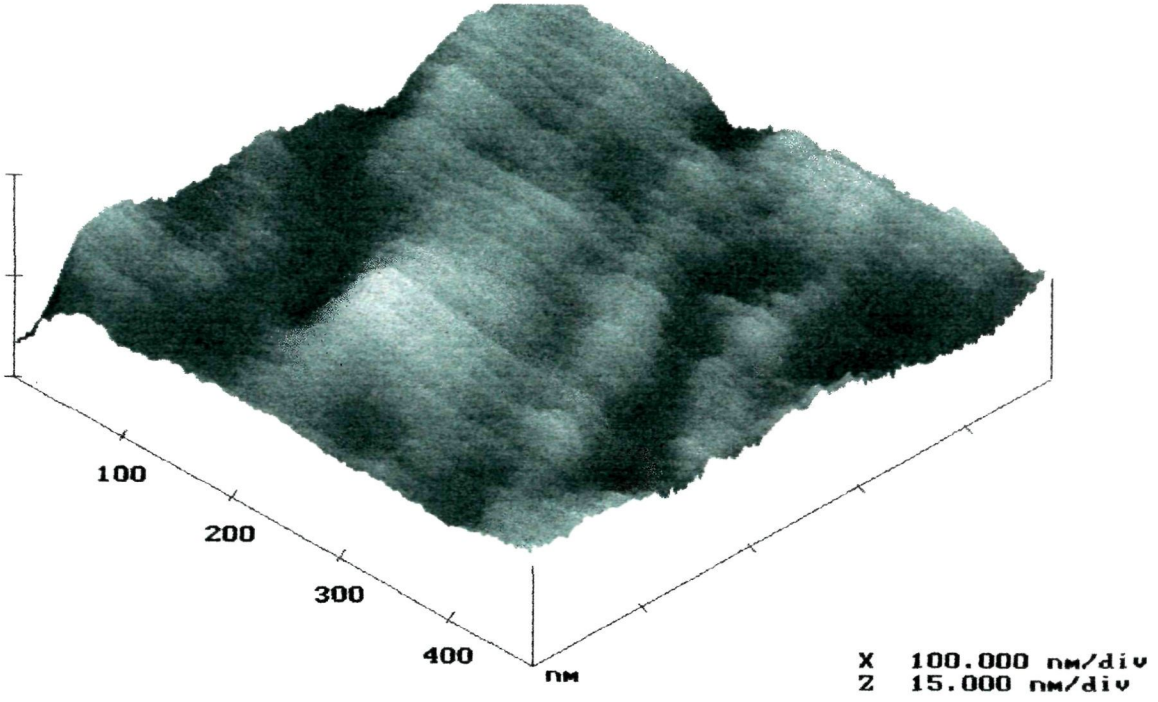

Fig. 2.25(b) AFM image of the electron irradiated PI (23 kGy).

2.5. CONCLUSION

On the basis of the results derived and the discussions thereon, the following conclusions have been drawn.

2.5.1. Electron induced modifications in Polyethylene terephthalate

- Amorphisation of the crystalline fraction of the polymer is evident from absorbance band of FT-IR spectra. Increase in absorbance indicates loss of crystallinity of the polymer. Amorphisation process is strongly enhanced because the polymer has been irradiated in oxygen atmosphere. Presence of aromatic groups in the polymer structure accounts for the stability of the polymer. Amorphisation of the polymer indicates that PET has undergone some chain-scission by electron bombardment. Electron irradiation has not been able to induce alkyne formation in PET.
- A decrease in thermal stability due to electron irradiation of the polymer by 40% has been observed from the results of TGA. Moreover, the temperature of complete decomposition was also observed to decrease by electron irradiation. The chain-scission leads to a decrease in the strength of the polymer, thus, decreasing its ability to withstand high temperatures. A decrease in the

melting temperature of the electron irradiated PET by 3% was also evidenced by DSC measurements.

- PET showed a decrease in its crystallinity due to electron irradiation, as evident from X-ray diffraction studies. The shift in main peak of X-ray diffraction spectra and 8% decrease in its intensity indicate the destruction of crystalline structure of the pristine polymer due to electron irradiation followed by the amorphisation.
- UV-Vis spectroscopic analysis showed that there is no shift of the absorption edge from UV to visible region in the polymer due to electron irradiation. There is no change in band-gap after irradiation, which might be due to presence of aromatic groups in the repeating unit of the polymer that accounts for the stability of the polymer against electron irradiation.
- The bulk etch-rate of the fission fragments increased due to the irradiation, as revealed from track studies. The activation energy of etching in pristine PET was calculated to be 33.0 kJ. $mole^{-1}$, which was found to be reduced to 30.0 kJ. $mole^{-1}$. So, due to 2 MeV electron irradiation on PET, a comparatively less energy is needed to activate the molecules. Moreover, the electron irradiation has

converted the polymer into an easily etchable material.

- Due to time lapse between the irradiation and the measurement, the Electron Spin Resonance studies represent the steady state of the polymer. No free radical signal has been recorded.
- The Atomic force microscopy showed that the surface roughness of the polymer has decreased by 35% after electron irradiation.

So, the main advantage of 2 MeV electron irradiation of 23 kGy dose on PET is that, its activation energy for etching decreases, thus, converting the polymer into an easily etchable material.

2.5.2. Electron induced modifications in Polypropylene

- It is evident from FT-IR spectral analysis that the isotactic nature of PP has not been destroyed due to electron irradiation. Moreover, the symmetric and asymmetric stretching, scissors or bending and wagging of CH_3 and CH_2 group frequencies are observed both in the pristine as well as the irradiated Polypropylene. The increase in absorbance of CH_2 wagging vibration due to irradiation indicates the increase in chain length of hydrocarbon due to addition of more CH_2 groups, which might be due to some cross-linking mechanism induced by electron irradiation in the polymer.

- Thermogravimetric analysis has indicated an increase of 36% in the thermal stability in PP due to electron irradiation. The irradiated polymer remains stable up to a relatively higher temperature. The slow decomposition zone as well as the fast decomposition zone of the irradiated PP started at a higher temperature than those of the pristine one. The temperature of complete decomposition is also higher in case of the irradiated PP. All these findings denote an improvement in the thermal behaviour of PP due to electron irradiation. The reason for this modification might be the predominant cross-linking occurring due to electron bombardment, which increases the molecular weight and compactness, imparting more strength to withstand the thermal strain.
- The increase in melting temperature from 212°C in pristine PP to 221°C in the electron irradiated PP, as obtained from DSC measurement can be correlated to recently observed 'secondary ion induced crystallisation' processes (SRIC) in gamma ray irradiated PP, where the radiation enhanced micro crystalline regions were verified by Transmission Electron Microscopy (Mateev and Karageorgiev, 2000). These new micro-crystalline regions were reported to be distributed inhomogeneously on the surfaces of

strongly stressed interlamella and interspherolite spaces, characterised by considerably high values of the mechanical surface energy. This supported the crystallisation exotherms as observed in case of irradiated PP. The increase in crystallinity of the PP has resulted in increase in melting temperature.

- Increase in crystallinity due to irradiation, which was revealed from Differential Scanning Calorimetry is further supported by X-ray diffraction patterns. The X-ray diffraction spectra showed that the intensity of the main peak is increased by 70% due to irradiation. Emergence of new peaks also supports the increase in crystallinity due to irradiation in the polymer.
- The decrease in optical band-gap from 5.2 eV in pristine to 4.9 eV in the irradiated Polypropylene has been observed from UV-Vis spectroscopy. Decrease in band-gap implies increase in conductivity of the polymer. This has been also been verified by the A. C. conductance measurement.
- The surface roughness was found to decrease after irradiation by 9%, i.e., from 7.2 nm to 6.6 nm. The cavities created by the electron bombardment might have been repaired by cross-linking of the polymer after irradiation.

So, irradiation by 2 MeV electron has increased the conductivity, thermal stability, crystallinity and the surface smoothness of Polypropylene. This conductive polymer with enhanced thermal stability and crystallinity can find extensive applications in *microelectronics*.

2.5.3. Electron induced modifications in Polytetrafluoro ethylene

- The analysis of the FT-IR spectra for the pristine and the irradiated PTFE showed C-F stretching vibration from 1300 cm^{-1} to 1000 cm^{-1}. The electron irradiated PTFE showed some additional bands assigned to carbonyl stretching vibrations and to terminal double bonds.
- The UV-Vis spectral analysis showed a shift of absorption edges from UV to visible region due to irradiation. A decrease in band-gap by 50% after electron bombardment has been observed. This indicates that the conductivity of the PTFE has increased due to 2 MeV electron irradiation.
- The ESR spectra showed the presence of free radical due to electron irradiation. This free radical is responsible for the decrease in

energy band-gap due to irradiation as revealed by UV-Vis spectral analysis. The formation of free radicals further supports the bond-cleavage due to irradiation.

- This is further supported by the TGA thermograms, which showed a decrease in thermal stability of the PTFE after irradiation. The chain-scission led to a decrease in the strength of the polymer, thus, decreasing its ability to withstand high temperatures. The TGA thermograms showed that, the pristine polymer remained stable up to 264°C, followed by slow decomposition up to 534°C, after which the fast decomposition occurred, till the pristine sample gets completely decomposed at 639°C. The electron irradiated PTFE remained stable up to a relatively lower temperature of 250°C. The fast decomposition started at 499°C and the irradiated sample was completely decomposed at 622°C. So, a decrease in thermal stability has been observed in this polymer due to 2MeV electron irradiation.
- A slight decrease in the melting temperature from 334°C in the pristine to 330°C in the irradiated PTFE was also observed from DSC measurements.
- The X-ray diffraction patterns showed a shift in the main peak

along with the decrease of 39% in its intensity in the irradiated PTFE. The intensity of the main peak was found to decrease implying a decrease in crystallinity due to electron irradiation in PTFE.

- Atomic Force Microscopy indicated an increase in surface roughness by 14%, i.e., from 19.4 nm to 22.0 nm due to electron irradiation.

Thus, electron irradiation in the polymer Polytetrafluoro ethylene induced chain-scission and bond-cleavage resulting in the formation of free radicals, which in turn increased the conductivity of the polymer. The crystallinity of the polymer is destroyed due to irradiation. Thermal stability is also reduced due to electron irradiation.

2.5.4. Electron induced modifications in Polyimide

- The Fourier transform spectral analysis showed that electron irradiation has led only to modification of existing lines, but not to the formation of entirely new structures. The increase in absorbance in the wide region between 3500 cm^{-1} to 3200 cm^{-1} presumably originated from oxidative degradation of hydrogen bonds of amides. This degradation process has been enhanced due to electron irradiation in presence of air. The degradation is characterised by

the decay of imide group. Aromatic additives or groups in the repeating units of polymer act as stabilising elements against electron irradiation induced degradation due to delocalisation of excitation energy in the aromatic units.

- The Electron Spin Resonance spectroscopy did not show any free radical signal. The ESR spectra actually represent the stationary state of the polymer since the measurements have been done after a few months of irradiation.
- There was no shift of absorption edge from UV to visible region, implyng that the optical band-gap remains constant. The presence of aromatic group in the repeating units of the polymer accounts for its stability towards radiation.
- The Thermogravimetric analysis showed the absence of any stable zone for the pristine and the irradiated PI. The slow decomposition zone of the irradiated Polyimide terminated at a relatively lower temperature. Moreover the irradiated PI decomposed completely at a relatively lower temperature. This implied that there was some chain-scissioning due to irradiation, which accounted for a 16% decrease in the complete decomposition temperature of the irradiated sample.

- The differential scanning calorimetry showed a decrease in melting temperature from 320°C in the pristine PI to 310°C in the irradiated PI.
- There was an increase in bulk etch-rate and hence a decrease in activation energy of etching due to chain-scissioning in the irradiated PI. The activation energy in the pristine sample was calculated to be 73.0 kJ. $mole^{-1}$, whereas that in the irradiated polymer was found to be reduced to 48.0 kJ. $mole^{-1}$. Thus, electron irradiation converted PI into an easily etchable material.
- The surface roughness in nanoscale in the pristine PI was found to be 5.6 nm, which was found to be reduced to 4.7 nm i.e. the electron irradiation resulted in about 16% reduction in the surface roughness of PI.

So, it is now further confirmed that PI can withstand 2 MeV of electron without undergoing any considerable change in its properties. The presence of aromatic groups in the structure of PI, which are not destroyed by 23 kGy dose of 2 MeV electron irradiation, is the main cause of radiation stability of the polymer. In a separate experiment of heavy ion (^{28}Si and ^{58}Ni) irradiation in PI, it was observed that the band-gap changes considerably at higher doses (Tripathy et al., 2000).

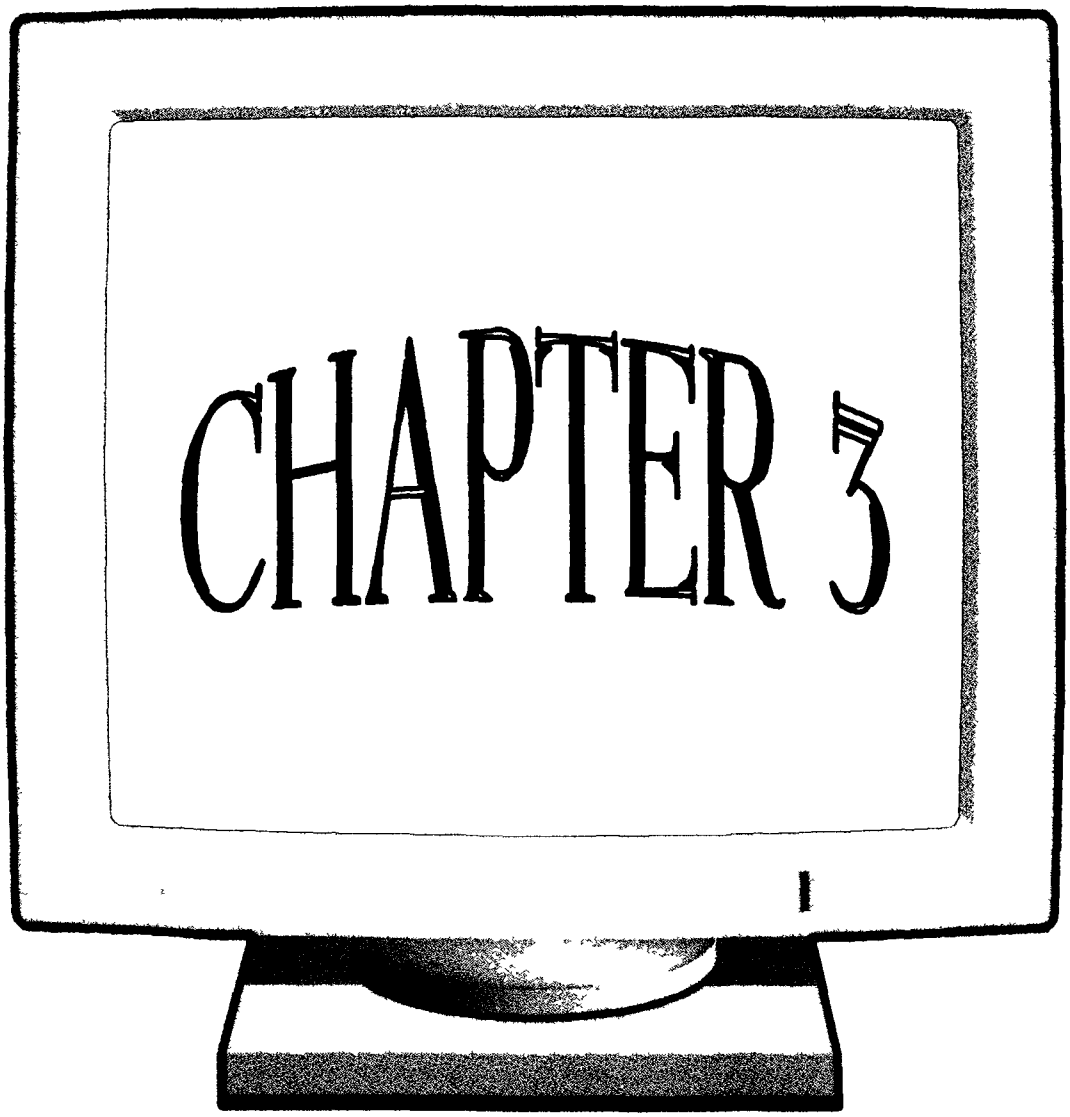
CHAPTER 3

CHAPTER 3

DOSE DEPENDENT MODIFICATION OF POLYALLYLDIGLYCOL CARBONATE BY 2 MeV ELECTRONS

3.1. INTRODUCTION

The field of polymer damage by energetic ions has gained considerable attention in the last decade since it has turned out that the ion beam modifies the electrical, electronic and optical properties of polymers, by depositing energy in the material, thus, enhancing their applicability in various technological fields. Polymer irradiation induces several inter-chain and intra-chain modifications as the incident ions scissor the polymer chains, break the covalent bonds, promote cross-linking while liberating certain volatile species, leading to changes in the macro-molecular weight distribution and in the

creation of new chemical groups. The optical absorption method is a powerful tool for investigating the optically induced transitions and for providing information about the band structure and energy gap in crystalline and non-crystalline materials (Higazy and Hussein 1995). The modifications induced are due to the large amount of energy storage in the electronic molecular environment, which overcomes the binding energies of simple organic molecules. The effectiveness of these changes produced in the polymer depends on the target parameters (structure, composition, molecular weight of the polymer as well as the irradiation parameters like ion energy, mass, fluence etc. Under irradiation, the energy transferred to the molecules of the medium results in primary ionisation and excitations (Chapiro, 1988). Polyatomic molecules having absorbed energy will suffer bond cleavages giving rise to free radicals and these are responsible for most chemical transformations observed in polymers.

Literature survey indicates that gamma irradiation of Polyallyldiglycol carbonate leads to change in refractive index in the entire bulk of the sample, while an ion beam irradiation leads to a localised and sufficient increase in polymer's refractive index to achieve optical wave-guides. Further it has been found that, refractive

index is an increasing function of dose in case of gamma rays and 200 keV proton beam (Darraud-Taupiac et al., 1997). UV-Vis spectrometry shows that, ion beam induced cluster formation sets in at a minimum transferred electronic energy density around 10^{-3} eV/Å^3 in case of high energy heavy ion impact whereas a higher threshold energy density around 10^{-1} eV/Å^3 is required, if the total deposited energy is accumulated by low energy ion or high energy electron impacts (Fink et al., 1996(b)). Decrease in energy band-gap after 16 MeV electron irradiation in Polyvinyl alcohol has already been reported (Fink et al., 1995). Formation of C=C double bonds due to ^{16}O heavy ion irradiation in Polyallyldiglycol carbonate becomes source of free carriers. Thus, conductivity increases and dielectric constant decreases. Conversion of C=C to C-C in Polyallyldiglycol carbonate due to ^{28}Si irradiation causes a decrease in free carriers by cross-linking and hence an increase in dielectric constant (Phukan et al., 1999). An increase in surface roughness and change in colour of Polyallyldiglycol carbonate has been observed when irradiated to higher gamma doses (Abu-Jarad et al., 1997). A decrease in optical transmittance and appearance of strong absorption bands resulting from the formation of CO_2, has been observed in Polyallyldiglycol carbonate due to X-ray irradiation

indicating the degradation of the polymer (Chong et al., 1997).

3.2. SPECIFICATION OF POLYALLYLDIGLYCOL CARBONATE

Polyallyldiglycol carbonate (PADC) belongs to polyen of type ~CH_2-CHR~ having the diethylene glycol carbonate links which, belong to polyester. It contains polyallyl chains joined by diethyleneglycol dicarbonate links which when hit by the electrons results in destruction of the polymer chains (Thang et al., 1995). PADC is an ideal polymer detector, which is optically clear, amorphous, highly transparent, homogeneous and isotropic. It is a radiation sensitive thermoset material that does not cross-link upon irradiation. It is about 100 times more sensitive than polycarbonate (Ghosh et al., 1994). Its thermosetting nature stands out clearly against other polymers, which are thermoplastic in nature. It is susceptible to interfacial degradation by a suitable etchant. It is light in weight and flexible. It neither softens on heating nor hardens on cooling. Its important properties are listed in Table 3.1. Its superb sensitivity, optical clarity and uniformity extends its applicability in high precision works like observation of heavy nuclei in cosmic radiation, neutron dosimetry and measurement of uranium content in

various materials. Its applicability further extends to windows of aeroplane and marine vessels, ophthalmic lenses, industrial gas mask lenses, biological test chambers, X-ray equipment and accessories, computer tape reels and watch crystals.

Table 3.1 Important properties of PADC

Properties	PADC
Commercially available as	CR-39
Monomeric composition	$C_{12}H_{18}O_7$
Molecular weight	274.0
Density (g/ml)	1.32
Refractive index	1.5
Thickness (μm)	1500
Uniformity	Good
Optical behavior	Transparent
Manufactured by	Homalite Corp. Wilmington, Del. USA.

In this chapter, we have studied the effect of different doses of 2 MeV electron beam on PADC by different characterisation techniques.

The optical absorbance studies leading to detailed analysis of variation in energy band-gap has been done by UV-Vis spectroscopy. The structural change has been studied by Fourier transform IR spectroscopy. Electron spin resonance spectroscopy has been done to observe any free radical formation. The thermal decomposition behaviour and the resulting phase transitions have been studied by Thermogravimetric analysis and Differential scanning calorimetry. Effect of irradiation on the amorphous nature of the PADC has been studied by X-ray diffraction technique. Finally the damage in the nanoscopic level of the polymer due to irradiation and the resulting roughness has been studied by Atomic Force microscopy.

3.3. TARGET PREPARATION AND IRRADIATION

Preparation of the targets

PADC samples of size (2x2) cm^2 were cut from commercially available sheets. They were then washed thoroughly with soap solution and then with deionised water. The cleaned samples were then dried inside vacuum desiccator.

Irradiation and cooling

Irradiation of the targets was done by 2 MeV electron from electron

generator at Hahn-Meitner Institute, Berlin. The electron beam was allowed to pass through a collimator and was allowed to fall on the target placed at a distance of 2 metres from the collimator. The dose of 2 MeV electron was varied to carry out a dose dependent study. The doses used were 2 kGy, 23 kGy, 46 kGy, 93 kGy, 139 kGy, 186 kGy and 235 kGy.

Irradiated samples were allowed to cool for about 24 hours. The samples were then taken and preserved in plastic boxes.

3.4. EXPERIMENTAL TECHNIQUES FOR CHARACTERISATION OF THE TARGET

The irradiated PADC samples were characterised by the different experimental techniques viz. spectroscopic, thermal, diffraction and surface analysis techniques as described below:

3.4.1. *UV-Vis spectroscopy*

UV-Vis spectroscopy for the irradiated samples was done by Beckman (DU-650) UV spectrophotometer. The samples were put inside a quartz shell keeping pristine PADC as reference. The scanning speed of the apparatus was 1200 nm/min and the scanning wavelength region was 330 nm to 500 nm. The absorption edge was found to be

within 330-370 nm wavelength range. Shift in absorption edges from UV to visible region was correlated with energy band-gap (E_g) by Tauc's expression (discussed in Chapter 2, eqn. 2.2). The shift in optical band-gap energy leads to the conclusion that energetic ion beams favour the formation of compounds with chemical structures having double- or triple - bonds and phenolate or quinonic structures (Fink et al., 1995). The error associated in E_g measurement was ± 0.1 eV.

3.4.2. *Fourier transform Infra-red Spectroscopy (FT-IR)*

All FT-IR spectra of the irradiated samples along with their pristine were recorded in transmission mode using model NICOLET, IMPACT 410 Fourier transforming instrument keeping air as reference. All the measurements were done in the wave number range of 4000 cm^{-1} to 500 cm^{-1}. The spectra were obtained for the polymer's transmittance as a function of wave number. The variation in transmittance (%) for the pristine and electron irradiated samples were inter-compared and the peak analysis was done to study the variation in position and intensity of the bands, disappearance of some existing bands and emergence of new bands. For a relatively ideal sample, the accuracy is expected to be from better than ± 1% to ± 3% of

the amount present.

3.4.3. *Electron Spin Resonance spectroscopy (ESR)*

All the ESR measurements have been done using a Varian (E-109, X-band) spectrophotometer with 100 kHz field modulation. Samples were cut into (0.5 x 0.5) cm^2, placed in quartz tube and spectra were recorded at room temperature. A 9.6 GHz frequency was used for this instrument. The instrumental conditions were:

Field set: 3382 Gauss; Scan range: 1000 Gauss; Time constant: 0.25 seconds; Scan time: 4 minutes; Modulation amplitude: 0.5x1; Receiver gain: $6.3x10^4$; Microwave power: 2 mW. The spectra obtained were analysed for emergence of free radicals.

3.4.4. *Thermogravimetric analysis*

An automatic Perkin Elmer instrument was used in the present study. The scanning rate for this instrument was adjusted to 20°C/min and Nitrogen was used as the flushing gas. The temperature range scanned was 30°C to 600°C. The study of thermal stability as a function of dose was done with the help of a thermogram, a plot of mass percent as a function of temperature, which was obtained by the Perkin Elmer instrument.

3.4.5. *Differential Scanning Calorimetry (DSC)*

All the measurements were done using a Perkin Elmer instrument. The scanning rate for this instrument was adjusted to 20°C/min. The temperature range scanned was 50°C to 520°C, in an inert atmosphere using Nitrogen as flushing gas.

3.4.6. *X-ray diffraction studies (XRD)*

X-ray diffraction patterns were recorded using Cu-Kα radiation (λ=1.54 Å) 8.04 keV energy from Rigaku θ-2θ spectromenter at Inter University Consortium, Indore, India. A rotating anode source and Sodium Iodine scintillation detector was used. Dimension of entrance slit was 0.2 mm and the step size was 0.04 mm. The value of 2θ ranged from 3° to 90°.

3.4.7. *Atomic Force Microscopy (AFM)*

AFM of the samples were done at Inter University Consortium, Indore, India, using Digital Nanoscope E instrument in contact mode. The cantilever moved according to the force acting on its tip (sensor). Thus, by sliding across the sample surface, the probe's tip measured the topography. The detector measured the sensor's response and the surface images were obtained. Further, the surface roughness of the irradiated samples was measured at 20 different places on the sample

surface at random and the mean was taken as the surface roughness of the sample.

3.5. RESULTS AND DISCUSSION

After characterisation of the irradiated samples by various mentioned techniques, the results were analysed and are discussed under different sub-headings.

3.5.1. *Spectroscopic analysis*

Spectroscopic analysis was done by comparing the results of three different techniques i.e. UV-Vis Spectroscopy, FT-IR Spectroscopy and Electron Spin Resonance Spectroscopy.

a) UV-Vis Spectroscopy

With increasing electron irradiation dose, the absorption edge at the lower wavelength side of PADC spectra shifted towards higher wavelength side as shown in Fig. 3.1. This finding was in accordance with the observations on heavy-ion irradiated polymer foils, and hence it was assumed that same destruction mechanism, which was derived for ions, also holds good for electron irradiation.

PADC network consists of polyallyl chains joined by diethylene glycol dicarbonate links. The target molecules when hit by the

electrons, having absorbed energy suffered bond cleavage giving rise to unsaturated fragments - free radicals (Thang et al., 1995). The mechanism is shown below:

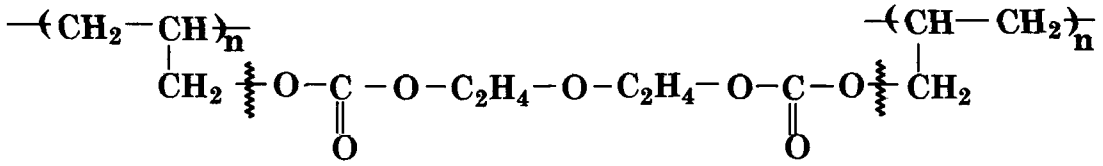

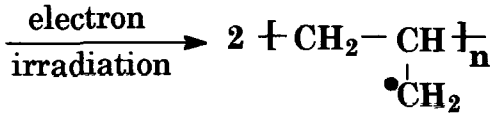

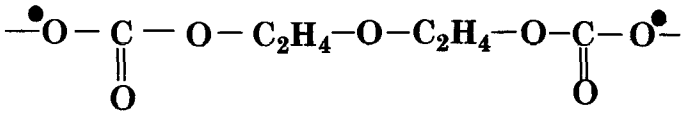

The absorption coefficient (ε) for different electron doses were determined. The values of $\sqrt{\varepsilon}/\lambda$ were calculated and plotted against $1/\lambda$ on X-axis. The straight line of the curve was then extrapolated and its intersection on the abscissa was determined. This wavelength corresponds to the gap-wavelength (λ_g). The band-gap (E_g) was then determined for the irradiated samples using eqn.(2.2).

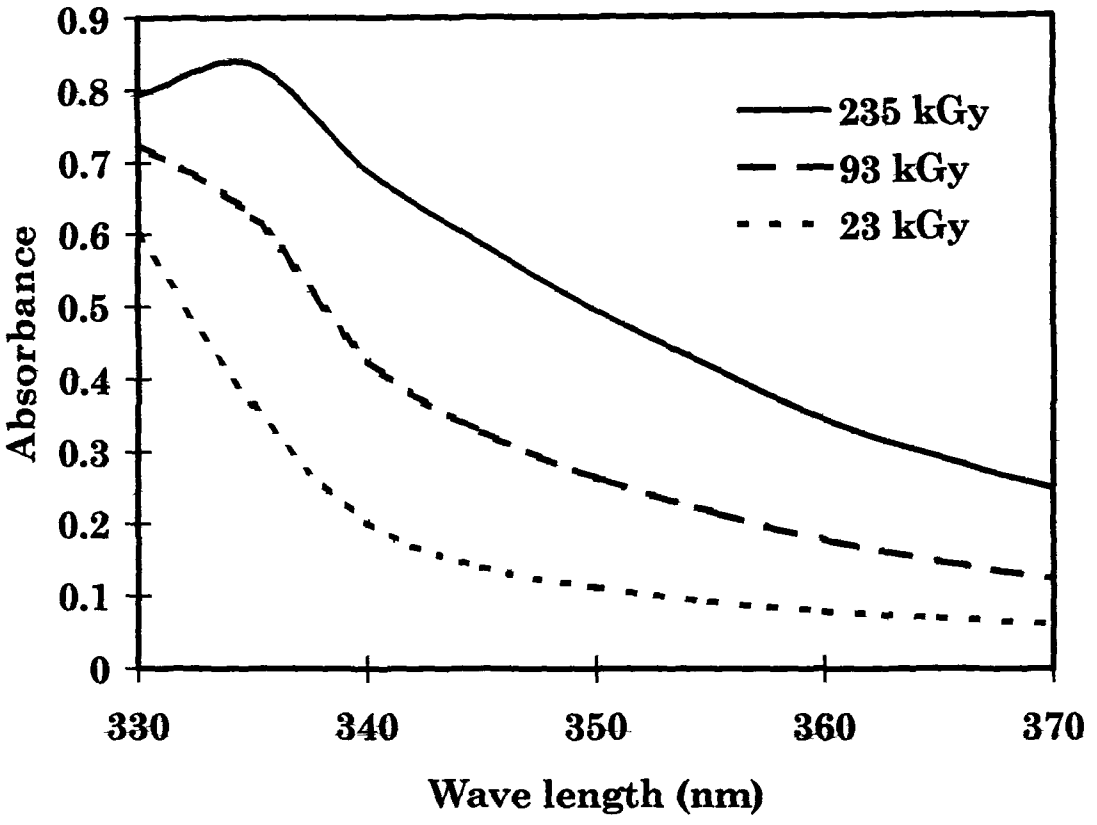

Fig. 3.1. UV-Vis spectra of the PADC irradiated to 23 kGy, 93 kGy and 235 kGy of 2 MeV electron.

Table 3.2 contains the data of electron dose dependent optical band-gap (E_g) and the gap wavelength (λ_g) at the point of intersection. E_g was found to be ranging from 3.6 eV to 3.1 eV for doses ranging from 2 kGy to 235 kGy with respect to pristine as shown in Table 3.2.

The absorbance was found to increase with increase in electron dose. The optical band-gap was found to be an inverse function of dose as evident from Fig. 3.2.

Table 3.2. Variation in gap-wavelength (λ_g) and optical band-gap (E_g) with electron dose in PADC.

Dose (kGy)	Gap-wavelength λ_g (nm)	Optical band-gap E_g (eV)
Pristine	345.5	3.6
2	345.5	3.6
23	350.2	3.5
46	365.7	3.5
93	370.0	3.4
139	380.6	3.3
186	386.1	3.2
235	394.0	3.1

The variation of energy band-gap with electron-dose can be represented in form of a mathematical equation, which is derived as

$$E_g = -0.0021\ D + 3.6 \qquad \text{---------- (3.1)}$$

where, E_g is the energy band-gap in eV and D is the 2 MeV electron dose in kGy.

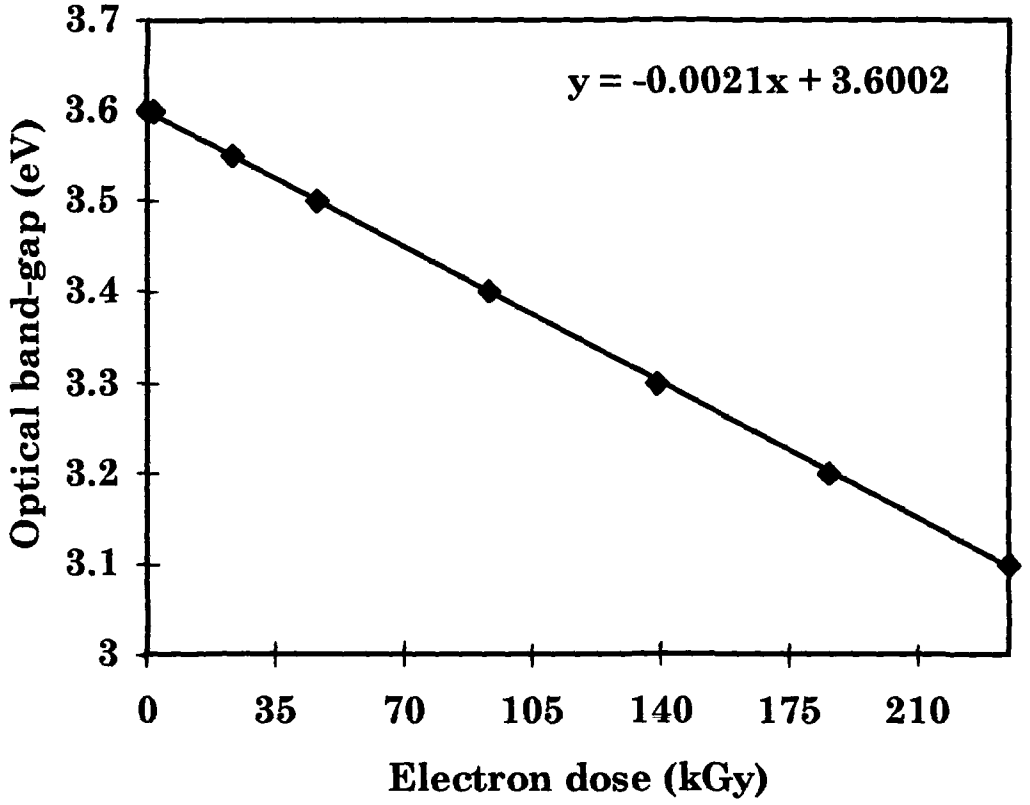

Fig. 3.2. The plot showing the variation of optical band-gap with electron dose in PADC.

b) FT-IR Spectroscopic analysis

The IR spectra obtained from FT-IR Spectroscopic analysis shows the variation of transmittance with wave number. In the present case, a dose dependent study was done to study the variation of transmittance with electron dose. The IR spectra of the pristine and the irradiated PADC (235 kGy) are shown in Fig. 3.3.

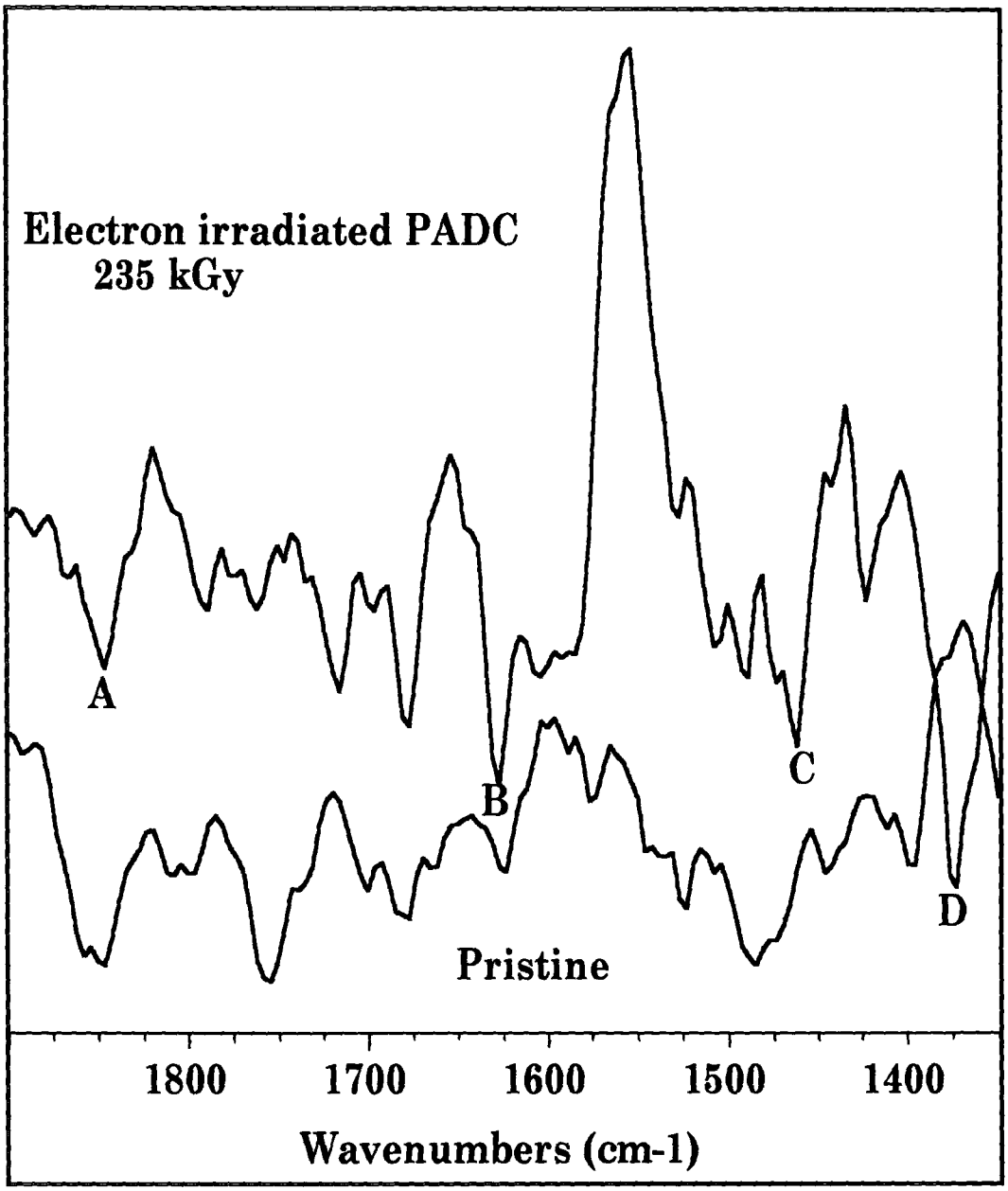

Fig. 3.3. FT-IR spectra of the pristine and the electron irradiated PADC (235 kGy dose).

Some characteristic bands have been identified. The C=O stretching vibration is observed from 1850 cm^{-1} (A) to 1630 cm^{-1} (B). The $-CH_2$-O- scissor vibration is observed at 1460 cm^{-1} (C). The CH_2 scissor vibration is observed at 1370 cm^{-1}(D).

From an analysis of the data for transmission (%) as a function of dose, the following results were derived:

i) From the constancy in position of the transmittance spectra of irradiated and unirradiated samples as evident from Fig. 3.3, it was assumed that interchain separation was not affected by electron irradiation. It could also be taken as an indication that there is no cross-linking after irradiation damage has broken the chemical bonds.

ii) A decrease in transmittance was observed with increase in electron dose.

iii) Variation of transmittance (%) with electron dose, for some selected wavelengths are listed in Table 3.3. Variation in transmittance was observed to be less at higher doses. In other words, decrease in transmittance was observed to be slower as the electron dose increased. So, it could be concluded that PADC track detector could be used as a reliable dosimeter for large doses of electron.

iv) An increase in brittleness of PADC was observed at higher doses (235 kGy), which was a sign of decreased strength presumably due to random chain-scission.

Table 3.3. Variation in transmittance% with different doses of 2 MeV electron in PADC.

Wave length (nm)	Transmittance (%)							
	a	b	c	d	e	f	g	h
2564	9.6	6.5	5.6	5.0	4.8	4.6	4.5	4.4
2597	13.0	9.0	7.9	7.1	6.7	6.5	6.4	6.3
2608	14.1	9.8	8.8	7.7	7.4	7.3	7.2	7.1
2620	15.3	10.6	9.4	7.9	7.4	7.3	7.2	7.2
2633	15.4	10.7	9.2	7.8	7.3	7.1	7.1	7.0
2646	15.3	10.5	9.2	7.5	6.8	6.5	6.4	6.3
2654	15.0	10.2	9.2	7.3	6.9	6.6	6.5	6.4
2671	14.6	9.6	8.8	6.7	6.3	6.0	5.9	5.8

where, a, b, c, d, e, f, g and h represent the different doses of 2 MeV electron with a = Pristine, b = 2 kGy, c = 23 kGy, d = 46 kGy, e = 93 kGy, f = 139 kGy, g = 186 kGy, h = 235 kGy.

c) Electron spin resonance spectroscopic analysis

Free radicals, generally the allyl radical, formed in the PADC after gamma and proton irradiation survive for at least six months (Darraud-Taupiac et al., 1997). The ESR spectra of the electron irradiated PADC did not show any significant modification. No free radical signal was recorded. Owing to the time lapse between the irradiation of the samples and their analysis, there was a possibility of annihilation of the radicals, which might have been formed due to electron irradiation.

3.5.2. *Thermal analysis*

Thermal analysis of the pristine and the irradiated samples were done by Thermogravimetric analysis and Differential Scanning Calorimetry. Dose dependent variation in thermal stability and thermal decomposition behaviour has been studied.

a) Thermogravimetric Analysis

Thermograms obtained from TGA measurements showed that all the samples displayed a stable zone without any weight loss, followed by a zone of slow decomposition and then terminated after a fast decomposition zone. Dose dependent variation in thermal behaviour is

shown in Table 3.4. Thermograms of the PADC samples irradiated to 23 kGy, 93 kGy and 235 kGy electron doses are shown in Fig. 3.4. The pristine PADC was stable in the temperature range of 30°C to 118°C after which the decomposition started and at a slower pace up to 332°C.

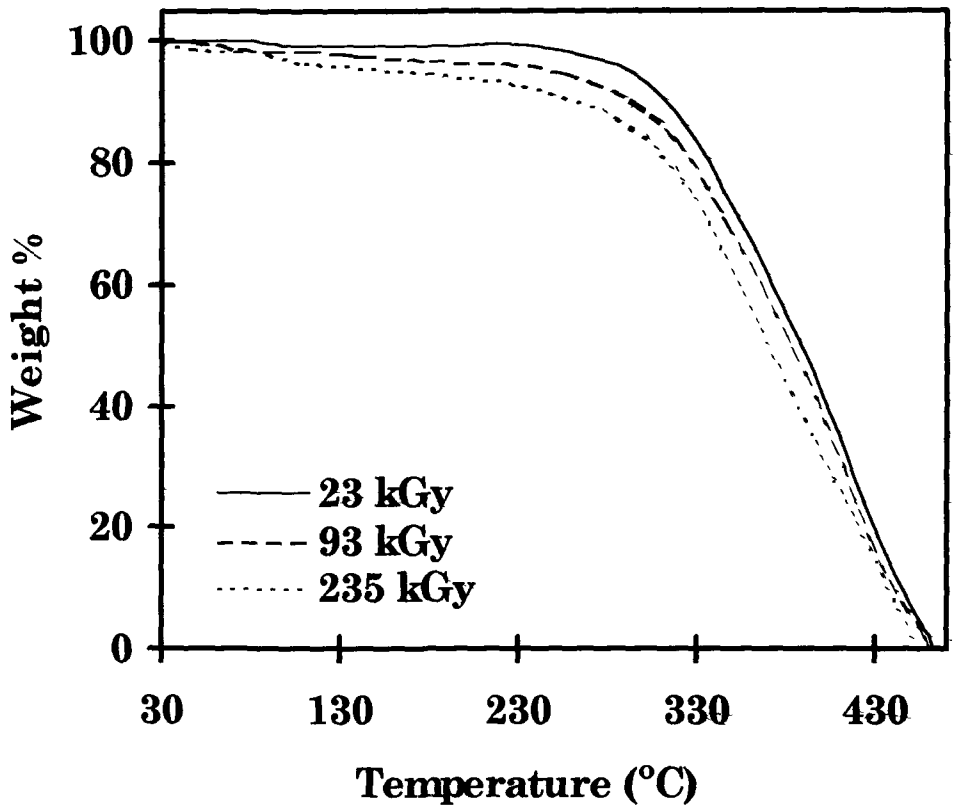

Fig. 3.4. TGA thermograms of PADC samples irradiated to 23, 93, 235 kGy doses of 2 MeV electron.

A faster rate of decomposition set in from 332°C to 481°C. It was followed by a residual decomposition. The stability of PADC towards rise in temperature gradually decreased with increase in dose. For PADC irradiated to 235 kGy dose, the polymer was stable up to 48°C, following the same trend of dehydration and then decomposition at a faster rate till complete decomposition at 455°C.

Table 3.4. Variation in thermal stability and decomposition with electron dose in PADC.

Dose (kGy)	Stability Zone (°C)	Slow Decomposition Zone (°C)	Fast Decomposition Zone (°C)
0(Pristine)	30 - 118	118 - 332	332 - 481
2	30 - 118	118 - 301	301 - 480
23	30 - 93	93 - 280	280 - 463
46	30 - 82	82 - 250	250 - 462
93	30 - 72	72 - 250	250 - 460
139	30 - 71	71 - 250	250 - 458
186	30 - 70	70 - 240	240 - 457
235	30 - 48	48 - 240	240 - 455

No residual decomposition was observed in the case of irradiated PADC samples. Electron irradiation led to chain-scissoning as a result

of which the irradiated polymer became more prone to decompose faster.

b) Differential scanning calorimetric analysis

A dose dependent study of the electron irradiated PADC samples were done by differential scanning calorimetry. In all the cases, we got a small exothermic peak at 317°C. The amount of heat involved in this exothermic process gradually decreased from 785.6 J/g in the pristine PADC to 261.3 J/g in the PADC irradiated to 235 kGy of 2 MeV electron. Further, in all the cases, this small exothermic peak was followed by a large exotherm starting from 321°C to 486°C, with the peak at 407°C. The heat involved in this exothermic reaction gradually decreased from 5362.6 J/g in case of pristine PADC to 3046.7 J/g in the PADC irradiated to 235 kGy of 2 MeV electron. These two exotherms were followed by a continuous endotherm of decomposition. Since the polymer PADC is completely amorphous in nature, there is no melting point as such associated with it. The decomposition temperature is rather the flow temperature at which the polymer changes from rubbery to liquid state.

The DSC thermograms obtained for the pristine and the PADC irradiated to 235 kGy dose of 2 MeV electron is shown in Fig. 3.5.

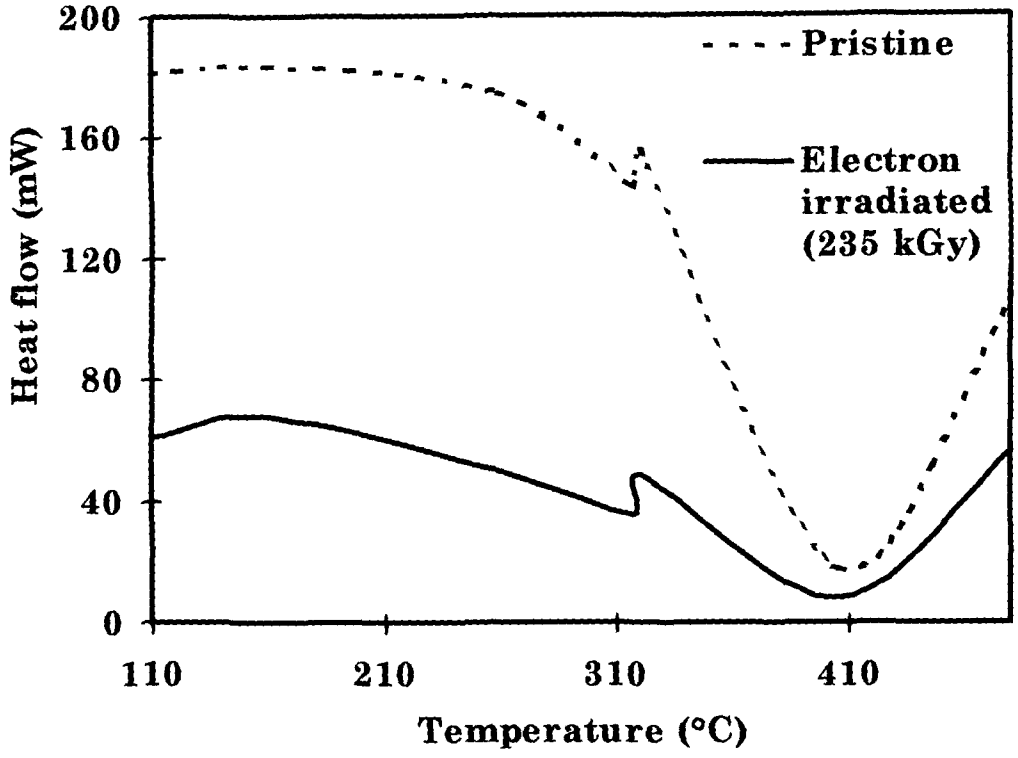

Fig. 3.5. DSC thermograms of the pristine and the PADC irradiated to 235 kGy of 2 MeV electron.

3.5.3. *Surface damage and roughness analysis*

The atomic force micrographs of the pristine along with PADC irradiated to 235 kGy electron dose are shown in Fig. 3.6 (a) and (b), which clearly showed that the extent of surface damage in the irradiated one. The surface roughness in the pristine and the irradiated PADC were measured in 20 different fields in 1 μm scanning range and the arithmetic mean was calculated to find the exact surface roughness. The surface roughness analysis showed that roughness in the pristine sample was 4.9 ± 0.4 nm was found to be reduced to 4.6 ± 0.4 nm in the PADC irradiated to the highest dose.

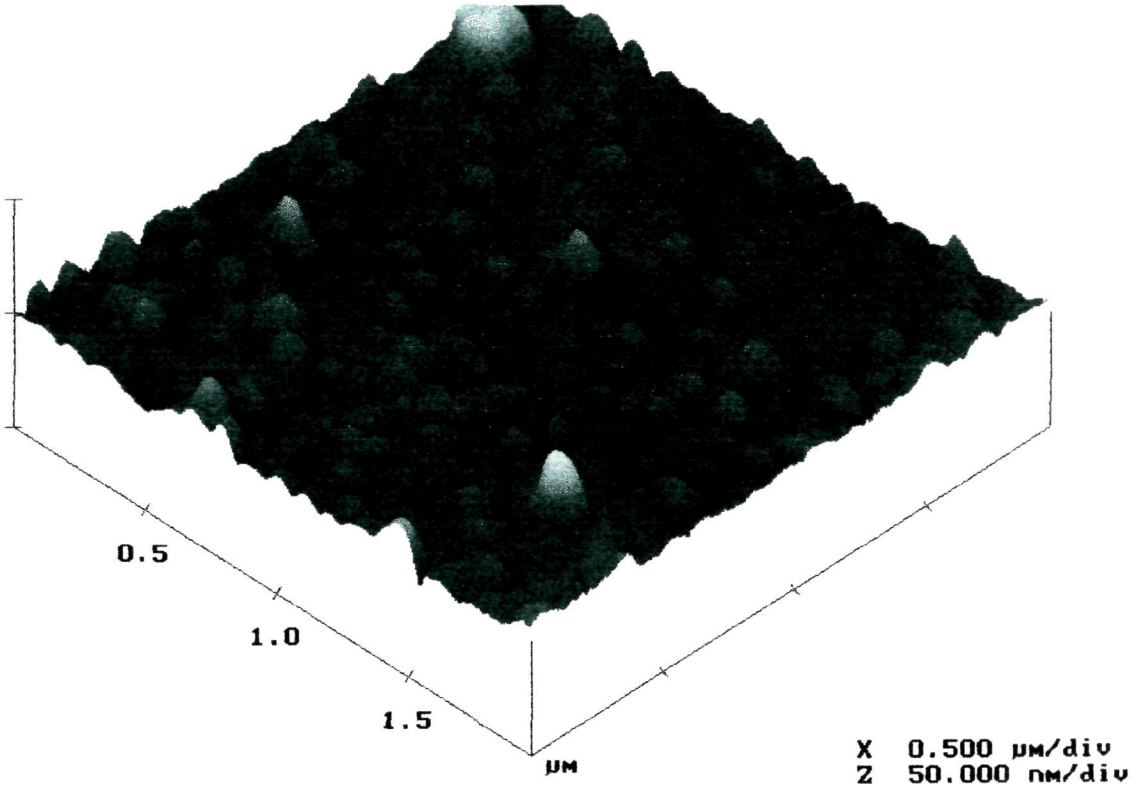

Fig. 3.6(a) AFM image of the pristine PADC.

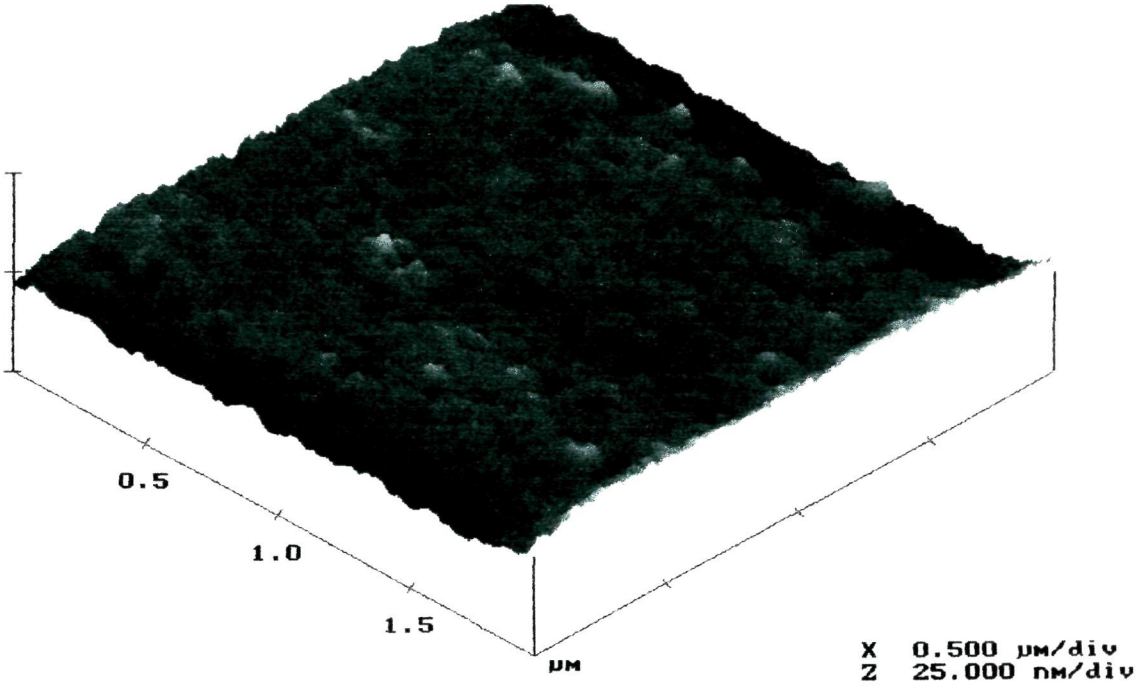

Fig. 3.6(b) AFM image of 235 kGy electron irradiated PADC.

3.5.4. *X-ray diffraction studies*

The diffraction patterns of the pristine along with PADC irradiated to a dose of 235 kGy of 2 MeV electron were recorded. As evident from the XRD spectra shown in Fig. 3.7, the maximum intensity of the main peak at $2\theta = 20.84°$ was reduced from 7120 counts in the pristine PADC to 5760 counts in case of PADC irradiated by 235 kGy dose of electron. Decrease in the intensity of the main peak could be interpreted as the result of chain-scission of the polymer by electron bombardment.

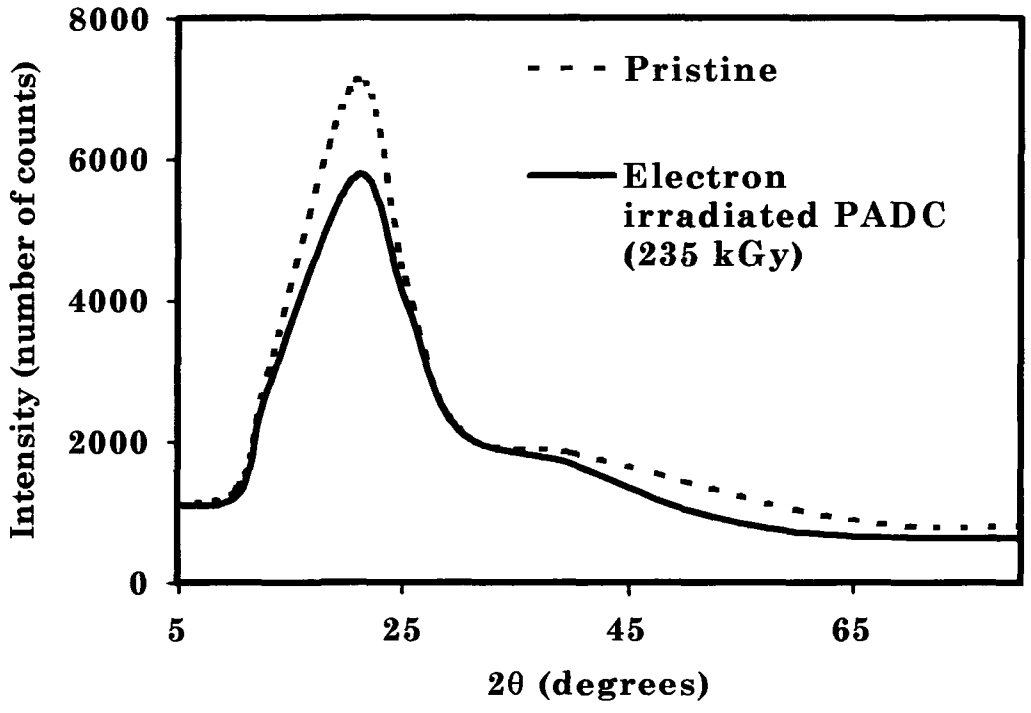

Fig. 3.7. XRD spectra of the pristine and 235 kGy dose of electron irradiated PADC.

3.6. CONCLUSION

1. The effect of different doses of 2 MeV electron irradiation on one of the most sensitive polymers, PADC, was studied and a gradual decrease in the optical band-gap was observed with increase in electron dose. There was a 14% decrease in band-gap in the PADC irradiated to 235 kGy of electron from that of the pristine. Thus, the energy band-gap was found to be an inverse function of electron dose. A relation was derived to calculate the energy-gap for PADC irradiated to different electron doses:

   $E_g = -0.0021\ D + 3.6$,

   where, D is the electron dose in kGy and E_g is the energy band-gap in eV.

2. The spectra recorded in the IR region showed that the inter-chain separation was not affected by electron irradiation and no cross-linking had taken place after the bond cleavage due to irradiation. Variation in transmittance was less for higher doses, which implied that it could be used as reliable dosimeter for large doses of electron.

3. Thermogravimetric analysis of the irradiated PADC samples showed an electron dose dependent variation in thermal stability. It was found that the higher the electron dose, lower was the thermal stability of the irradiated polymer. A gradual decrease in the stability zone, slow decomposition zone and fast decomposition zone was observed with increase in the electron dose. In the PADC irradiated to 235 kGy electron dose, the stability zone decreased by 59%, the slow decomposition zone decreased by 28% and the fast decomposition zone decreased by 5% from that of the pristine PADC.

4. DSC thermograms of the pristine PADC and the PADC samples irradiated to different doses of electron showed two exothermic peaks at 317°C and 407°C. The heat involved in the exothermic processes decreased with increase in dose. A decrease of 75% and 51% in the heat involved during the exothermic reaction at 317°C and 407°C respectively was observed in the PADC irradiated to 235 kGy of electron as compared to that of the pristine. No sharp melting point was recorded, rather, the two exotherms were followed by a continuous endotherm in the pristine as well as the

irradiated PADC samples.

5. A broad peak in the diffraction patterns of the XRD spectra for the pristine as well as the irradiated PADC showed the amorphous nature of the polymer. No shift was observed in the position of the main peak, but a decrease in the intensity of the main peak by 19% was observed in the PADC irradiated to 235 kGy of electron from that of the pristine PADC.

6. The AFM photomicrographs of the pristine PADC and the PADC irradiated to 235 kGy of electron showed a decrease in surface roughness by electron irradiation. In the scale of 1μm scanning range, the surface roughness was found to be decreased from 4.9 ± 0.4 nm in case of the pristine PADC to 4.6 ± 0.4 nm in the PADC irradiated to 235 kGy of electron. This 6% decrease in surface roughness by electron irradiation can be attributed to a splash phenomena which is expected due to the swelling of the nearby surface in atomic scale around the impinging ions.

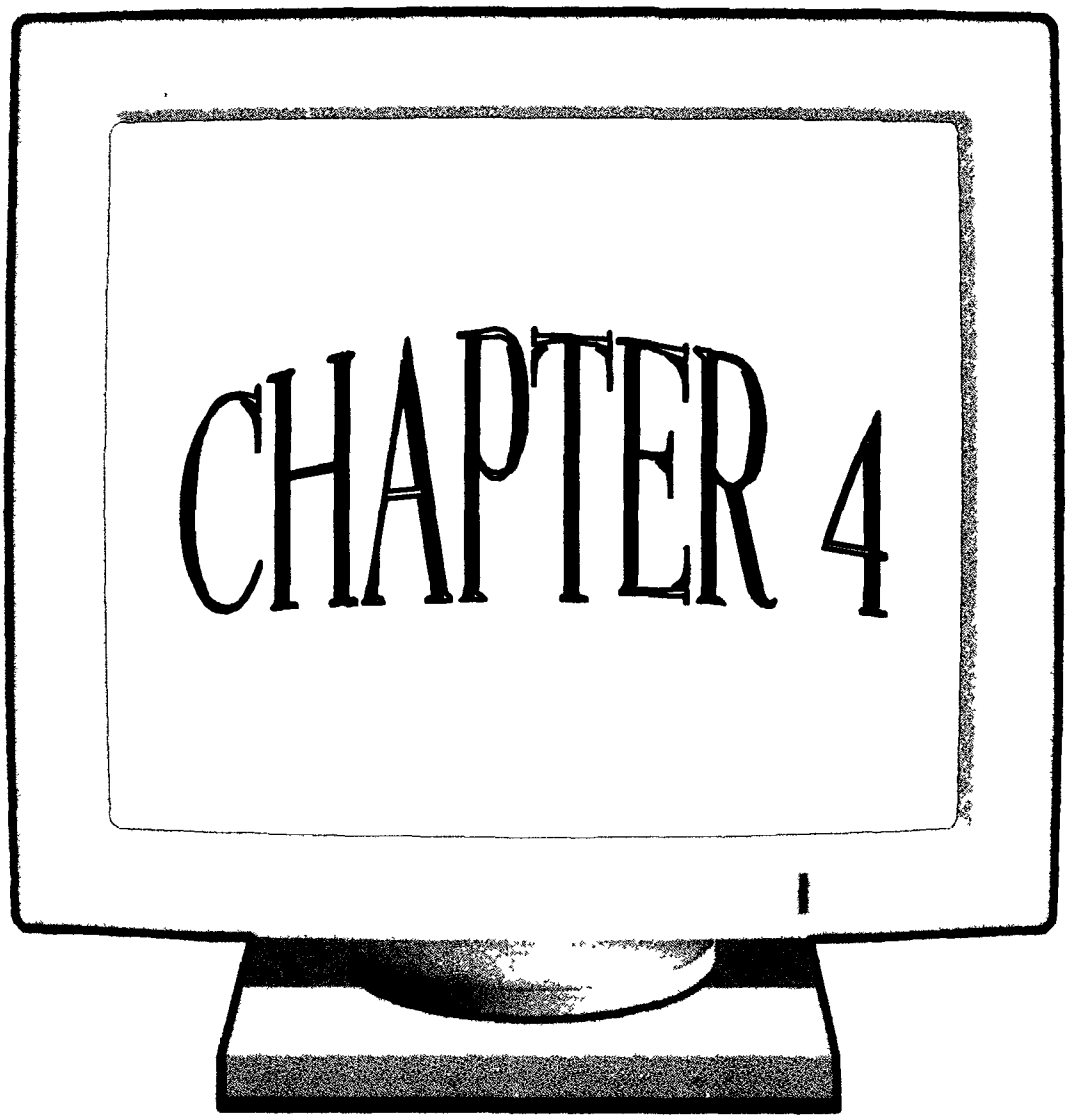
CHAPTER 4

CHAPTER 4

IMPACT OF ELECTRON IRRADIATION ON ETCHING RESPONSE IN POLYALLYLDIGLYCOL CARBONATE (PADC)

4.1. INTRODUCTION TO TRACK TECHNIQUE

The use of ion beams for polymer modification requires information on the morphology of tracks created by impinging ions. Tracks of energetic particles in polymers are complicated primarily because of greater multiplicity of chemically active defects that can occur i.e. displaced atoms, broken molecular chains, free radicals etc. Since, energy transfers needed to produce these defects are generally lower, polymers are a class of more sensitive track detectors.

When the projectile consists of electrons, collision between two

particles of equal mass can transfer the whole of kinetic energy to the stationary particle. Large energy transfers are thus possible and the path-length is much less well defined. Further, a light particle is much more readily deviated by the nucleus and so scattering angles will be larger and the path-length much more crooked. It follows that the range of an electron is not necessarily as great as its path-length. The large energy transfer results in appearance of additional electron tracks branching off the track of the incident particle - δ rays and represent 30% of total energy originally present in the incident electron. At higher energies (kinetic energy > 1 MeV), the energy-loss of an electron is chiefly due to bremsstrahlung and the probability of this process increases with energy. Linear energy transfer (LET) is a measure of rate of energy deposition and is defined as the linear rate of loss of energy by an ionising particle traversing a material medium. Electrons are low LET radiations and mostly affect the physical and chemical properties of polymeric films. Though the electrons cannot create etchable tracks of their own, yet they can affect etch-rate values of the detectors and other heavy ion tracks depending on the absorbed dose (Frank and Benton, 1970). With electron irradiation, the damage is dispersed in an atomic scale, so that it is not possible to see the

individual etched features resulting from the defects responsible for accelerated etching.

Heavy ions traversing an insulating medium produce narrow regions of atomic defects. In polymers the track core consists of a zone of drastically reduced molecular weight, corresponding to broken molecular bonds, surrounded by a track halo where the chemically reactive species undergo secondary reactions. Because of large free energy associated with the disordered structure, radiation damaged trails are generally much more chemically reactive than a normal unirradiated material. In polymeric solids less energy is required to break chemical bonds than to ionise atoms. Consequently, formation of high density of broken bonds along the particle trajectory effectively decreases the average molecular weight of the polymer thereby increasing its chemical reactivity. Chemical etching transforms the latent tracks into optically visible tracks by supplying required amount of energy for the enlargement process. Etched tracks of 100 μm diameter, for example, has the volume 10^8 times larger than the volume of original latent track.

The geometry of track etching is dictated in the simple case by the simultaneous action of two etching processes:

- The chemical dissolution along the particle track at a constant linear rate.
- Constant and isotropic general attack on the surface of the etched track at a lesser rate.

Homogeneity of the track detector and absence of polycrystallinity are the track-etch requirements. The track etching in a given substance can be affected by the choice of the etchant, its concentration, the temperature of chemical attack and the orientation of the attacked surface. The amount of chemical change depends both on the total quantity of radiation energy available and on the rate at which energy is deposited. The modifications in registration characteristics are attributed to structural changes produced by deposited doses. Two competing processes account for the structural changes. The cross-linking of the polymer molecule reduces the dissolution rate whereas chain rupture or scission enhances degradation and, thus, increases the etching rates (Zamani and Charalambous, 1985; Singh and Singh, 1988). In the last few years, a lot of work has been done to characterise and improve track detectors for better detection sensitivity (Mishra et al., 1999) as well as charge and energy resolutions. The nuclear track technique is quite versatile,

simple and accurate (Dwivedi, 1991). The importance of latent tracks lies in the fact that they are the characteristic signatures of the charged particles producing them. The shape of the etched track is formed as a result of competition between bulk etch-rate and track etch-rate. Polyallyldiglycol carbonate (PADC) belongs to the polyen of the type $-CH_2-CHR-$ having the diethyleneglycol carbonate links which belong to polyester. The structure of PADC is characterised by two main parameters: 1. The concentration of effective diethylene dicarbonate cross-links which, actually join two polyallyl chains and

2. The average length of polyallyl chains.

Both parameters contribute to overall density of cross-links in PADC networks (Ahmed and Stejny, 1991). All polymers containing the ester functional group in their molecule can be written as:

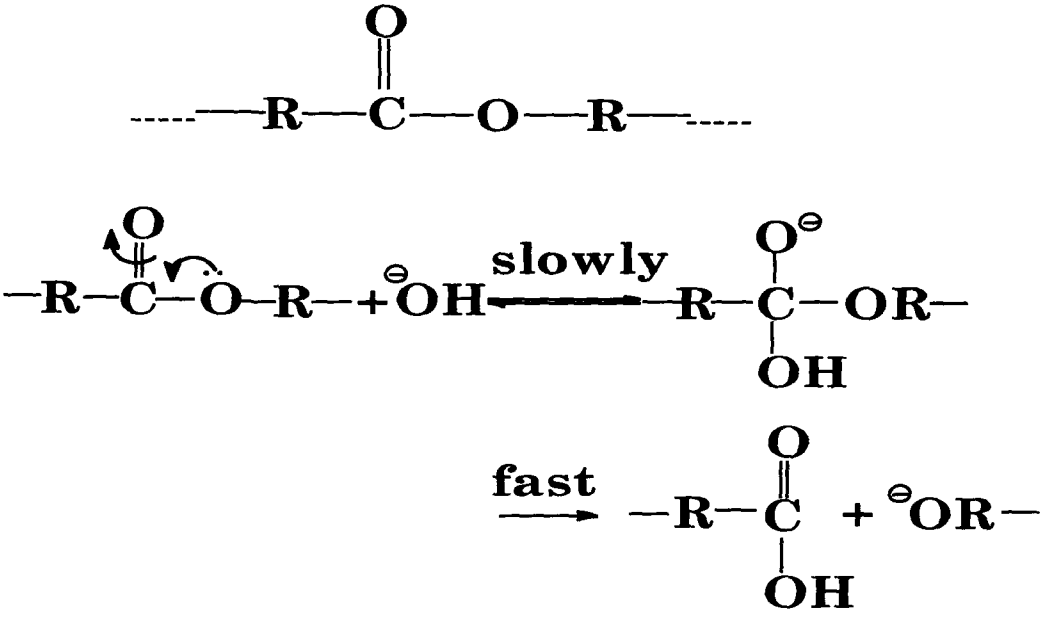

Such polymer is capable to alkali hydrolysing reaction by the above mentioned mechanism. PADC is essentially one macromolecule with less positive density and stronger space shielding effect. Therefore it is insoluble and not easily amenable to alkali hydrolyse. Due to this, the bulk etching-rate of this polymer is less compared to that of other detectors.

PADC is a highly sensitive track recording plastic. It is a thermoset polymer that does not cross-link upon irradiation and is susceptible to interfacial degradation by a convenient etchant which make it an ideal polymer detector. Their amorphous nature and radiation sensitivity further enhance the track detection property (Ghosh et al., 1994). It is about 100 times more sensitive than polycarbonate.

Earlier studies indicate a modification in track registration properties of PADC on exposure to high gamma dose (Frank and Benton, 1970; Akber et al., 1980; Zamani et al., 1986; Portwood and Henshaw, 1986; Sharma et al., 1991; Sinha et al., 1997; Abu-Jarad et al., 1997; Sinha and Dwivedi 1998). The effects of Co-60 gamma rays and 25 MeV pulsed electrons have been investigated on PADC and the bulk etch-rate was found to be increasing exponentially with the

absorbed dose (Oda et al., 1997). An increase in etch-rate values and the sensitivity of PADC has been observed for higher doses (5 x 10^5 Gy) of gamma rays, whereas a drop in these parameters is observed for lower gamma doses (Abu-Jarad et al., 1997).

In the present study, an attempt has been made to improve the detection and track registration efficiency of PADC by electron bombardment. The electron dose dependence on heavy-ion track registration properties of PADC, the most widely used polymer for charge detection, has been investigated. The surface damage was also analysed by scanning electron microscopy.

4.2. MEASURABLE TRACK PARAMETERS

BULK ETCH-RATE

An etchant attacks both the radiation-damaged area as well as the undamaged area. The increase of track-diameter with etching time gives a measure of the bulk etch-rate (V_G) along the surface plane, which is the rate of etching of the undamaged portion.

$$V_G = (d / 2t) \qquad \text{----------(4.1)}$$

where, d is the diameter of the track after etching time t.

TRUE TRACK LENGTH

The true track lengths can be calculated from measured projected track lengths using the formulations as follows:

The true track length,

$$L = (l / \cos\varphi) + (V_G t / \sin\varphi) - V_G (t - t_C) \quad \text{---------(4.2)}$$

where, l is the projected track length as observed by microscope,

φ is the angle of irradiation,

$(V_G t / \sin\varphi)$ is the surface etching correction,

t is the etching time,

t_C is the complete etching time that corresponds to a fixed value of track diameter which is independent of temperature of a given etchant and dielectric (Dwivedi, 1997),

$V_G(t-t_C)$ is the over-etching correction .

TRACK ETCH-RATE

The linear rate of chemical attack along the track is termed as the track etch-rate (V_T). It depends on the amount of damage located in the track core region and, hence, on the properties of the track forming material. V_T can be obtained by measuring the track length increase at different etching times. If over a small etching time period Δt, the increase in track length is ΔL, then

$V_T \cong \Delta L / \Delta t.$ ---------(4.3)

ETCHING RESPONSE

The ratio of V_T / V_G is the etching response of the detector. The larger its value, the better is the track developing efficiency of the detector.

CRITICAL ANGLE OF ETCHING

Critical angle of etching is defined as the angle at or below which the damage trail of an impinging particle is not detectable. If V_T is a varying function of etching time, the critical angle of etching θ_C is given by:

$\theta_C = \sin^{-1} (V_G / V_T).$ -------(4.4)

Critical angle, in turn, controls the efficiency of the detector. Moreover, it puts a limitation to the maximum projected track-lengths.

DETECTION EFFICIENCY

The detection efficiency of the detector may be defined as the ratio of number of tracks created to the number of impinging particles. It depends on the angle of incidence of the particles on to the detector. It can be calculated using the formula:

$\eta = 1 - \sin \theta_C$ -------(4.5)

4.3. EXPERIMENTAL ASPECTS

4.3.1. *Preparation of the targets*

PADC samples (composition: $C_{12}H_{18}O_7$, density: 1.32 $g.cm^{-3}$) of sizes (2x2) cm^2 were cut from commercially available sheets (thickness $\approx$ 1.5 mm), manufactured by Homalite Corporation, Wilmington, Del. (USA). After removing the surface protective layers, these detector plates were washed thoroughly with soap solution and then with deionised water to remove surface contamination. The cleaned samples were then dried inside vacuum desiccator.

4.3.2. *Irradiation and cooling*

Irradiation of the targets was done by 2 MeV electron from an electron generator at the Hahn-Meitner Institute, Berlin. The electron beam was allowed to pass through a collimator and was allowed to fall on the target placed at a distance of 2 metres from the collimator. The dose of 2 MeV electron was varied to carry out a dose dependent study. The doses used were 2 kGy, 23 kGy, 46 kGy, 93 kGy, 139 kGy, 186 kGy and 235 kGy. Irradiated samples were allowed to cool for about 24 hours. The samples were then preserved in plastic boxes.

4.3.3 *Exposure to 140 MeV ^{28}Si*

PADC detectors pre-irradiated to different doses of a 2 MeV

electron beam, were again exposed to well collimated beam of ^{28}Si ions with an initial energy of 140 MeV. The beam was allowed to fall on the gold foil scatterer of thickness 3μm and the optimum flux of ^{28}Si was measured to be 10^5 ions.cm^{-2}.sec^{-1}. The current measured by the Faraday cup on the scatterer during irradiation was 0.8 pnA. The irradiation was done in the 20° port of the General Purpose Scattering Chamber (GPSC) of the 15 UD Pelletron Accelerator at the Nuclear Science Centre, New Delhi. The scattered beam was allowed to fall at an angle of 45° on the targets mounted on a specially designed zig-zag ladder. The irradiation geometry has been illustrated in Fig.4.1. After irradiation, the samples were allowed to cool and then were stored in plastic boxes.

4.3.4. *Chemical treatment*

The samples were washed thoroughly in lukewarm soap solution to avoid non-uniformity in etching due to surface contamination. Then the cleaned samples were etched in 6 N NaOH solution at an etching temperature of 55°C. Successive etching was performed till the tracks were completely etched. After every etching, the samples were washed in running water and dried under vacuum.

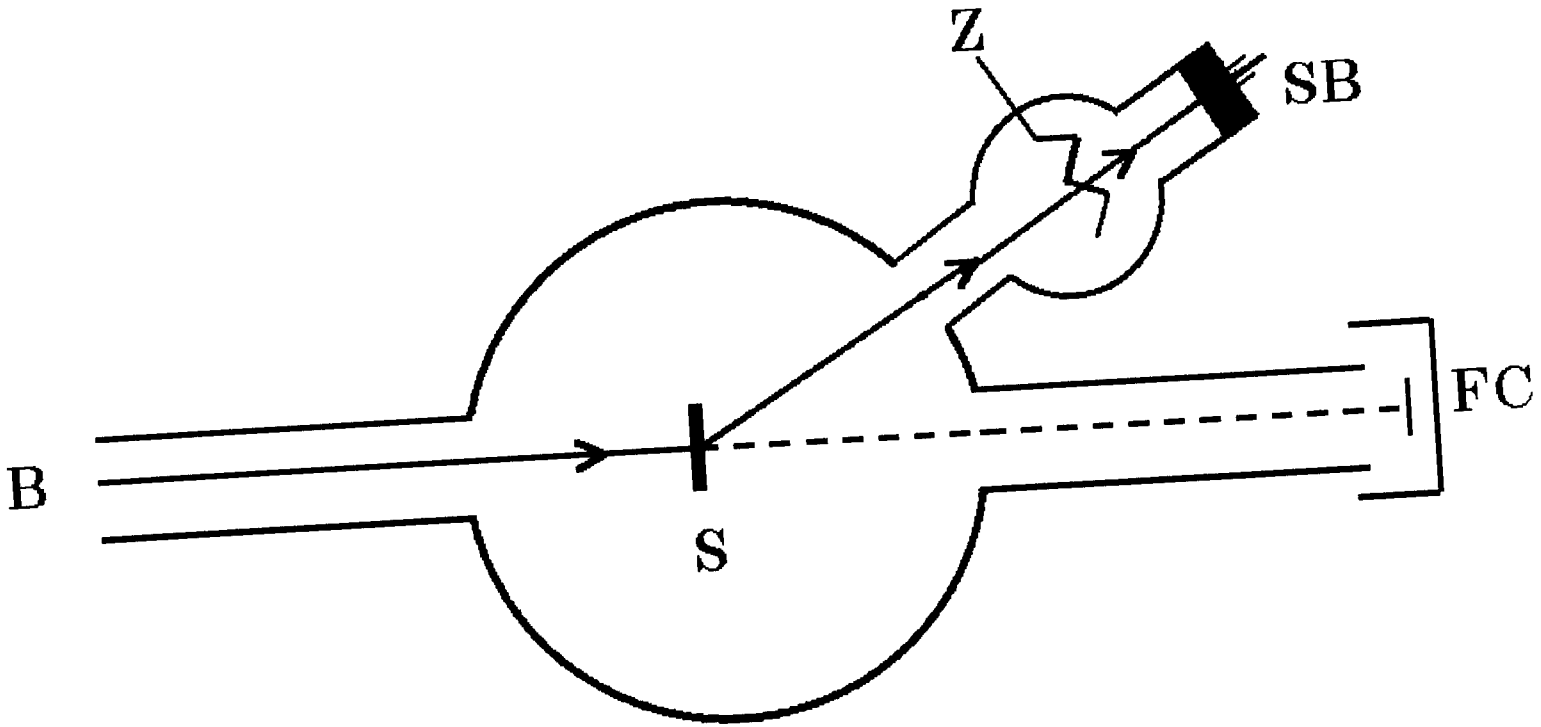

B: ^{28}Si beam
S: Gold scatterer
SB: Surface barrier detector
FC: Faraday cup
Z: Zig-zag ladder

Fig. 4.1. The irradiation geometry of the General Purpose Scattering Chamber.

4.3.5. *Measurement of track parameters*

The track parameters were measured by Leitz optical microscope at a magnification of 625x. The diameters of 50 Silicon ion tracks were measured in each detector to find out the most probable track-diameters at different etching times. The track lengths and the corresponding track-diameters were measured to an accuracy of ± 1.12μm. The bulk etch-rate (V_G) were calculated from the slope of the plot between silicon ion track diameters versus etching time. After every successive etching, the track-lengths were measured at random all over the detector surface to average out the effects due to non-uniformity of the targets. The true maximum etchable track-lengths were then calculated from projected track lengths. The track etch-rate (V_T) was calculated from the slope of the plot between silicon ion track lengths versus etching time. The errors associated with etch-rate measurement lies between 0.3 to 0.6μm/h.

4.3.6. *Scanning electron microscopy of the etched samples*

The etched samples were washed thoroughly in running water and then dried. Gold plating of all the samples was done by Ion Sputter JFC-1100. The gold coating was applied for 15 minutes under vacuum at 10 mA and 1 kV conditions. The approximate thickness of

the gold plating was 150 nm. Gold plating was done to make the polymer surface conducting. After 15 minutes the system was allowed to cool and the samples were taken out from the chamber. Scanning electron microscopy of these uniformly gold coated samples were done by a JSM-35 CF Scanning electron microscope under complete vacuum conditions. The surface damage was studied by the photo-micrographs of the samples.

4.4. RESULTS AND DISCUSSION

The silicon track diameters were found to be an increasing function of dose. V_G of PADC as the function of electron dose is shown in Fig. 4.2. Though all PADC samples were irradiated to ^{28}Si under similar conditions, yet their bulk etch-rates were different. The bulk etch-rate of PADC pre-irradiated to 235 kGy dose of 2 MeV electron was found to be nearly 4 times higher than that of pristine PADC which is not irradiated by electron as shown in Table 4.1.

Electron irradiation has promoted chain-scissioning, thereby, increasing the V_G and converting them into rapidly etchable materials.

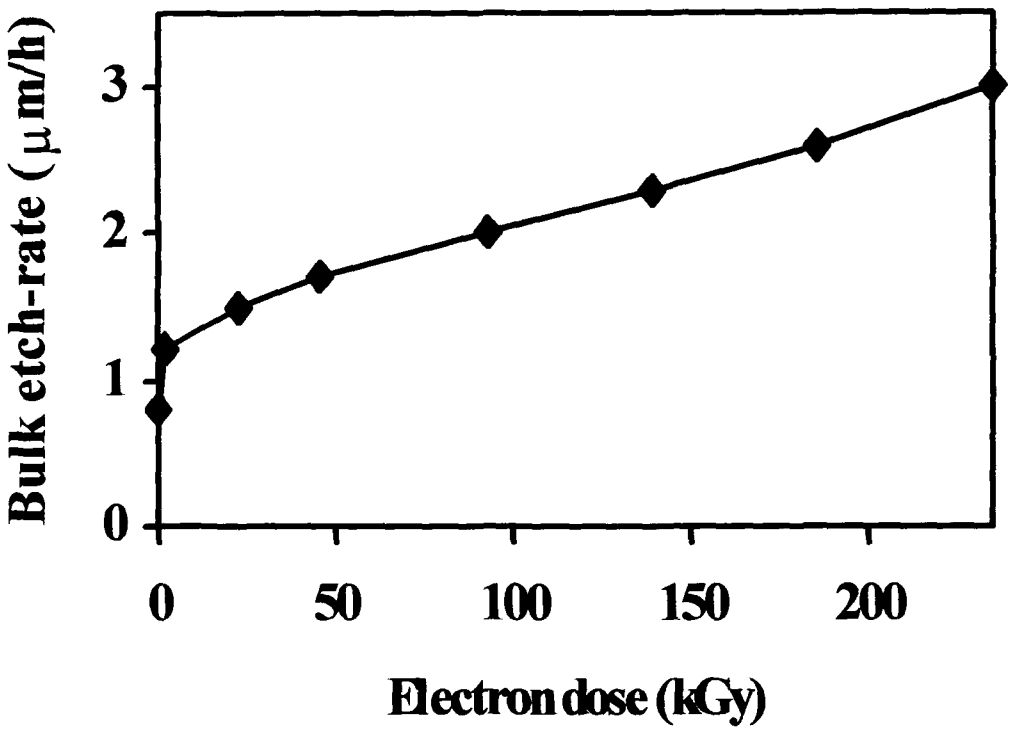

Fig. 4.2. Variation in bulk etch-rate of PADC with electron dose.

As the particle slows down, its ionisation rate increases. The track etch-rate (V_T) increases with ionisation rate. Energy loss rate slightly increases along track trajectory. Therefore, increase in V_T is probable with increasing etched track length (Kocsis et al., 1997). The track etch-rate was also found to be increasing with increase in electron dose as shown in Fig. 4.3.

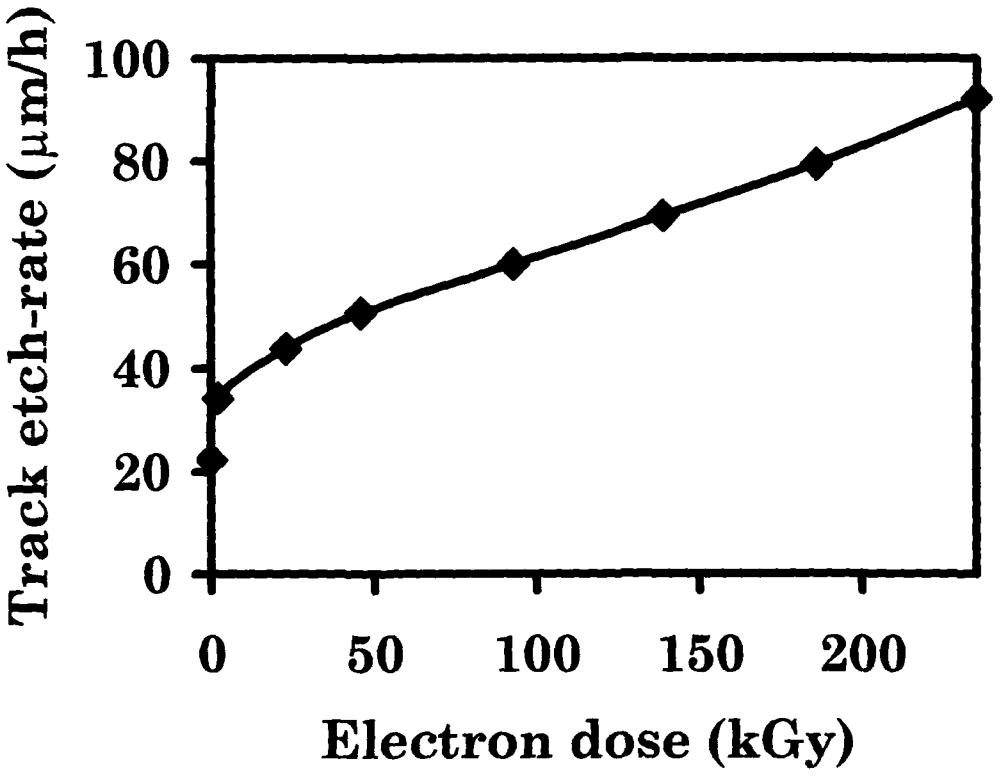

Fig. 4.3. Variation in track etch-rate of PADC with electron dose.

The etching response is the etch-rate ratio V_T/V_G, which was found to increase with increase in electron dose as shown in Table 4.1. Variation of etching response in PADC with electron dose is shown in Fig. 4.4. The etching response is also known as the etching sensitivity of the detector. The larger its value, the better is the track developing efficiency of the detector. The electron irradiation improved the sensitivity of the detector. In other words, electron irradiation can be used to sensitise the detector.

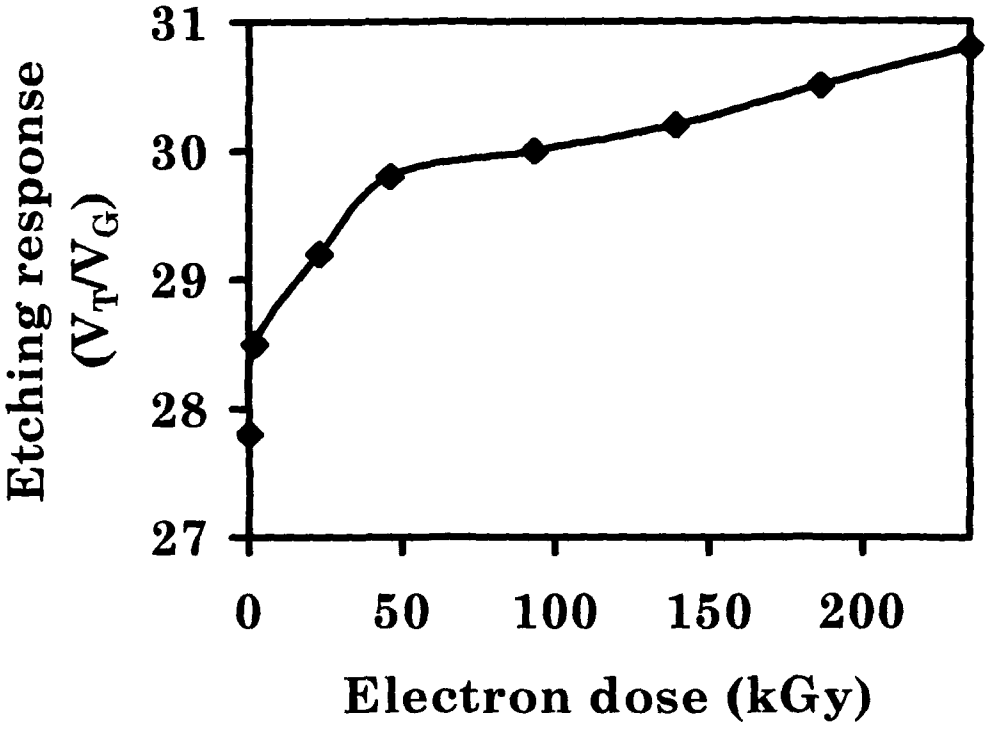

Fig. 4.4. Variation of etching response of PADC with electron dose.

The critical angle of etching, (θ_C) was found to decrease with electron dose as evident from Table 4.1. The cone angles of etched tracks are bigger for detectors having higher values of critical angle. The detection efficiency of the detector was improved by increasing the electron dose on PADC, as shown in Table 4.1.

Table 4.1. Variation of bulk etch-rate (V_G), track etch-rate (V_T), etching response (V_T/V_G), critical angle of etching (θ_c) and detection efficiency (η) of PADC with electron dose.

Electron Dose (kGy)	V_T (μm/h)	V_G (μm/h)	V_T/V_G	θ_c (degrees)	η
0 (Pristine)	22.2	0.8	27.8	2.1	0.96
2	34.2	1.2	28.5	2.0	0.96
23	43.8	1.5	29.2	1.96	0.97
46	50.6	1.7	29.8	1.92	0.97
93	60.0	2.0	30.0	1.91	0.97
139	69.5	2.3	30.2	1.90	0.97
186	79.4	2.6	30.5	1.88	0.97
235	92.3	3.0	30.8	1.86	0.97

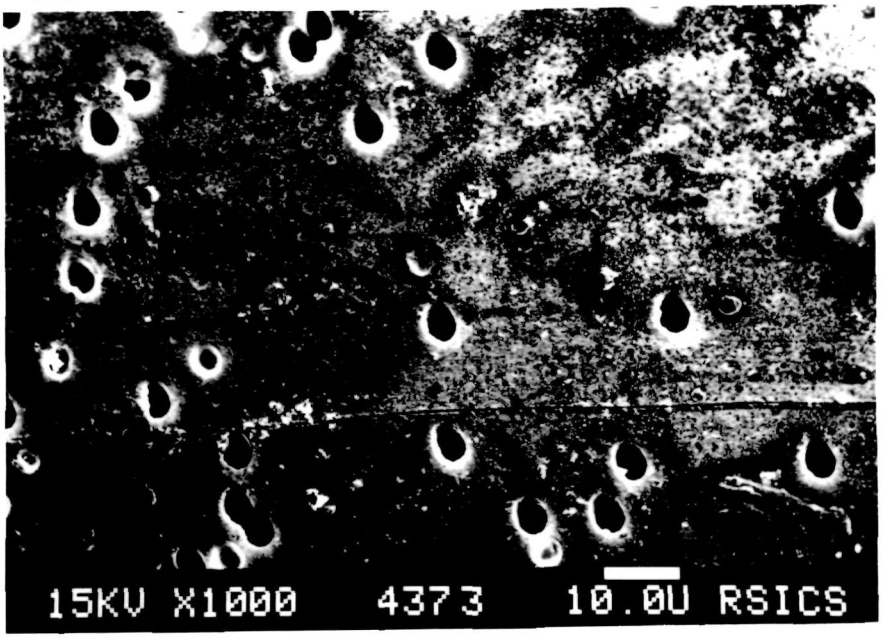

a

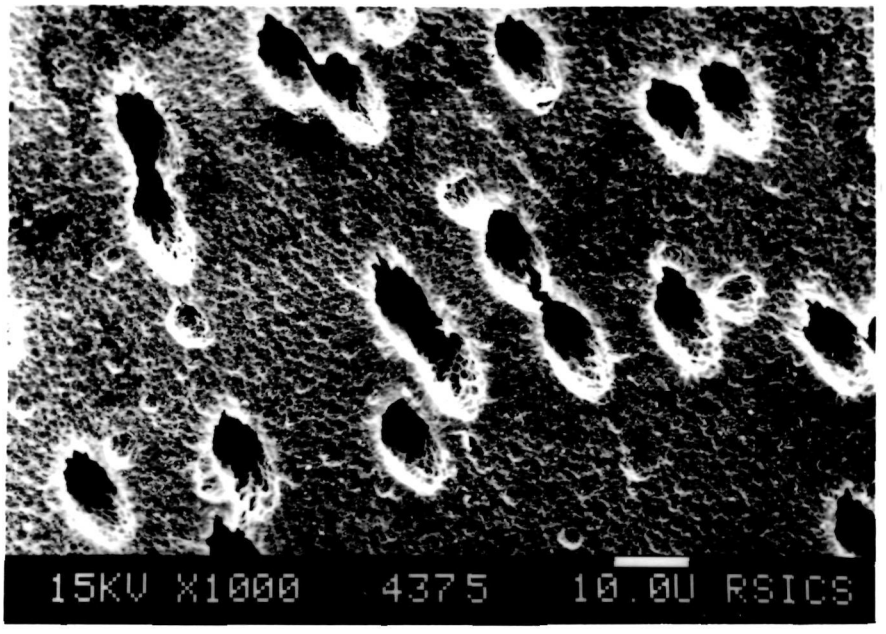

b

Fig. 4.5 a. ^{28}Si tracks in pristine PADC

b. ^{28}Si tracks in electron irradiated PADC (23 kGy).

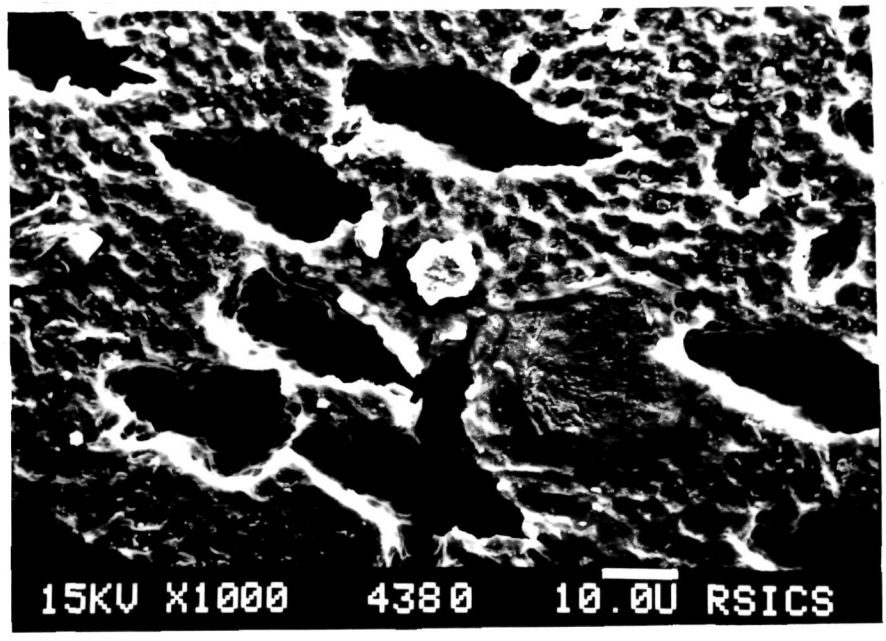

c

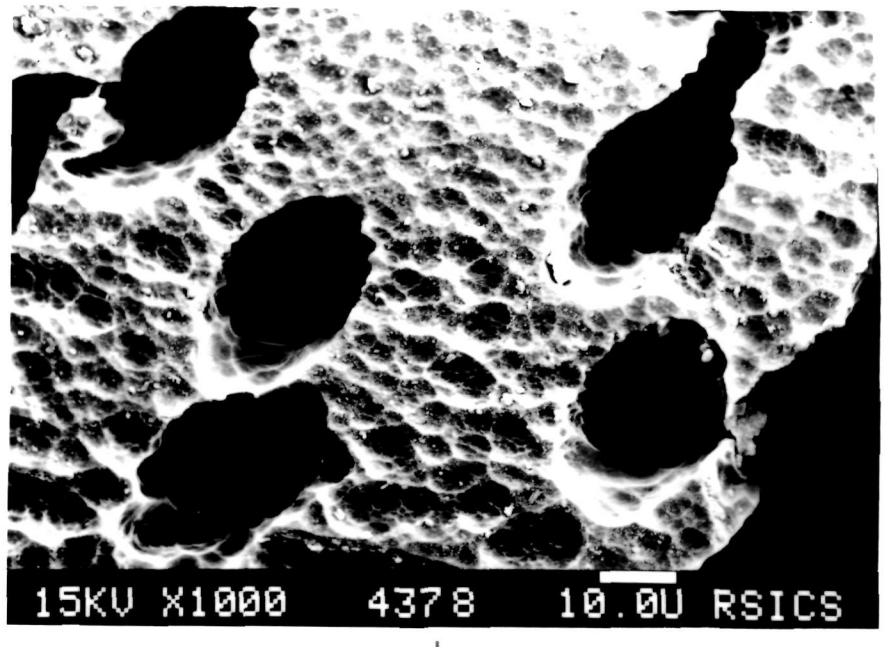

d

Fig. 4.5 c. ^{28}Si tracks in electron irradiated PADC (139 kGy).

d. ^{28}Si tracks in electron irradiated PADC (235 kGy).

The scanning electron micro-graphs of the samples after complete etching, as shown in Fig.4.5, revealed that the diameters of Silicon tracks were maximum for the PADC pre-irradiated to 235 kGy dose of 2 MeV electron. The etched ^{28}Si tracks are of larger diameters in the pre-electron irradiated samples. In the pristine sample, it was observed that the surface other than the etched tracks was smooth. But, the sample surface other than the tracks, showed maximum damage in case of electron irradiated samples. This extra damage was caused by electron irradiation. It could also be observed from the photomicrographs that the portion of the sample other than the tracks had suffered maximum damage in the 235 kGy dose electron irradiated sample.

4.5. CONCLUSION

The dependence of track parameters on different doses of 2 MeV electrons was studied. The electron irradiation has promoted chain-scissioning in PADC, which in turn affected the etch-rates of PADC detectors. Bulk etch-rate and track etch-rate were directly related to electron dose. The bulk etch-rate of PADC irradiated to 235 kGy dose of electron was found to be 4 times higher than that of pristine PADC.

The electron irradiation made the PADC easily etchable. Moreover, the PADC irradiated by 235 kGy electron dose required a comparatively less time for complete etching. Electron irradiation improved the etching response and the detection efficiency of the detector. Thus, it can be concluded that, the heavy-ion track registration capacity of the PADC can be improved by pre-irradiating it with electrons. In other words, the electron irradiation can be used to sensitise the detector, PADC.

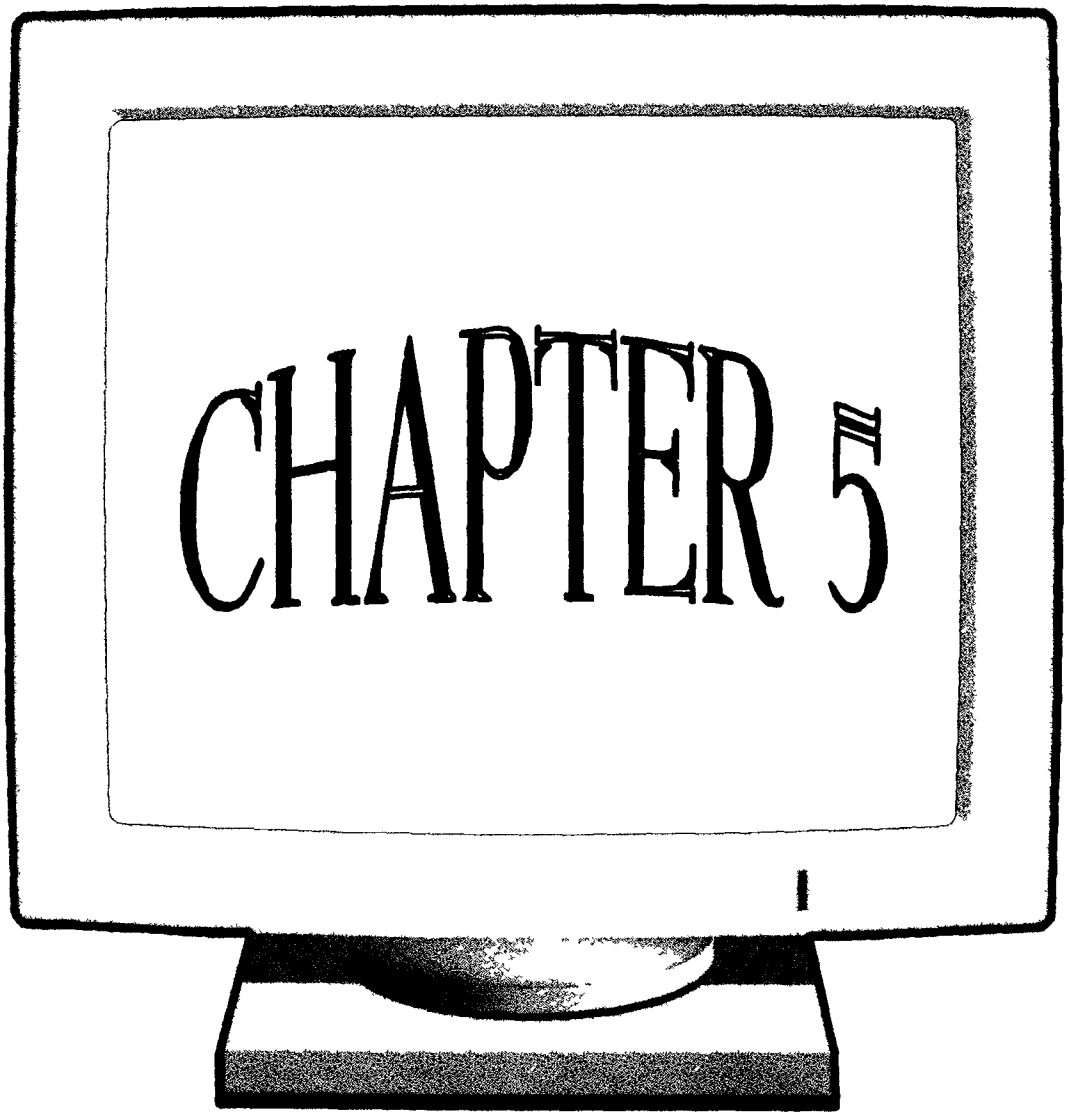
CHAPTER 5

CHAPTER 5

MODIFICATION OF PADC THROUGH ELECTRON-TARGET COLLISION

5.1. INTRODUCTION

In a passage of an initially homogenous beam of electrons through a target, the apparent straggling is pronounced by scattering of electrons into different directions, giving rise to different path-lengths of electrons traversing the same thickness of the absorber. The electrons are deflected much more readily than heavier particles by which imprecision can be introduced in measuring the thickness of the absorber needed to stop the electrons of a given energy (Beiser, 1997). When compared with heavy charged particles, fast electrons lose energy at a lower rate and follow a more torturous path through the absorbing materials. Nuclear scattering is responsible for most of the large angle deflections, although energy-loss is caused almost entirely by interactions with electrons. Electron interaction with matter has

some peculiarities because of its low mass and the moving electrons are identical with atomic electrons from which the greatest part of the energy of the particles is transferred under the decelerating action of Coulomb force (Tayal, 1992).

The energy-loss per unit path-length, -dE/dx, for a heavy particle with charge ze, moving at a velocity v << c is given by (Klimov, 1975):

$$-\frac{dE}{dx} = \frac{e^4}{4\pi\xi_o{}^2 m}\frac{z^2}{v^2} N Z \ln\frac{m v^2}{2 I \sqrt{e/2}} \qquad \text{-------(5.1)}$$

where,

m is the mass of the target material,

ξ_o is the permittivity of vacuum = 8.85×10^{-12} F/m,

NZ is the number of atoms per unit volume of the target material

$= \rho N_A (Z/A)$,

ρ is the density of the target material,

N_A is the Avagadro's number = 6.023×10^{23} mol^{-1},

A is the atomic weight of the target,

Z is the atomic number of the target,

I is the mean excitation energy of atoms of the medium $\approx$ 13Z eV.

Since energy-loss by ionisation varies approximately as $1/v^2$, –dE/dx is much smaller for electrons (whose velocity is higher for a

given energy) than for heavy particles at low and moderate energies (Ehrharat, 1984). Electrons with kinetic energy greater than 0.01 MeV are relativistic particles having low ionisation losses. The specific energy-loss by relativistic electrons is determined by the expression (Spinks and Woods, 1990):

$$-\frac{dE}{dx}=\frac{e^4 NZ}{8\pi\xi_o{}^2 m_e v^2}\left\{\ln\frac{m_o v^2 E}{2I^2(1-\beta^2)}-\left(2-\sqrt{1-\beta^2}-1+\beta^2\right)\times\ln 2+1-\beta^2+\frac{1}{8}\left(1-\sqrt{1-\beta^2}\right)^2\right\}$$

--------(5.2)

where,

E is the kinetic energy of the electron,

e is the elementary charge = 1.6 x 10^{-19} C,

m_o is the rest mass of the electron = 9.1 x 10^{-31} kg,

v is the velocity of the electrons,

β is v/c,

c is the velocity of light,

Z is the atomic number of the stopping material.

At lower velocities, β→0, this relation reduces to eqn. (5.1)

When v→c, β→1,

$$-\frac{dE}{dx}=\frac{e^4 NZ}{8\pi\xi_o{}^2 m_o c^2}\left(\ln\frac{E^3}{2m_o c^2 I^2}+\frac{1}{8}\right)$$

---------(5.3)

Energy-loss by emission of radiation is dominant for high energy electrons (>1 MeV). These radiative losses take the form of 'Bremsstrahlung' or braking electromagnetic radiation, which can emanate from any position along the electron track. An electron passing by the target nucleus experiences a Coulomb force and is deflected. The deceleration of the charged particle results in the emission of electromagnetic radiation known as 'Bremsstrahlung' (Sorensen, 1996). Thus, slowing down of electron in the nuclear field is accompanied by the emission of γ-rays with energy equal to the energy lost by the electron and can be any value down to the value of the initial kinetic energy of the electron. The probability of energy emission during the heavy ion interaction is 10^6 to 10^7 times lower than during electron deceleration. Bremsstrahlung is an important means of energy-loss only for electrons where $(z/m_e)^2 \approx 3\text{x}10^6$, with z and m_e being the charge and mass respectively of the incident electron.

The intensity of Bremsstrahlung at a given energy of the incident particle is directly proportional to $(z/m_e)^2 Z^2$, where Z is the charge of the target nucleus. Thus, in heavy materials such as Lead (Pb), the radiation loss becomes appreciable even at 1 MeV.

The probability of emission of Bremsstrahlung increases with energy of the electron beam. Bremsstrahlung predominates over ionisation at high energies and in heavy substances. Total linear stopping power for electrons is the sum of the collisional and radiative losses. The ratio of energy-loss by radiation to energy-loss by ionisation in an element of atomic number Z is approximately equal to EZ/800, i.e.,

$$\frac{\left(\frac{dE}{dx}\right)_{bremsstrahlung}}{\left(\frac{dE}{dx}\right)_{ionisation}} \cong \frac{EZ}{800} \qquad \text{---------(5.4)}$$

In lead, the rate of energy-loss by bremsstrahlung becomes equal to that by ionisation for electron of energy ~10 MeV, whereas in air bremsstrahlung remains small until electron energy reaches above ~100 MeV.

In the present work, the effect of 2 MeV electrons on Polyallyl diglycol carbonate (PADC), passing through three different metal targets viz. Lead, Gold and Molybdenum was studied.

5.2. EXPERIMENTAL ASPECTS

5.2.1. *Preparation of the target stacks*

PADC samples (composition: $C_{12}H_{18}O_7$, density: 1.32 g.cm^{-3}) of sizes (2x2) cm^2 were cut from commercially available sheets (thickness $\approx$ 1.5 mm), manufactured by Homalite Corporation, Wilmington, Del. (USA). After removing the surface protective layers, these detector plates were washed thoroughly with soap solution and then with deionised water to remove surface contamination. The cleaned samples were then dried inside a vacuum desiccator.

Three different types of metal foils were used for preparing the target stack. These were Lead foils (Z = 82, Thickness: 125 μm, density: 1.35 g.cm^{-3}), Gold foils (Z = 79, Thickness: 3 μm, density: 9.32 g.cm^{-3}) and Molybdenum foils (Z = 42, Thickness: 25 μm, density: 10.22 g.cm^{-3}). The target stacks were prepared placing six metal foils and five PADC samples alternately as shown in Fig. 5.1. For three metal foils three different target stacks were prepared.

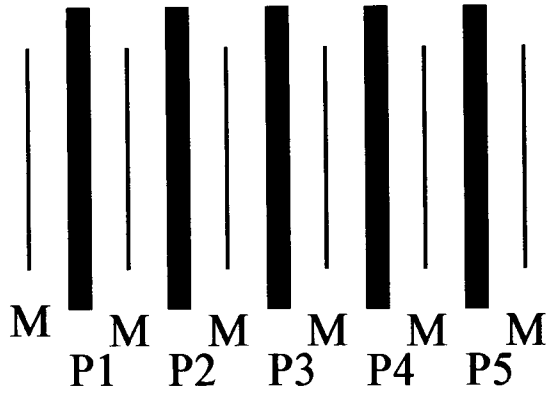

Fig. 5.1. Arrangement of metal foils (M) and PADC samples (P1, P2, P3, P4, P5) for each target stack.

5.2.2. *Irradiation and cooling*

Irradiation of the target stacks was done by a 23 kGy dose of 2 MeV electron beam from an electron generator at the Hahn-Meitner Institute, Berlin. The electron beam was allowed to pass through a collimator and was allowed to fall on the target stack placed at a distance of 2 metres from the collimator. Irradiated samples were allowed to cool for about 24 hours. The stacks were then taken and preserved in plastic boxes.

5.2.3. *Exposure to fission fragments*

The PADC samples were separated from the target stacks and small pieces of three PADC samples (P1, P3, P5) of each stack were further exposed to fission fragments from a ^{252}Cf source having a fission

activity of 5.7×10^3 s^{-1}. The PADC samples were mounted on a perspex holder kept at a distance of 1 cm from the source ^{252}Cf and exposed at an angle of 90°. An unstacked electron irradiated PADC was taken as pristine and it was also exposed to fission fragments in a similar manner. After irradiation, the samples were allowed to cool and then were stored in plastic boxes.

5.2.4. *Chemical treatment*

The samples were washed thoroughly in lukewarm soap solution to avoid non-uniformity in etching due to surface contamination. Then the cleaned samples were etched in 6N NaOH solution at an etching temperature of 55°C. Successive etching was performed till the tracks were completely etched. After every etching, the samples were washed in running water and dried in vacuum.

5.2.5. *Measurement of track parameters*

The track diameters of fission fragments were measured by Leitz optical microscope at a magnification of 625x. The bulk etch-rate (V_G) was calculated from the slope of the plot between normally incident fission-fragment track diameters (D_{ff}) versus etching time (t), using the track diameter method:

$$V_G = D_{ff} / 2t \qquad \text{.....(5.5)}$$

The error associated with the etch-rate measurements is ± 0.4 μm/h.

5.2.6. *Thermal analysis*

A simple automatic Perkin Elmer instrument was used for the thermal analysis of the 1st, 3rd and 5th PADC samples of each stack. The scanning rate for this instrument was adjusted to 20°C/min with nitrogen as flushing gas. The samples were crimped in small aluminium pans, weighed in a thermobalance and were scanned in the temperature range from 30°C to 600°C. The study of thermal stability was done with the help of thermogram, i.e., a plot of mass percent as a function of temperature which was obtained by the Perkin Elmer instrument. The error associated in recording the thermograms is ± 2°C.

5.3. RESULTS AND DISCUSSION

During the transition from one layer to another the cross-sections of electron scattering changes abruptly and the characteristics of electrons, both transmitted and reflected, depends upon the chemical composition of the layers (Balashov, 1999; Idoeta, 2000). The passage of electrons through the metallic target is accompanied by scattering and absorption, owing to the energy losses in collisions. The depth-dose distribution arises as a consequence of two processes:

energy-loss due to ionisation and excitation of target atoms and multiple scattering of electrons in the target. The stopping power depends on the atomic number and atomic weight of the target material. Both scattering and slowing down of electrons increase with increasing target-atom mass. The transmission coefficient of electrons for a target made of heavy atoms is less than for a target consisting of light atoms. The energy spectra of the transmitted electrons vary from almost Gaussian for small target thicknesses to a broad assymetric curve for large thicknesses. For the targets consisting of lighter atoms the number of low energy electrons in the spectrum decreases owing to reduction in generation of secondary electrons and weaker scattering. The maximum energy of the spectrum decreases too. The reflection coefficient is influenced both by a single large angle scattering and by multiple small angle scatterings. The heavier the target atoms, the higher is the number of singly scattered electrons. The reflected intensity increases with increasing thickness of the reflector except that for thickness greater than about one-third of the range of the electrons, saturation is achieved and further increase in thickness does not add to the reflected intensity. For generation of bremsstrahlung, the targets with high atomic number are used as a rule due to rapid increase of production cross-section with target

atomic number. The efficiency of conversion of kinetic energy to bremsstrahlung increases with increasing electron energy and with increasing charge of the target. Moreover, if thickness of the heavy layer increases, the emission coefficient of bremsstrahlung grows.

The electrons with kinetic energy 2 MeV are already relativistic. Ionisation-loss constitute the basic energy-loss mechanism of electrons moving with energy less than 10 MeV.

ENERGY-LOSS CALCULATION FOR LEAD

From eqn. (5.3), the energy-loss for lead can be derived as:

For Lead, $\frac{e^4 NZ}{8\pi\xi^2 mc^2} = 1.1 \text{ x } 10^{-11}\text{kg.m/s}^2$, $\left(\ln\frac{E^3}{2mc^2 I^2}+\frac{1}{8}\right) = -7.1577.$

Specific energy-loss by ionisation for lead was calculated to be,

$$-\frac{dE}{dx}=\frac{e^4 NZ}{8\pi\xi^2 mc^2}\left(\ln\frac{E^3}{2mc^2 I^2}+\frac{1}{8}\right) = -7.8735 \text{ x } 10^{-11} \text{ kg.m/s}^2.$$

Energy-loss by ionisation in lead foil of (125 μm) = 0.062 MeV.

Energy-loss by radiation of lead foil calculated from eqn.(5.4) was found to be approximately equal to 0.001 MeV.

ENERGY-LOSS CALCULATION FOR MOLYBDENUM

Similarly for Molybdenum, using eqn. (5.3) we get,

$$\frac{e^4 NZ}{8\pi\xi^2 mc^2} = 1.096 \text{ x } 10^{-11}\text{kg.m/s}^2, \left(\ln\frac{E^3}{2mc^2 I^2}+\frac{1}{8}\right) = -5.82.$$

Specific energy-loss by ionisation for Molybdenum was calculated to

be, $-\frac{dE}{dx}=\frac{e^4 NZ}{8\pi\xi^2 mc^2}\left(\ln\frac{E^3}{2mc^2 I^2}+\frac{1}{8}\right) = -6.379 \times 10^{-11}$ kg.m/s^2.

Energy-loss by ionisation in Molybdenum foil (25 μm) = 0.01 MeV.

Energy-loss by radiation by Molybdenum foil was found to be approximately equal to 0.0001 MeV.

ENERGY-LOSS CALCULATION FOR GOLD

For Gold, $\frac{e^4 NZ}{8\pi\xi^2 mc^2} = 1.898 \times 10^{-11}$kg.m/s^2, $\left(\ln\frac{E^3}{2mc^2 I^2}+\frac{1}{8}\right) = -7.085$.

Specific energy-loss by ionisation for Gold foil was calculated to be,

$-\frac{dE}{dx}=\frac{e^4 NZ}{8\pi\xi^2 mc^2}\left(\ln\frac{E^3}{2mc^2 I^2}+\frac{1}{8}\right) = -13.447 \times 10^{-11}$ kg.m/s^2.

Energy-loss by ionisation in Gold foil (3 μm) = 0.002 MeV.

Energy-loss by radiation of Gold foil was found to be approximately equal to 0.0003 MeV.

All the energy-loss data calculated for the three metallic foils is tabulated in Table 5.1. Total energy-loss is the sum of the energy loss by ionisation and that by radiation. As evident from the calculated energy-loss values, the maximum energy loss of 2 MeV electron has taken place when it passes through the lead foil. It is quite clear that, the energy-loss of the electron beam depends on the thickness of the

metallic foil. Owing to less thickness of the Gold foil, the energy-loss of electron beam was found to be low. The track diameters of the fission fragments from ^{252}Cf source in the PADC samples of the three stacks are tabulated in Table 5.2. The fission fragment track diameters in stacked PADC samples were found to be less than that in pristine PADC because in stacked PADC samples the amount of energy reaching the PADC samples was reduced due to energy-loss of electron.

Table 5.1. Energy-loss data calculated for 2 MeV electron beam passing through different metallic foils.

Metallic foil, Thickness (μm), and density ($g.cm^{-3}$)	Energy-loss by ionisation (MeV)	Energy-loss by bremsstrahlung (MeV)	Total energy-loss (MeV)
Lead, 125, 11.35	6.2×10^{-2}	0.1×10^{-2}	6.3×10^{-2}
Molybdenum, 25, 10.22	1.0×10^{-2}	0.01×10^{-2}	1.01×10^{-2}
Gold, 3, 19.32	0.2×10^{-2}	0.03×10^{-2}	0.23×10^{-2}

Table 5.2. Fission fragment track diameters in 1st (P1), 3rd (P3) and 5th (P5) PADC samples of the Lead, Molybdenum and Gold stack and that in pristine PADC.

Etching time (hours)	Fission fragment track diameters (μm)									
	Pristine	Lead stack			Molybdenum stack			Gold stack		
		P1	P3	P5	P1	P3	P5	P1	P3	P5
1.0	5.3	2.7	2.7	2.7	3.6	2.7	2.7	3.6	3.6	2.7
2.0	8.9	5.3	4.9	4.6	6.2	5.6	4.8	7.1	6.2	5.3
2.5	10.7	7.1	6.4	5.8	8.5	7.5	6.3	9.2	8.2	7.6
3.0	12.8	9.2	7.8	7.1	10.0	9.1	8.1	11.3	9.7	8.4
3.5	15.2	10.8	9.2	8.5	12.0	10.9	9.1	13.2	11.9	10.2

Among the stacked PADC samples, the track diameters were found to be maximum in the PADC of Gold stack because the energy loss by electrons was minimum for Gold foils. Thus, maximum energy has reached the PADC samples of Gold stack, resulting in increasing the bulk etch-rate probably due to chain-scission in PADC, as explained in Chapter 4. Again among all the PADC samples of the Gold stack, the diameters were found to be maximum in the 1st PADC

(P1) and were found to be gradually decreasing for 3rd and 5th PADC. The track diameters were found to be minimum for the PADC samples of the Lead stack because energy-loss was maximum in Lead foil. The track diameters in the 1st, 3rd and 5th PADC of all the stacks are shown in Fig. 5.2. The bulk etch-rate was calculated by using eqn. (5.5) and is tabulated in Table 5.3. The bulk etch-rate of pristine (stackless) PADC was found to be maximum, i.e., 2.2 μm/h.

Table 5.3. Variation of bulk etch-rate (V_G) of pristine along with the irradiated PADC samples (P1, P3, P5).

Sample	V_G (μm/h)
Pristine PADC (electron irradiated unstacked PADC)	2.2
P1 of Lead stack	1.5
P3 of Lead stack	1.3
P5 of Lead stack	1.2
P1 of Molybdenum stack	1.7
P3 of Molybdenum stack	1.5
P5 of Molybdenum stack	1.3
P1 of Gold stack	1.9
P3 of Gold stack	1.6
P5 of Gold stack	1.4

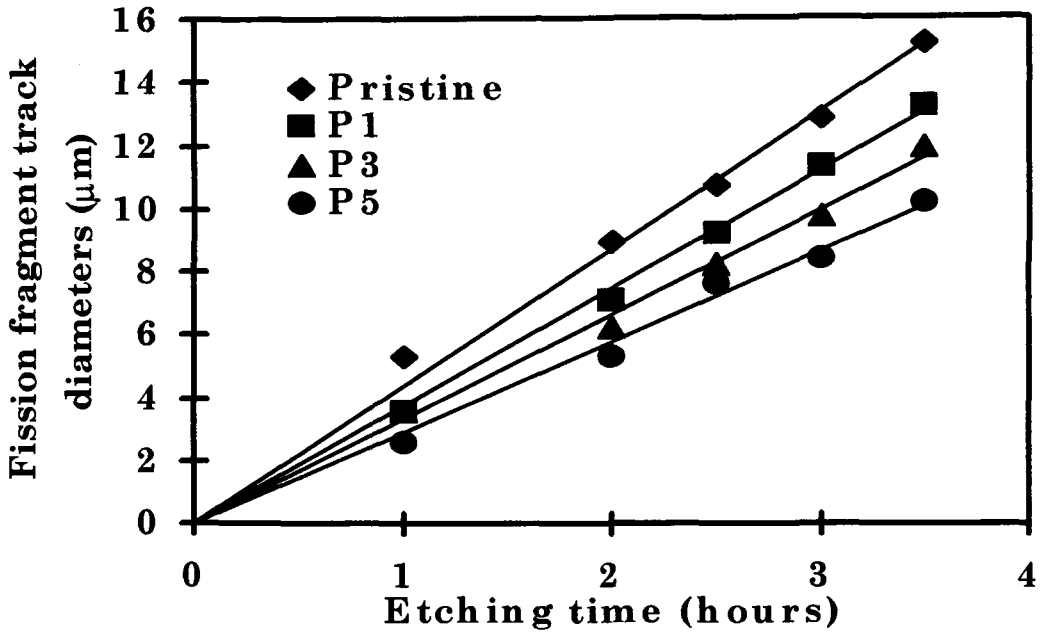

(I)

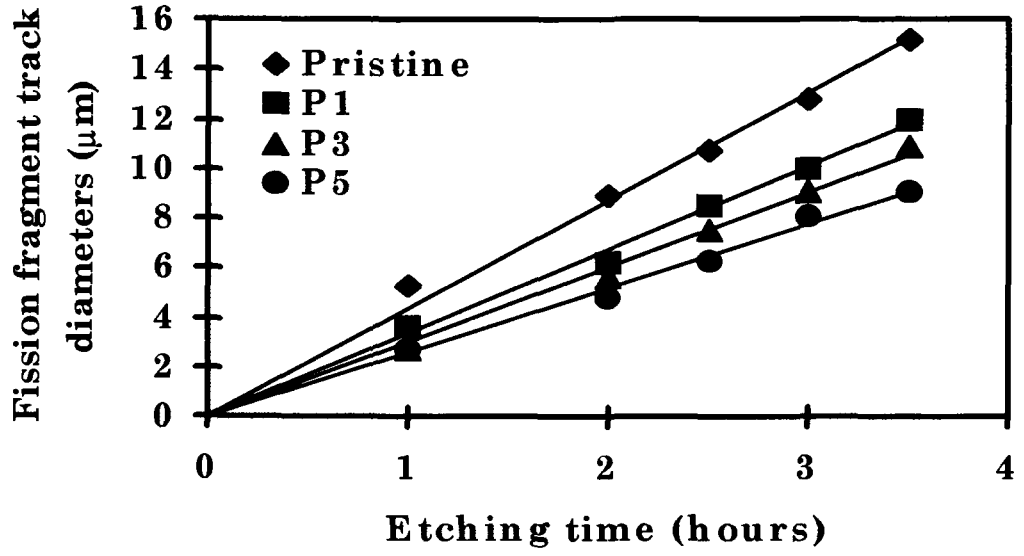

(II)

Fig. 5.2. The plot of fission track diameters versus etching time in 1st (P1), 3rd (P3) and 5th (P5) PADC samples along with the pristine PADC in
(I) Gold stack and (II) Molybdenum stack

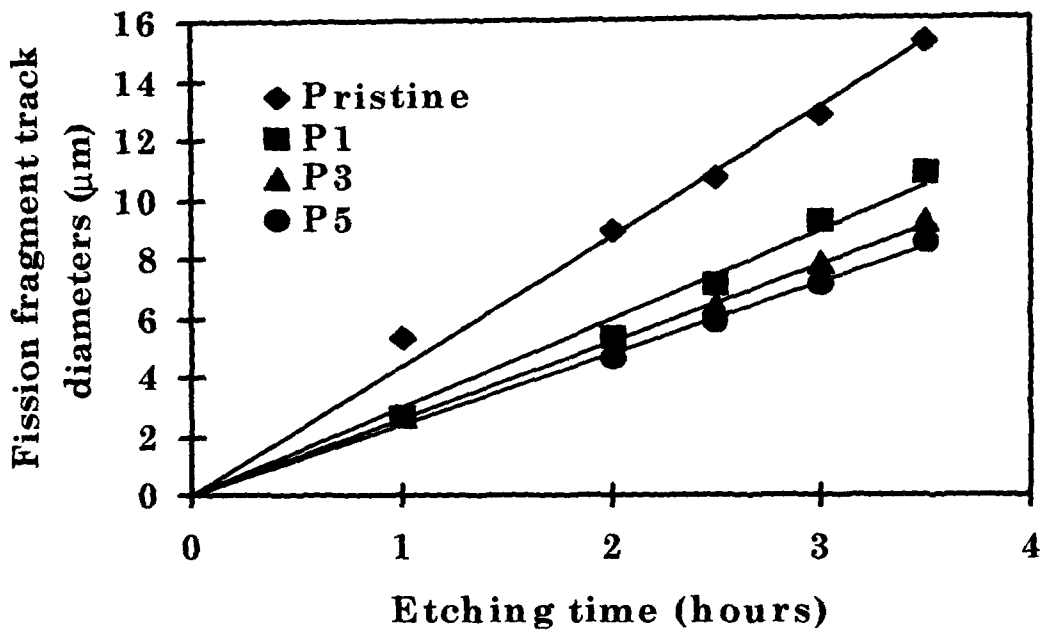

(III)

Fig. 5.2. The plot of fission track diameters versus etching time in 1st (P1), 3rd (P3) and 5th (P5) PADC samples along with the pristine PADC in (III) Lead stack

Among the stacked PADC samples, the maximum bulk etch-rate was found to be 1.9 μm/h for 1st PADC of Gold stack and the minimum was found to be 1.2 μm/h for 5th PADC of Lead stack. The energy-loss of electrons through Lead foil was maximum resulting in minimum bulk etch-rate. Thermal analysis of the samples showed that the pristine PADC was most stable. The pristine (stackless) PADC remained stable from up to 93°C. The 1st PADC (P1) of Gold stack was

least stable among all the stacked PADC samples. The bulk etch-rate of this PADC was maximum. This implied that the chain-scission mechanism is more prominent in this PADC, which in turn, indicated that more electron energy was incident on the sample.

In each stack, thermal stability increased with increase in the penetration depth of the electrons. The last PADC sample in each stack was most stable denoting that less energy was deposited in this sample. The data for the stable zone of all the samples have been compiled in Table 5.4. The thermograms for the 1st PADC samples of all the three stacks are shown in Fig. 5.3.

As it is evident from the thermogram that, due to maximum energy-loss by electrons for Lead, minimum electron energy was deposited on the 1st PADC of Lead stack in comparison to 1st PADC samples of other two stacks. So, the extent of chain-scission (as a function of the deposited energy) seems to be less in this sample (1st PADC of Lead stack), thus leading to its more stability than that of the 1st PADC samples of the other stacks.

Table 5.4. Thermal stability of the pristine PADC (P) along with that of the PADC samples (1st: P1, 3rd : P3 and 5th: P5) of different stacks.

Stack	Sample	Thermal Stability(°C)
---	Pristine (P)	30 - 93
Lead	P1	30 - 107
	P3	30 - 125
	P5	30 - 131
Molybdenum	P1	30 - 100
	P3	30 - 125
	P5	30 - 131
Gold	P1	30 - 95
	P3	30 - 122
	P5	30 - 130

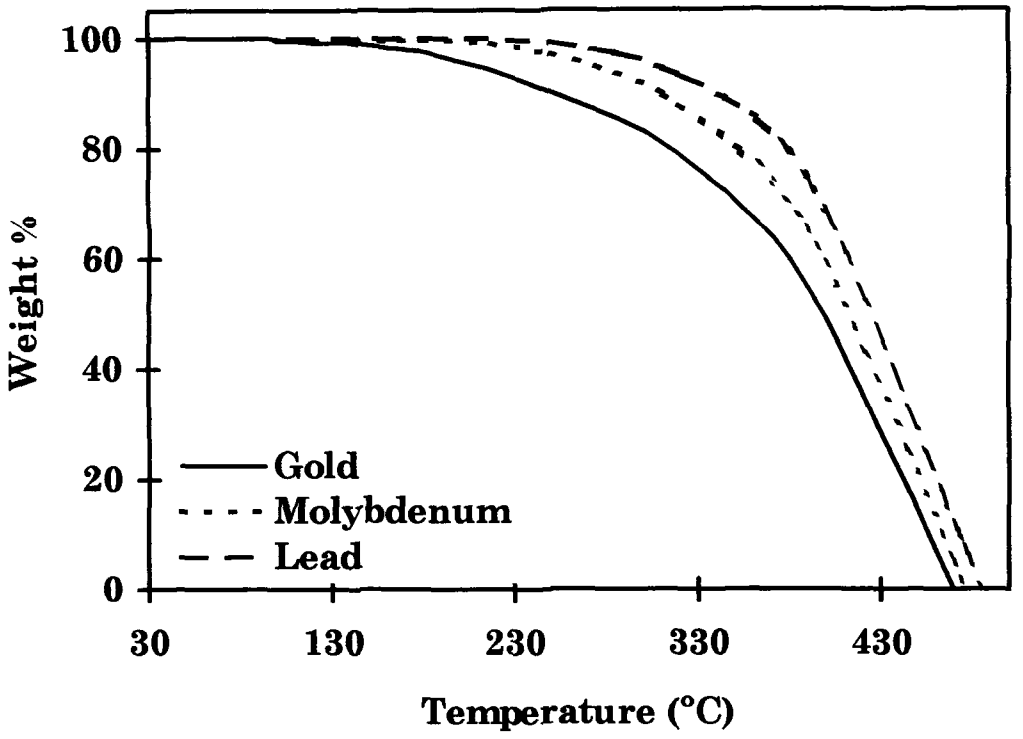

Fig. 5.3. The thermograms of the 1st PADC samples of all the three stacks (Gold, Molybdenum and Lead), showing their thermal decomposition behaviour.

5.4. CONCLUSION

2 MeV electrons, while traversing through a material medium loses energy through ionisation and radiative emission. The total energy-loss by the electron beam is the sum of the ionisation and radiation energy-loss. The energy-loss by electrons was found to be

dependent on the charge, mass, thickness and density of the target material. The energy-loss by electrons was found to be high for Lead foil because of its large atomic number and thickness. The energy-loss of electron while traversed through the Molybdenum foil was found to be more than the energy-loss, when it passed through Gold foil because, though the density and atomic number of Gold foil was more than that of Molybdenum, yet the thickness of the Gold foil was only 3μm. These results were further confirmed by track studies and thermogravimetric analysis. The fission track diameters in the 1st PADC samples of each stack were observed to be more than that in other PADC samples of the same stack. This is due to gradual energy-loss of the electron beam as it traverses deeper through the stack. The maximum energy was deposited in the 1st PADC samples of each stack and hence, the effect of chain-scissioning was relatively more, which resulted in faster bulk etch-rate. Among the 1st PADC samples of all the three stacks, the PADC of Gold stack was found to be having the highest bulk etch-rate due to minimum energy-loss of electron beam while passing through the Gold foil. The bulk etch-rate of the PADC of Lead stack was found to be minimum because of the maximum energy-loss by electron while traversing through the Lead foil. The thermal analysis of the PADC sample showed that the PADC

of Lead stack was comparatively more stable. This might be due to less energy deposition by the electrons, on the PADC sample because of maximum energy-loss of electron through the Lead foil. So, the PADC of the Lead stack is comparatively more thermally stable than the PADC samples of other two stacks.

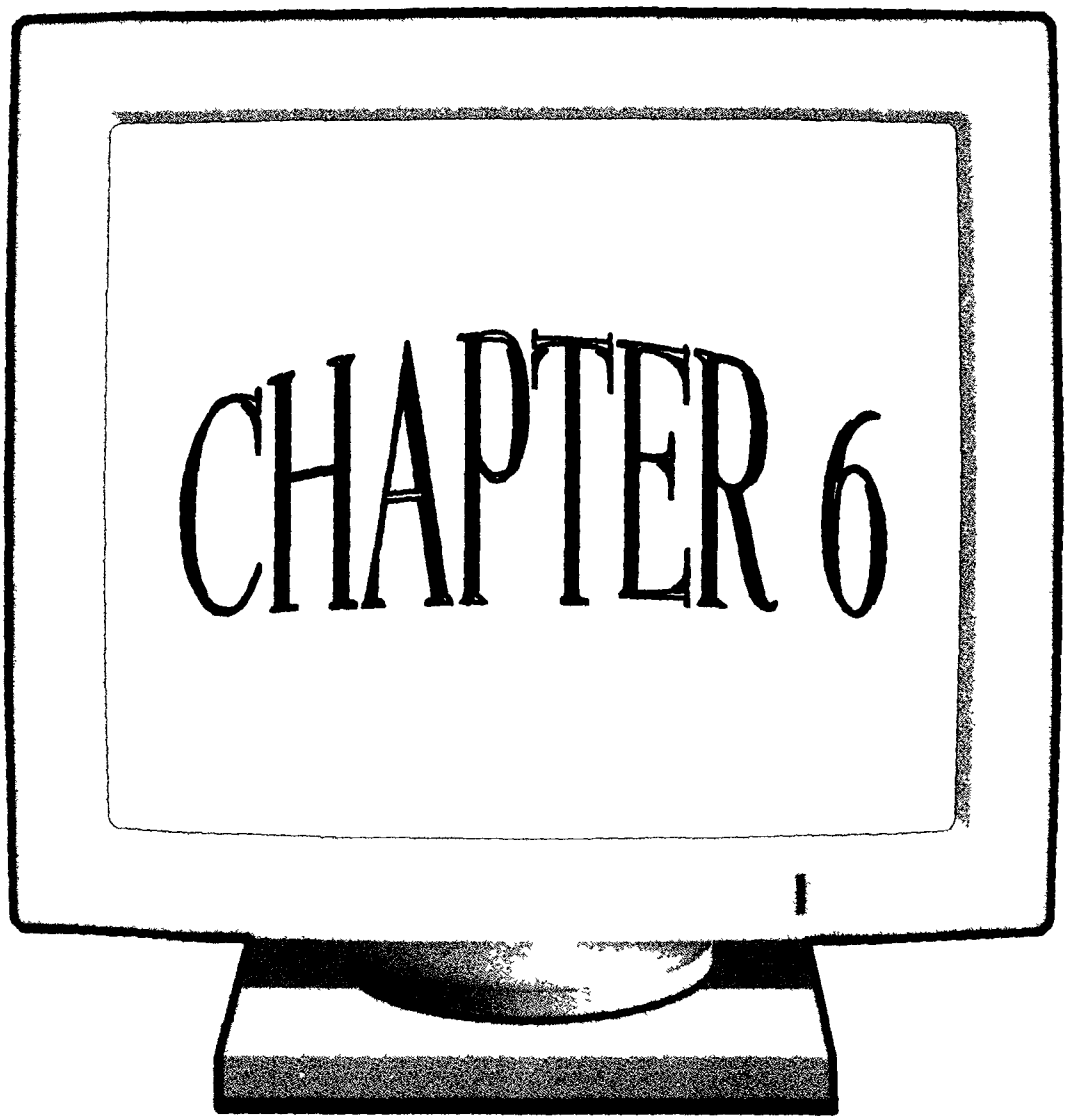
CHAPTER 6

CHAPTER 6

SUMMARY OF THE WORK AND FUTURE PERSPECTIVES

6.1. SUMMARY OF THE WORK

The widespread applications and technological importance of the polymers evoked us to induce some desirable modifications in their properties so as to enhance their applicability. The main challenge was to modify the polymers with low LET particles like electrons. In the preceding chapters, electron induced modifications in physical, chemical, structural and topological properties of some selected polymers have been studied by different characterisation techniques. The salient features of the present work are summarised polymer wise as follows:

6.1.1. *Dose dependent modification induced in Polyallyl diglycol carbonate (PADC) by 2 MeV electrons*

Modification in different properties of PADC has been studied as a function of 2 MeV electron-dose.

- A 14% decrease in optical band-gap from that of the pristine has been observed in the PADC irradiated by 235 kGy of electron.
- The optical band-gap was found to be an inverse function of electron dose. A relation has been derived to calculate the energy-gap for PADC irradiated to different electron doses:

  $E_g = -0.0021\ D + 3.6$,

  where, D is the electron dose in kGy

  E_g is the energy band-gap in eV.

  So, there is a possibility of decreasing the energy band-gap by bombarding higher doses of electron.
- The inter-chain separation was not affected by electron irradiation and no cross-linking was observed after the bond cleavage due to irradiation.
- Variation in transmittance was found to be less for higher doses of 2 MeV electron, which implies that it can be used as a reliable dosimeter for large doses of electron.

- The thermal stability of PADC could not be improved by electron irradiation because of chain-scission in the polymeric structure. Thermal stability was observed to be decreasing with increase in electron dose. No residual decomposition was observed in the electron irradiated PADC samples.
- The heat involved in the exothermic phase transition was found to be decreasing with increase in electron dose.
- Increase in dose of electron irradiation enhanced the amorphous nature of PADC.
- The electron irradiation promoted chain-scissioning in PADC, which in turn affected the etch-rates of PADC detectors.
- Bulk etch-rate and track etch-rate was found to be increasing with increase in electron dose. The bulk etch-rate of PADC irradiated to 235 kGy dose of electron was found to be 4 times higher than that of the pristine PADC.
- The track registration sensitivity and the etching response of PADC was improved by increasing the dose of electron irradiation.
- The heavy-ion track registration capacity of the PADC can be improved by pre-irradiating it with electrons. In other words, electron irradiation can be used to sensitise the PADC detector.

6.1.2. *Electron induced modification in Polypropylene*

The effect of 23 kGy of 2 MeV electron on PP has been studied and the following conclusions were drawn.

- The isotactic nature of PP was not destroyed due to electron irradiation.
- The increase in absorbance of CH_2 wagging vibration after electron irradiation indicated the increase in chain length of hydrocarbon due to addition of more CH_2 groups, which might be due to some cross-linking induced by electron irradiation in the polymer.
- An increase in thermal stability of PP was observed after electron irradiation, which can be attributed to pre-dominant cross-linking by electron bombardment.
- The increase in melting temperature due to electron bombardment has been attributed to secondary ion induced crystalline regions distributed inhomogeneously on the surfaces of strongly stressed interlamella and interspherolite spaces, characterised by considerably high values of mechanical surface energy.
- A broad region of crystallisation exotherms was observed in the case of irradiated PP.

- The increase in main peak intensity and emergence of new peaks after electron irradiation indicated an increase in crystallinity of the irradiated PP.
- The decrease in optical band-gap in the irradiated PP implies an increase in conductivity of the polymer, which has been also verified by A. C. conductance measurement.
- The surface roughness of PP was found to decrease after electron irradiation.

6.1.3. *Electron induced modifications in Polyethylene terephthalate*

The modifications induced 23 kGy dose of 2 MeV electron in PET are summarised as follows:

- Increase in absorbance of the characteristic bands in PET in the FT-IR region indicate the amorphisation of the polymer. The process of amorphisation was enhanced because of the irradiation of the samples in air.
- The presence of aromatic groups in the polymer structure accounted for the stability of the polymer.
- Amorphisation of the polymer indicated that PET underwent some chain-scission by electron bombardment.

- A decrease in thermal stability of the polymer was observed due to electron irradiation, which is due to chain-scission in the polymer.
- The melting temperature of PET was also decreased by electron irradiation.
- The shift in main peak of X-ray diffraction spectra and decrease in its intensity indicated the destruction of crystalline structure of the pristine polymer due to electron irradiation followed by the amorphisation.
- There was no change in the optical band-gap of PET after electron irradiation.
- The bulk etch-rate for the fission fragments in PET increased due to electron irradiation thereby, decreasing the activation energy of etching.
- The electron irradiation has converted the PET into an easily etchable material.
- The surface roughness of the polymer decreased after electron irradiation.

6.1.4. *Electron induced modifications in Polyimide*

The modifications induced 23 kGy dose of 2 MeV electron in PI are summarised as follows:

- The degradation of PI by electron irradiation is characterised by the decay of the imide group.
- Oxidative degradation of hydrogen bonds of amides was further enhanced due to electron irradiation in the presence of air.
- There was no change in the optical band-gap observed due to the electron irradiation.
- The thermal stability of PI decreased by electron irradiation. Though the stable zone remained the same in the pristine and the irradiated PI, yet the irradiated PI decomposed completely at a relatively lower temperature.
- The irradiated PI showed a decrease in the melting temperature also.
- There was an increase in bulk etch-rate and hence a decrease in activation energy of etching due to chain-scissioning in the irradiated PI.
- Electron irradiation converted the PI into an easily etchable material.
- The surface roughness of the pristine PI was reduced by electron irradiation.

6.1.5. *Electron induced modifications in Polytetrafluoro ethylene*

The modifications induced 23 kGy dose of 2 MeV electron in PTFE are summarised as follows:

- An increase in absorbance and emergence of some additional absorbance bands in the electron irradiated PTFE is evident from FT-IR studies.
- A 50% decrease in the optical band-gap of PTFE by electron bombardment show the impact of electron irradiation in enhancing polymer's conductivity.
- The stable free radical detected from ESR spectra of the irradiated PTFE was responsible for decrease in energy band-gap.
- A decrease in thermal stability of the PTFE was observed due to chain-scission, leading to a decrease in the strength of the polymer after electron irradiation.
- The melting temperature of PTFE was reduced by electron irradiation.
- The decrease in intensity of the main peak in the electron irradiated PTFE, in the diffraction spectra, further supports the decrease in crystallinity by electron irradiation.

- The chain-scissioning and formation of smaller fragments might be the reason for increase in roughness of the irradiated PTFE.

6.1.6. *Modification of PADC through electron-target collision*

The mode of energy-loss by 2 MeV electrons when they pass through different metallic layers, the impact of energy-loss phenomena on the track registration property and thermal characteristics of PADC were studied.

- The total energy-loss by the electron beam is the sum of the energy-loss due to ionisation and that due to radiation. The energy-loss by electrons was found to be a direct function of the charge, mass, thickness and density of the target material.
- The energy-loss by electrons was calculated to be maximum in Lead foil because of its large atomic number and thickness followed by that in Molybdenum and then in Gold foil.
- The effect of chain-scission was observed to be maximum in the 1st PADC sample of each stack due to high energy deposition, resulting in a higher bulk etch-rate than the successive PADC samples of the same stack.

- The 1st PADC of Gold stack was found to be having the highest bulk etch-rate owing to minimum energy-loss of electron beam while passing through the Gold foil.
- The bulk etch-rate of the PADC of Lead stack was found to be minimum because of the maximum energy-loss by electron while traversing through the Lead foil.
- The thermal analysis of the PADC sample showed that the PADC of the Lead stack was comparatively more stable due to maximum energy-loss of electron through the Lead foil. A minimum energy deposited on the 1st PADC sample of the Lead stack caused the least damage to it.

Thus, the energy-loss by electrons can be controlled by placing suitable metal foils accordingly. In addition to this, desirable modifications in the detectors can be achieved by controlling the energy-loss of ion beams by placing appropriate metal foils.

6.2. FUTURE PERSPECTIVES

6.2.1. *Future applications of the modified polymers*

The present work has resulted in providing some important data base regarding the modifications produced in the selected polymers by electron irradiation, which will further enhance the technological applicability of the polymers.

- PADC can be satisfactorily used as a reliable dosimeter for high-energy electrons.
- The modification in etching response and efficiency of PADC by electron irradiation will further enhance its utility as a track detector.
- The 235 kGy dose of 2 MeV electron increased the bulk etch-rate of PADC by four times. This indicates that the use of still higher doses can improve the track registration sensitivity of PADC. In other words, electron irradiation can be used to sensitise the PADC detector.
- As the ability of Polypropylene to withstand thermal strain increases after electron irradiation, this modified polymer can be used in high temperature works.

- The conductivity of Polypropylene has also been improved by electron irradiation. This lightest polymer may possibly find its application in micro-electronics.
- The formation of stable free radical and a 50% decrease in the optical band-gap by electron irradiation in Polytetrafluoro ethylene further enhances the applicability of this widely used polymer.
- Electron induced degradation of PTFE extends its applicability as lubricants and in production of perfluoro intermediates useful in textile industries.
- Electron irradiation has enhanced the bulk etch-rate, thereby decreasing the activation energy of etching in Polyimide and Polyethylene terephthalate. This enhances the applicability of these polymers as track detectors and in development of nulear track micro/nano- filters (NTMF).

6.2.2. *Future extension of the present work*

Following subsequent investigations may augment present studies for a deeper understanding of the induced modifications in the polymers:

- Online measurements and study of energy-loss phenomena of electrons by Electron Energy Loss Spectrophotometer (EELS) can provide a deeper insight to the entire energy-loss process.
- Positron annihilation spectroscopy (PAS) can be employed to study the free volume in the irradiated polymers.
- Depth profiling techniques can be used to probe implanted or penetrating matter along the ion tracks in the irradiated polymers.
- Simulations of tracer mobility along the ion tracks in polymer i.e., Diffusion simulations can be performed to understand non-trivial shapes of the measured depth profiles of implanted ions or penetrants.
- The electrons with energy above the critical value, which results in a considerable radiative loss by bremsstrahlung emission, can be used to study the effect of bremsstrahlung on the detectors.
- Some other investigations on the irradiated polymers like thermoluminesence, annealing characteristics, hydrogen loss

studies, etc. can provide more information on the induced modifications.

- Studies at higher doses of electron will be significant for alkyne group formation in Polyethylene terephthalate, in decreasing the band-gap in Polyimide and in improving the etching response of these two polymers to electron irradiation.
- The impact of heavy ion irradiation on the same polymers can be done in order to have a comparative study on the effect of the low and high LET radiation on polymers.
- The study of the impact of electron irradiation on polymers can be extended to some other polymers like Polycarbonates, Polyvinyl chloride, Cellulose nitrate, Silicon rubber, SR-86 etc.

REFERENCES

Abu-Jarad F., Hala A. M., Farhat M. and Islam M. (1997) Effect of high gamma dose on the CR-39 properties. *Radiat. Meas.* **28**, 111-116.

Ahmad S. and Stejny J. (1991) Polymerisation, Structure and track recording properties of CR-39. *Nucl. Tracks Radiat. Meas.* **19**, 11-16.

Akber R. A., Nadeem K., Majid C. A., Hussain A., Zaman N., Chaudhary M. A. and Khan H. A. (1980) Studies of structural changes produced by high doses of gamma rays in some plastic track detectors. *Nucl. Instr. Meth.* B **173**, 217-222.

Alpert N. L., Keiser W. E. and Szymanski H. A. (1970) IR- Theory and Practice of Infrared Spectroscopy. *A Plenum/Rosetta edition, Published by Plenum Publishing Corporation, New York,* 184-300.

Apel P., Spohr R., Trautmann C. and Vutsadakis V. (1999) Track structure in polyethylene terephthalate irradiated by heavy ions: LET dependence of track diameter. *Radiat. Meas.* **31**, 51-56.

Balashov A. P., Kostin D. V. and Shipatov E. T. (1999) Penetration of fast electrons in layered targets. *Nucl. Instr. and Meth.* **B 115**, 25-35.

Beardmore K. and Smith R. (1995) Ion bombardment of Polyethylene. *Nucl. Instr. Meth.* B **102**, 223-227.

Beiser Arthur. (1997) Concepts of Modern Physics. *Tata McGraw-Hill Publishing Company Ltd, New Delhi. 5th Edition,* 474-478.

Betz N., Peterson E., Le Moël A. (1996) Swift heavy ion effects in fluoro polymers: radicals and crosslinking. *Nucl. Instr. and Meth.* B **116**, 207-211.

Bohidar N. (1994) Radiation – Induced Polymerisation and Effects of Nuclear radiation on Polymers. *J. T. R. Cem.* **1**, 31-39.

Calcagno L., Compagnini G. and Foti G. (1992) Structural modification of polymer films by ion irradiation. *Nucl. Instr. and Meth.* B **65**, 413-422.

Caro J. C., Lappan U. and Lunkwitz K. (1999) Sulphonation of fluoropolymers induced by electron beam irradiation. *Nucl. Instr. and Meth.* B **151**, 181-185.

Chapiro A. (1988) Chemical modifications in irradiated Polymers. *Nucl. Instr. and Meth.* B **32**, 111-114.

Chong C. S., Ishak I., Mahat R. H. and Amin Y. M. (1997) UV-Vis and FTIR spectral studies of CR-39 plastics irradiated with X-rays. *Radiat. Meas.* **28**, 119-122.

Darraud-Taupiac C., Bennamane B., Decossas J. L. and Vareille J. C. (1997) CR-39 (poly(diethylene glycol bis(allyl carbonate)) under γ-rays & proton beams. *Nucl. Instr. and Meth.* B **131**, 198-204.

Das A., Bera S., Dhara S. and Patnaik A. (1998) Physical and chemical implications of 100 keV proton implantation of laser ablated PPS thin films. *Nucl. Instr. and Meth.* B **134**, 377-384.

Davenas J., Baiteux G. and Jardin C. (1997) Electronic and mass transport in ion beam nano structured polymers: Role of the irradiation energy. *Nucl. Instr. and Meth.* B **131**, 91-96.

Dwivedi K. K. and Mukherji S. (1979) Heavy ion track lengths in Solid dielectric track detectors. *Nucl. Instr. Meth.* B **161**, 317-326.

Dwivedi K. K. (1991) Range and energy loss measurement of heavy ions by a nuclear track technique. *Nucl. Tracks Radiat. Meas.* **19**, 71-76.

Dwivedi K. K. (1997) On the Critical Etching Parameters of Track Detectors. *Int. J. Radiat. Appl. Instr. (Part D): Radiat. Meas.* **27**, 453-456.

Dwivedi K. K., Ghosh S., Fink D., Mishra R., Tripathy S. P., Kulshreshtha A. and Khathing D. T. (1999) Modification of Track Registration Response of PADC detector by energetic protons. *Radiat. Meas.* **31**, 127-132.

Eßer M. and Fuhrmann J. (1999) Polymer chain orientation in latent ion tracks. *Nucl. Instr. Meth.* B **151**, 118-122.

Ehrhardt H. (1984) Electron impact ionisation. *Electronic and Atomic Collisions, J. Eichler, I. V. Hertel, N. Stolterfoht (eds.),* 21-29.

Fink D., Hosoi F., Omichi H., Sasuga T. and Amaral L. (1994) IR transmission of ion iradiated polymers. *Radiat. Eff. and Def. in Solids* **132**, 313-328.

Fink D., Chung W. H., Klett R., Schmoldt A., Cardoso J., Montiel R., Vazquez M. H., Wang L., Hosoi F., Omichi H. and Goppelt-Langer P. (1995) Carbonaceous Clusters in irradiated polymers as revealed by UV-Vis spectrometry. *Radiat. Eff. and Def. in Solids* **133**, 193-208.

Fink D., Chung W., Klett R., Dobeli M., Synal H. A., Chadderton L. T. and Wang L. (1996) On the dying of ion tracks in polymers. *Nucl. Instr. and Meth.* B **108**, 377-384.

Fink D., Klett R., Chadderton L. T., Cardoso J., Montiel R., Vazquez H. and Karnovich A. A. (1996) Carbonaceous Clusters in irradiated polymers as revealed by small angle X-ray scattering and ESR. *Nucl. Instr. and Meth.* B **111**, 303-314.

Frank A. L. and Benton E. V. (1970) Dielectric plastics as high exposure gamma ray detectors. *Radiat. Eff.* **2**, 269-272.

Gangal S. V. (1989) in: *Encyclopedia of Polymer Science & Engineering, H. F. Mark, N. M. Bikales, C. G. Overberger (Eds.) 2nd Edition, Wiley, New York* **16**, 557-580.

Ghosh S., Raju J. and Dwivedi K. K. (1994) Tracklengths of energetic ^{132}Xe ions in CR-39 detectors. *Radiat. Eff. and Def. in Solids* **129**, 155-159.

Gowariker V. R., Viswanathan N. V. and Jayadev S. (1996) Polymer Science. *New Age International (P) limited, Publishers. 9th Edition,* 150-173.

Higazy A. A. and Hussein A. (1995) Optical absorption studies of gamma irradiated magnesium phosphate glasses. *Radiat. Eff. and Def. in Solids* **133**, 225-235.

Idoeta R. (2000) Penetration of beta rays through gold absorbers. *Nucl. Instr. Meth.* B **160**, 250-256.

Khan H. A., Asharf M. A., Yameen S., Haroon M. R., Hussain A. (1975) Effects of high gamma doses on the response of plastic track detectors. *Nucl. Instr. Meth.* B **127**, 105-108.

Klimov A. (1975) Nuclear Physics and Nuclear Reactors. *Mir Publications, Moscow,* 180-189.

Kocsis ZS., Dwivedi K. K. and Brandt R. (1997) Studies on the Track Formation Mechanism of the Heavy Ions in CR-39. *Int. J. Radiat. Appl. Instr. (Part D): Radiat. Meas.* **28**, 177-180.

Lee E. H., Lewis M. B., Blau P. J. and Mansur L. K. (1991) Improved Surface properties of Polymer materials by multiple ion beam treatment. *J. Mater. Res.* **6**, 610-628.

Lee E. H. (1999) Ion beam modification of polymeric materials - fundamental principles and applications *Nucl. Instr. Meth.* B **151**, 29-41.

Marletta G. and Iacona F. (1995) Chemical and Physical property modifications induced by ion irradiation in Polymers. Materials and Processes for surface & interface Engineering. *Kluwer Academic Publishers,* 597-640.

Mateev M. and Karageorgiev S. (2000) Radiation induced transformation of Polypropylene – Morphology and viscoelastic behaviour. *Radiat. Eff. and Def. in Solids* **152**, 109-138.

Matzke Hj. (1982) Radiation damage in crystalline insulators, oxides and ceramic nuclear fuels. *Radiat. Eff.* **64**, 3-33.

Mishra R., Tripathy S. P., Kulshreshtha A., Srivastava A., Dwivedi K. K. and Avasthi D. K. (1999) Ranges and energy loss measurement of 1.0-4.7 MeV/u ^{28}Si ions in Makrofol-G using PADC as detector. *Radiat. Eff. and Def. in Solids* **147**, 273-281.

Mishra R., Tripathy S. P., Sinha D., Dwivedi K. K., Ghosh S., Khathing D. T., Müller M., Fink D. and Chung W. H. (2000) Optical and electrical properties of some electron and proton irradiated polymers. *Nucl. Instr. and Meth.* B **168**, 59-64.

Oda K., Yoshida K., Yamauchi T., Honda Y., Ikeda T. and Tagawa S. (1997) Effects of low LET radiations on CR-39 track detector. *Radiat. Meas.* **28**, 85-88.

Papaléo R. M. Farenzena L. S., De Araújo M. A. and Livi R. P. (1999) Surface tracks in polymers induced by MeV heavy ion impacts. *Nucl. Instr. Meth.* B **151**, 135-139.

Phukan T., Kanjilal D., Goswami T. D. and Das H. L. (1999) Dielectric response of heavy ion irradiated PADC track detector. *Nucl. Instr. Meth.* B **155**, 116-119.

Popok V. N., Odjhaev V. B., Kozlov I. P, Karpovich I. A. and Sviridov D. V. (1997) Ion beam effects in polymer films: Structure evolution of implanted layer. *Nucl. Instr. Meth.* B **129**, 60-64.

Portwood T. and Henshaw D. L. (1986) The effect of gamma dose on alpha response of CR-39. *Nucl. Tracks* **12**, 105-108.

Sasuga T. (1988) Oxidative irradiation effects on several aromatic polyimides. *Polymer* **29**, 1562-1568.

Saxena A. and Dwivedi K. K. (1986) Chemical etching characteristics of glass detectors. *Nucl. Tracks and Radiat. Meas.* **12**, 161-164.

Schierholz K., Lappan U., Lunkwitz K. (1999) Electron beam irradiation of polytetrafluoroethylene in air: investigations on thermal behavior. *Nucl. Instr. and Meth.* B **151**, 232-237.

Sharma S. L., Pal T., Rao V. V. and Enge W. (1991) Effect of gamma irradiation on bulk etch rate of CR-39. *Nucl. Tracks Radiat. Meas.* B **18**, 385-389.

Singh S. and Singh B. (1988) The effects of gamma irradiations on etching characteristics of some solid state track detectors. *Nucl. Tracks Radiat. Meas.* **15**, 199-202.

Sinha D., Ghosh S., Srivastava A., Dedgaonkar V. G., Dwivedi K. K. (1997) Effect of gamma rays on PADC detectors. *Radiat. Meas.* **28**, 145-148.

Sinha D., Dwivedi K. K. (1998) Modifications of radiation detection response of PADC track detectors by photons. *Radiat. Physics and Chemistry* **53**, 99-105.

Sorensen A. M. (1996) Channeling, Bremsstrahlung and Pair Creation in Single crystals. *Nucl. Instr. and Meth.* **B 119**, 1-29.

Spinks J. W. T. and Woods R. J. (1990) Introduction to Radiation Chemistry. *Wiley Interscience Publication. 3rd Edition,* 14-22.

Steckenreiter T., Balanzat E., Fuess H. and Trautmann C. (1997) Chemical modifications of PET induced by SHI. *Nucl. Instr. Meth.* B **131**, 159-166.

Steckenreiter T., Balanzat E., Fuess H. and Trautmann C. (1999) Pyrolytic Effects induced by energetic ions in Polymers. *Nucl. Instr. and Meth.* B **151**, 161-168.

Tayal D. C. (1992) Nuclear Physics. *Himalaya Publishing House, 5th Edition*, 102-112.

Thang N. X. and Doan T. T. (1995) Structure effect in response function of CR-39 detector. *Radiat. Meas.* **25**, 185-187

Trautmann C., Bouffard S. and Spohr R. (1996) Etching Threshold for ion tracks in Polyimide. *Nucl. Instr. and Meth.* B **116**, 429-433.

Tripathy S. P., Mishra R., Khathing D. T., Kulshrestha A., Dwivedi K. K., Srivastava A., Ghosh S. and Fink D. (2000) Optical absorption properties in heavy ion irradiated polymers. (communicated).

Wang Y. Q., Giedd R. E., Moss M. G. and Kaufmann J. (1997) Electronic properties of ion implanted polymer films. *Nucl. Instr. Meth.* B **127/128**, 710-715.

Xu X. L., Yuehui Yu., Zixin L., Lizhi C., Fang F., Zuyao Z., Shichang Z., Gendi D. and Guanqun X. (1991) Shrinkage of Polyimide films under ion beam irradiation. *Nucl. Instr. and Meth.* B **59/60**, 1267-1270.

Yoshida K. and Iwaki M. (1987) Structure and Morphology of ion-implanted Polyimide films. *Nucl. Instr. and Meth.* B **19/20**, 878-881.

Zamani M. and Charalambous S. (1985) Dose rate dependence on response of CR-39 SSNT-detector. *Int. J. Appl. Radiat. Isot.* **36**, 525-529.

Zamani M., Sampsonidis D., Charalambous S. (1986) Dose rate effects on CR-39 SSNT detector. *Nucl. Tracks* **12**, 125-128.

CURRICULUM VITAE

Name : Rosaline Mishra.

Date of birth : 20th July, 1974.

Educational qualifications:

Examination	Board/University	Year	Result	% of Marks
A.I.S.S.C.E	C.B.S.E.	1989	1st Div.	79 %
A.I.S.S.E.	C.B.S.E.	1991	1st Div.	72 %
+3 Science (Physics)	Utkal University.	1994	1st Div.	67 %
M.Sc. (Physics)	Utkal University.	1996	1st Div.	72 %
Ph.D. (Physics)	N.E.H.University.	1997	***	***

Computer proficiency: MS-DOS, Windows 9x, BASIC programming, Word star, Lotus-1,2,3, MS-Word, Excel, Web designing.

CONFERENCE / WORKSHOP:

[1] Eleventh National Symposium on "Solid State Nuclear Track Detectors". October 12-14, 1998, G. N. D. University, Amritsar.

[2] International Conference on "Swift Heavy Ions in Materials Engineering and Characterisation (SHIMEC-98)", October 20-22, 1998, Nuclear Science Centre, New Delhi.

[3] Nuclear and Radiochemistry Symposium (NUCAR '99), Bhabha Atomic Research Center, Mumbai. Paper awarded.

[4] National workshop on Radiochemistry and applications of Radio-isotopes. December 5-13, 1996, NEHU, Shillong.

[5] Regional workshop on Analytical Techniques (Trace Elements) in Earth sciences. March 12-15, 1997, NEHU, Shillong.

[6] School on accelerator based technology. April 14-24, 1998, Nuclear Science Centre, New Delhi.

[7] National Workshop on Radon/Helium Precursors for Earthquake Studies. October 12-17, 1998, G. N. D. University, Amritsar.

[8] School on Swift Heavy Ions in Materials: Basic phenomena and Applications. October 24, 1998, Nuclear Science Centre, New Delhi.

[9] Awareness programme on Applications of radioisotopes and radiation technology, November 26-27, 1999, R. S. I. C., Shillong.

[10] National Workshop on recent trends in Electron Microscopy. April 26-27, 2000, R. S. I. C., Shillong.

Scholarship/ Fellowship awarded:

Junior Research Fellowship (D.A.E.) : 18/11/96 - 18/11/98.
Senior Research Fellowship (D.A.E.) : 18/11/98 - 10/10/99.
Senior Research Fellowship (C.S.I.R.) : 10/10/99 onwards.

Membership:

Life member of Nuclear Track Society of India.

List of Research Papers:

[1] **Energy loss and Mean Ranges of ^{129}Xe in Mica and Makrofol-KG.**
A. Kulshreshtha, C. Laldawlgliana, **R. Mishra**, S. Ghosh, K. K. Dwivedi, R. Brandt and D. Fink. *Radiation Effects and Defects in Solids. Vol.147 (1999) 151-164.*

[2] **Ranges and Energy Loss Measurement of 1.0-4.7 MeV/u ^{28}Si ions in Makrofol-G using PADC as detector.**
R. Mishra, S. P. Tripathy, A. Kulshreshtha, A. Srivastava, K. K. Dwivedi and D. K. Avasthi. *Radiation Effects and Defects in Solids. vol.147 (1999) 273-281.*

[3] **Modifications in Track Registration Response of PADC detector by energetic protons.**
K. K. Dwivedi, S. Ghosh, D. Fink, **R. Mishra**, S. P. Tripathy, A. Kulshreshtha and D. T. Khathing. *Radiation Measurements. vol.31 (1999) 127-132.*

[4] **Concentration of Radon and Thoron in some dwellings of North Eastern India.**
R. Mishra, S. P. Tripathy, L. Pachuau, C. Laldawngliana, R. Lalramengzami, S. Ghosh, K. K. Dwivedi, D. T. Khathing, T. V. Ramachandran. *Indoor+ Built Environment. vol.8 (1999) 322-326.*

[5] **Assessment of Indoor Radon Level in Shillong.**
M. Sen, **R. Mishra**, S. P. Tripathy, D. Sinha, A. Kulshreshtha, K. K. Dwivedi, P. Deka and B. Bhattacharjee. *J. As. Sc. Soc. 39(3) (1998) 106.*

[6] **Optical and Electrical properties of some electron and proton irradiated polymers.**
R. Mishra, S. P. Tripathy, D.Sinha, D. T. Khathing, K. K. Dwivedi, S. Ghosh, M. Muller, D. Fink and W. H. Chung. Presented in NUCAR'99, BARC(**Awarded**). *Nuclear Instrumentation and Methods in Physics Res. B, 168 (2000) 59-64.*

[7] **Impact of Electron Irradiation on particle track etching response in Polyallyldiglycol carbonate (PADC).**
R. Mishra, S. P. Tripathy, A. Kulshrestha, A. Srivastava, S. Ghosh, K. K. Dwivedi, D. T. Khathing, M. Muller and D. Fink. *Pramana, vol.54(5) (2000)* 777-784.

[8] **Optical Absorption and Track studies of Gamma- irradiated ZnP glass.**
A. Kulshreshtha, D. Sinha, **R. Mishra**, S. P. Tripathy, K. K. Dwivedi, S. Ghosh and D. Fink. Presented in the 19th International Conference on Nuclear Tracks in Solids, Besancon, France. *Radiation Measurements. vol.32(3) (2000) 169-172.*

[9] **Effect of high gamma doses on etch rate values of different types of PADC detectors.**
D. Sinha, **R. Mishra**, S. P. Tripathy, K. K. Dwivedi. *Radiation Measurements, 000 (2000) 000.*

[10] **Simultaneous Determination of Radon, Thoron and their progeny in dwellings.**
K. K. Dwivedi, **R. Mishra**, S. P. Tripathy, A. Kulshreshtha, D. Sinha, A. Srivastava, P. Deka, B. Bhattacharjee, T. V. Ramachandran and K. S. V. Nambi. *Radiation Measurements, 000 (2000) 000.*

[11] **Electron Induced Modification in Poly(ethylene terephthalate).**
R. Mishra, S. P. Tripathy, K. K. Dwivedi, D. T. Khathing, S. Ghosh, M. Muller and D. Fink. *Radiation Effects and Defects in Solids. 000 (2000) 000.*

[12] **Effect of proton irradiation through metal foils on PADC.**
S. P. Tripathy, **R. Mishra**, A. Kulshreshtha, K. K. Dwivedi, D. T. Khathing, A. Srivastava, S. Ghosh and D.Fink. Presented in SHIMEC'98, NSC, Delhi. *Radiation Measurement, 000 (2000) 000.*

[13] **Electron irradiation on poly(allyl glycol carbonate).**
R. Mishra, S. P. Tripathy, A. Kulshreshtha, D. T. Khating, K. K. Dwivedi, S. Ghosh and D. Fink. Presented in the International conference SHIMEC '98, NSC, Delhi. *Radiation Effects and Defects in Solids. 000 (2000) 000.*

[14] **Gamma-photon induced modification of Polyvinylchloride (PVC) film.**
D. Sinha, S.P.Tripathy, **R.Mishra**, K.K.Dwivedi. *Communicated to Radiation Effects and Defects in Solids.*

[15] **Optical absorption studies in heavy ion irradiated polymers.**
S. P. Tripathy, **R. Mishra**, A. Kulshreshtha, D. T. Khathing, K. K. Dwivedi, A. Srivastava, S. Ghosh and D.Fink. Presented in 11th National Symposium on SSNTDS, 1998, GNDU, Amritsar. *Radiation Effects and Defects in Solids, 000 (2000) 000.*

[16] **Range of ^{28}Si ions in Makrofol.**
S. P. Tripathy, **R. Mishra**, S. Shyam, A. K. Mawar, K. K. Dwivedi, D. T. Khathing and A. Srivastava. Presented in 11th National Symposium on SSNTDS, 1998, GNDU, Amritsar. *Radiation Measurements, 000 (2000) 000.*

[17] **Electron Induced Modification in Polypropylene.**
R. Mishra, S. P. Tripathy, K. K. Dwivedi, D. T. Khathing, S. Ghosh, M. Muller and D. Fink. *Radiation Measurements, 000 (2000) 000.*

[18] **Modifications in etching characteristics and surface topography of some electron irradiated polymers.**
R. Mishra, S. P. Tripathy, K. K. Dwivedi, D. T. Khathing, S. Ghosh and D. Fink. Presented in International conf. on Nucl. Tracks, 2000, Slovenia. *Radiation Measurements, 000 (2000) 000.*

[19] **Modificatins induced by proton irradiation in Polyallyl diglycol carbonate.**
S. P. Tripathy, **R. Mishra**, K. K. Dwivedi, D. T. Khathing, S. Ghosh and D. Fink. Presented in International conf. on Nucl. Tracks, 2000, Slovenia. *Radiation Measurements, 000 (2000) 000.*

[20] **Range and Energy loss rate of 118 MeV ^{28}Si in some Polymers using PADC as Detector.**
D. T. Khathing, S. P. Tripathy, **R. Mishra**, B. K. Verma and K. K. Dwivedi. Presented in International conf. on Nucl. Tracks, 2000, Slovenia. *Radiation Measurements, 000 (2000) 000.*

[21] **Proton Induced Modification in Polyethylene Terephthalate (PET).**
K. K. Dwivedi, S. P. Tripathy, **R. Mishra**, D. T. Khathing, S. Ghosh and D.Fink. Presented in International con. on Nucl. Tracks, 2000, Slovenia. *Radiation Measurements, 000 (2000) 000.*

[22] **Optical and electrical properties of gamma irradiated PADC detector.**
D. Sinha, T. Phukan, S. P. Tripathy, **R. Mishra** and K. K. Dwivedi. Presented in International conf. on Nucl. Tracks, 2000, Slovenia. *Radiation Measurements, 000 (2000) 000.*

[23] **Effect of Electron irradiation on Polytetrafluoroethylene.**
R. Mishra, S. P. Tripathy, K. K. Dwivedi, D. T. Khathing, S. Ghosh, M. Muller and D. Fink. *Communicated to Nuclear Instrumentation and Methods in Physics B.*

[24] **Spectroscopic and Thermal Studies of Electron irradiated Polyimide.**
R. Mishra, S. P. Tripathy, D. T. Khathing, K. K. Dwivedi, S. Ghosh, M. Muller and D. Fink. *Communicated to Radiation Physics and Chemistry.*

[25] **Range and Energy loss rate of 118 MeV ^{28}Si in some polymers.**
S. P. Tripathy, **R. Mishra**, A. Kulshreshtha, A. Srivastava, D. T. Khathing and K. K. Dwivedi. Presented in NUCAR'99, BARC, Mumbai **(Awarded)**. *Communicated to Indian journal of Pure and Applied Physics.*

[26] **On the Isothermal and Isochronal Annealing of ZnP glass track detector.**
S. P. Tripathy, **R. Mishra**, K. K. Dwivedi and D. T. Khathing. *Communicated to Journal of Phys: D, Applied Physics.*